Inaugural dissertation

for

obtaining the doctoral degree

of the

Combined Faculty of Mathematics, Engineering and Natural Sciences

of the

Ruprecht - Karls - University

Heidelberg

Presented by

M.Sc. Nora Heike Heber

born in: Freiberg

Oral examination: 29.11.2023

The Impact of Cycling Hypoxia on the Phenotype of HPV-Positive Cervical Cancer Cells

Referees:

Prof. Dr. Ralf Bartenschlager

Prof. Dr. Felix Hoppe-Seyler

Table of contents

Summary

Persistent infections with high-risk human papillomavirus (HPV) types, such as HPV16 and HPV18, are the major risk factor for the development of cervical cancer. The global incidence of cervical cancers is expected to rise in the next decades. Therefore, a better understanding of critical parameters determining the malignant phenotype of HPV-positive cancer cells, as well as the development and improvement of therapeutic strategies for cervical cancer treatment, is highly warranted. The extent of hypoxia in solid cancers can critically affect tumor aggressiveness and their therapy response. Besides chronic hypoxia, cycling hypoxia (cycH) is a prevalent but much less investigated form of tumor hypoxia, in which cancer cells are exposed to recurrent phases of hypoxia and reoxygenation. Importantly, cycH may lead to a particularly aggressive and therapy-resistant cellular phenotype. The effects of cycH in cervical cancer cells were thus far unknown.

The results of this thesis reveal distinct effects of cycH on the phenotype of HPV-positive cancer cells. Unlike under chronic hypoxia, cervical cancer cells under cycH maintain HPV *E6/E7* oncogene expression and function. In addition, they exhibit an increased resistance to radiotherapy, as well as to pro-senescent and pro-apoptotic chemotherapy. Interestingly, the resistance of cervical cancer cells to the pro-apoptotic effects of Cisplatin, the key chemotherapeutic drug for cervical cancer treatment, is particularly pronounced in cells treated under cycH, exceeding even their increased resistance under chronic hypoxia. Proteome analyses reveal that cervical cancer cells exposed to cycH exhibit a unique proteome signature, which includes a significant downregulation of luminal lysosomal proteins, such as the potentially pro-apoptotic Cathepsins B and L. Additionally, a reduction in autophagic flux under cycH is detectable. Comprehensive analyses of the differential susceptibility of cervical cancer cells to Cisplatin treatment under different oxygen conditions were performed. Whereas they did not provide evidence that this phenomenon is linked to the observed lysosomal alterations, they revealed that the Caspase 8-linked activation of the pro-apoptotic BH3 interacting domain death agonist (BID) protein plays a crucial role. Under cycH, Cisplatin-treated cells generate much less truncated BID protein, the active form of BID, resulting in impaired mitochondrial outer membrane permeabilization and pro-apoptotic Cytochrome c release. In summary, these results show that cycH profoundly influences the phenotype of HPV-positive cancer cells, including the virus/host cell crosstalk, the proteomic signature, and key cellular processes such as the composition of lysosomal contents or autophagy regulation. Furthermore, cycH critically alters the therapeutic susceptibility in that cervical cancer cells exposed to cycH are especially resistant to Cisplatin and thus could represent a particularly challenging cellular subpopulation for cervical cancer chemotherapy.

Zusammenfassung

Persistierende Infektionen mit onkogenen Typen humaner Papillomaviren (HPV), wie HPV16 und HPV18, sind Hauptrisikofaktoren für die Entstehung von Zervixkarzinomen. Die weltweite Inzidenz von Zervixkarzinomen wird vermutlich zukünftig weiter steigen. Daher ist ein besseres Verständnis der kritischen Parameter, die für den malignen Phänotyp HPV-positiver Tumorzellen verantwortlich sind, sowie die Verbesserung von Therapiestrategien dringend erforderlich. Tumorhypoxie kann die Aggressivität von Tumoren und ihre Therapieresistenz steigern. Neben der chronischen Hypoxie ist die zyklische Hypoxie (cycH) eine prävalente, aber viel weniger untersuchte Form der Tumorhypoxie, bei der Tumorzellen rekurrenten Phasen von Hypoxie und Reoxygenierung ausgesetzt sind. CycH wird mit einem besonders aggressiven und therapieresistenten Phänotyp in Verbindung gebracht. Die Auswirkungen auf HPV-positive Tumorzellen waren bisher nicht erforscht.

Die Ergebnisse dieser Arbeit decken distinkte Effekte von cycH auf den Phänotyp von HPV-positiven Tumorzellen auf. Anders als unter chronischer Hypoxie erhalten HPV-positive Zellen unter cycH die Expression und Funktion der HPV E6/E7-Onkogene aufrecht. Darüber hinaus zeigen die Zellen unter cycH eine erhöhte Resistenz sowohl gegenüber Bestrahlung, als auch gegenüber pro-seneszenter und pro-apoptotischer Chemotherapie. Die Cisplatin-Resistenz von Zervixkarzinomzellen ist unter cycH besonders ausgeprägt und übersteigt sogar die Resistenzsteigerung unter chronischer Hypoxie. Proteomanalysen zeigen, dass Zervixkarzinomzellen unter cycH eine spezifische Proteom-Signatur aufweisen, die sich u. a. durch eine signifikante Herunterregulierung luminaler lysosomaler Proteine, wie der potenziell pro-apoptotischen Cathepsine B und L, auszeichnet. Zudem ist eine Verminderung des autophagischen Flusses unter cycH zu beobachten. Experimentell ergab sich kein Anhalt dafür, dass die von den Sauerstoffbedingungen abhängige differentielle Empfindlichkeit von HPV-positiven Tumorzellen gegenüber Cisplatin mit den beobachteten lysosomalen Veränderungen zusammenhängt. Vielmehr zeigt sich, dass hierfür die Caspase 8-vermittelte Aktivierung des pro-apoptotischen BID-Proteins eine zentrale Rolle spielt. Zellen, die unter cycH mit Cisplatin behandelt werden, weisen vergleichsweise nur sehr geringe Mengen an trunkiertem BID, der aktiven Form von BID, auf, was in einer ineffizienten Permeabilisierung der äußeren Mitochondrienmembran und einer stark reduzierten Freisetzung von Cytochrom c resultiert. Zusammenfassend zeigt diese Arbeit, dass cycH zu ausgeprägten und spezifischen phänotypischen Veränderungen in HPV-positiven Zellen führt. Die Ergebnisse weisen zudem darauf hin, dass Zervixkarzinomzellen unter cycH eine besonders herausfordernde Zellpopulation für die therapeutische Wirksamkeit von Cisplatin darstellen könnten.

Acknowledgements

First of all, I would like to thank Prof. Dr. Felix Hoppe-Seyler for giving me the opportunity to conduct my dissertation in his group, for his guidance and support. Likewise, I am truly grateful to Prof. Dr. Karin Hoppe-Seyler for inspiring discussions, advice, and encouragement. We've had the pleasure of working together since 2019 when I initially became part of your lab during my lab rotation. This was followed by my master's thesis and, eventually, my PhD. You gave me the necessary freedom and support to develop my own research questions and grow personally and professionally as a scientist. Additionally, I learned a lot about endurance, Wagner, and debating politics. Both of you create such a pleasant atmosphere in the group that I will definitely miss.

Furthermore, I am grateful to Prof. Dr. Ralf Bartenschlager for being the first referee of this thesis and a valuable member of my TAC committee. I also want to thank Prof. Dr. Stefan Duensing for joining my TAC committee. Likewise, I thank Prof. Dr. Martin Müller and Dr. Tim Waterboer for joining the committee for my thesis defense.

Next, I would like to thank Dr. Bianca Kuhn and Prof. Dr. Jeroen Krijgsveld (DKFZ) for the collaboration on performing mass spectrometry analyses and helpful discussions on data analysis. Furthermore, I wish to thank Dr. Vladimir Gonçalves Magalhães (DKFZ) for unconditional helpfulness and advice during the process of writing. I also want to sincerely thank Tom Holz for his help with all IT-related problems at any time.

Importantly, I would like to extend my sincere thanks to the members of the F065 lab. First, I am deeply grateful to Julia Bulkescher, Angela Holzer and Claudia Lohrey for the help and technical expertise. You always offered your generous support and comfort when the work started piling up on my lab bench. Furthermore, I would like to thank all past and present lab members: Alicia Avenhaus, Kristin Frensemeier, Anja Herrmann, Julia Mändl, Tobias Strobel, Milica Velimirovic, Maria Weber and Dongyun Yang. I truly appreciated the helpful discussions and advice, the supportive working atmosphere, and, of course, our coffee breaks. I will always cherish the great times we spent together, inside but especially outside the lab - whether it was playing laser tag, pub quizzes, or traveling together.

Many thanks also to my friends who accompanied and supported me the whole time, and especially to Tim. I am deeply grateful for your never-ending emotional support, encouragement, and enthusiasm, which significantly contributed to this thesis. Finally, I would like to thank my family for always believing in me, for supporting and encouraging me throughout my entire academic journey. Without all of you, I would have never come this far and, of course, would have had much less fun along the way.

Publications and Presentations

Publications

Heber N, Kuhn BJ, Strobel TD, Lohrey C, Krijgsveld J, Hoppe-Seyler K, Hoppe-Seyler F. The Impact of Cycling Hypoxia on the Phenotype of HPV-Positive Cervical Cancer Cells. Manuscript submitted for publication.

Strobel TD, Weber M, Heber N, Holzer A, Hoppe-Seyler K, Hoppe-Seyler F. Revisiting the role of STAT3 in cervical cancer. Manuscript in revision.

Presentations

Heber N, Kuhn BJ, Krijgsveld J, Hoppe-Seyler K, Hoppe-Seyler F. Phenotypic characterization of HPV-positive cervical cancer cells under cycling hypoxia. Helmholtz International Graduate School for Cancer Research 2023 PhD Retreat. 17-19.07.2023. Löwenstein, Germany. Poster Presentation.

Heber N, Kuhn BJ, Krijgsveld J, Hoppe-Seyler K, Hoppe-Seyler F. Phenotypic characterization of HPV-positive cervical cancer cells under cycling hypoxia. i3 Immunology, Infection and Inflammation @ DKFZ Seminar Series. 15.12.2022. Heidelberg, Germany. Oral Presentation.

Heber N, Kuhn BJ, Krijgsveld J, Hoppe-Seyler K, Hoppe-Seyler F. Phenotypic characterization of HPV-positive cervical cancer cells under cycling hypoxia. Helmholtz International Graduate School for Cancer Research 2022 PhD Poster Presentation. 18.11.2022. Heidelberg, Germany. Poster Presentation.

Heber N, Kuhn BJ, Krijgsveld J, Hoppe-Seyler K, Hoppe-Seyler F. Phenotypic characterization of HPV-positive cervical cancer cells under cycling hypoxia. 15th International PhD Student Cancer Conference. 08.-10.06.2022. Heidelberg, Germany. Poster Presentation.

CHAPTER 1

INTRODUCTION

1 Introduction

1.1 Human papillomaviruses and cancer

Cancer is a global health burden and a leading cause of death worldwide.[1] In 2020, 19.3 million new cancer cases and nearly 10 million cancer-related deaths were estimated, with a rising trend attributed to changes in demographics and lifestyle.[2] Risk factors for the development of cancer are, apart from genetic predispositions and ageing, mainly behavioral and environmental factors, such as smoking, alcohol consumption, obesity, exposure to UV light, chemical mutagens or radiation, as well as infection and inflammation.[3] Infectious agents contribute to a significant proportion of cancer cases, with approximately 13% of cancer cases in 2018 attributed to infections with, for instance, Human Papillomaviruses (HPVs), *Helicobacter pylori*, Hepatitis B and C Virus or Epstein-Barr Virus.[4] HPV infections, in particular, are responsible for approximately 4.5% of the cancer burden worldwide and cause various anogenital cancers, including cervical, anal, penile, vaginal, and vulvar cancers, as well as an increasing number of head and neck cancers.[4,5]

1.1.1 HPV classification

Human papillomaviruses are a group of small DNA viruses characterized by a non-enveloped icosahedral capsid. HPVs belong to the family of *Papillomaviridae* and primarily infect epithelial cells in the skin and mucosal tissues.[6] HPVs are commonly spread during sexual contact; however, most HPV infections remain asymptomatic and are efficiently cleared by the host immune system within approximately two years.[7,8]

HPVs display great genomic diversity and to date, more than 200 different HPV genotypes have been identified.[9,10] HPVs are classified into five phylogenetic HPV genera based on the sequence of their capsid protein-coding *L1* genes: alpha-papillomaviruses, beta-papillomaviruses, gamma-papillomaviruses, mu-papillomaviruses, and nu-papilloma-viruses.[9,11] Additionally, the HPV genotypes are further categorized into low-risk and high-risk HPV types based on their association with clinical outcomes.[6] Low-risk HPV types, for instance HPV6 or HPV11, can cause benign lesions, such as cutaneous or anogenital warts. In contrast, persistent infections with high-risk HPV types are a substantial risk factor for carcinogenesis.[6,12] Among the high-risk HPV types, twelve are classified as carcinogenic: HPV16, 18, 31, 33, 35, 39, 45, 51, 52, 56, 58, and 59.[8] Additionally, there are several other HPV types that are considered possibly carcinogenic in rare cases.[8]

1.1.2 HPV genome organization and life cycle

HPVs possess a circular, double-stranded DNA genome with an approximate size of 8 kilobase (kb) pairs. Among the various HPV genotypes, the HPV16 genome is of particular interest. It consists of eight open reading frames (ORFs) that encode six early genes (E1, E2, E4, E5, E6, and E7) and two late genes (L1 and L2), which are expressed at different stages of the viral life cycle in the differentiating epithelium (Figure 1).[6] The long control region (LCR), also known as the upstream regulatory region (URR), contains the origin of replication and transcription factor binding sites. The expression of HPV genes is tightly regulated by early and late promoters (HPV16: P97 and P670) as well as post-transcriptional messenger RNA (mRNA) splicing.[6,8,13]

The viral gene products can be further divided into highly conserved core proteins and accessory proteins that exert more diverse, HPV-type dependent functions.[8] The core proteins E1 and E2 are mainly involved in viral genome replication and transcriptional regulation. L1 and L2 code for the structural major and minor capsid proteins, respectively, and are responsible for capsid assembly, formation of viral particles and delivery of the viral genome.[6] The accessory proteins E4, E5, E6 and E7 promote different stages of the viral life cycle, modify the infected host cell, and enable evasion of host immune defenses. HPV E4 protein is involved in genome amplification as well as the release and transmission of virions from epithelial cells.[14] In the case of high-risk HPV types, E5, and particularly E6 and E7 are the responsible oncoproteins that promote the initiation and progression of HPV-induced carcinogenesis.[15] The HPV E5 protein contributes to the transformation process and malignant progression by stimulating growth factor receptors, such as epidermal growth factor receptor (EGFR), or by downregulating major histocompatibility complex class I (MHC-I) receptors, supporting immune evasion.[16–18] Additionally, E5 has been shown to prevent apoptosis, e.g. by decreasing Fas receptor expression and by inducing proteasomal degradation of the pro-apoptotic BAX protein (see chapter 1.2).[19,20] The major viral oncoproteins, HPV E6 and E7, directly contribute to carcinogenesis by interfering with key cellular regulatory pathways, such as the Retinoblastoma protein (pRb) and p53 tumor suppressors, and ensuring the maintenance of the transformed phenotype (see chapter 1.1.5).[21]

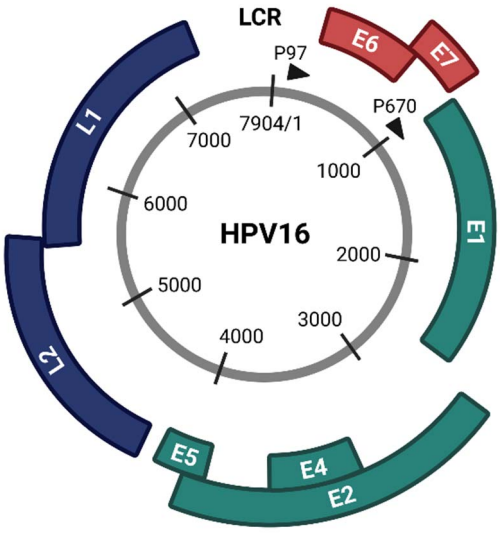

Figure 1. HPV genome organization.

The genome of high-risk HPV16 consists of six early ORFs, namely E1, E2, E4, E5 (green), E6, and E7 (red) and two late ORFs (L1 and L2, blue). Viral gene expression is regulated by the early (P97) and late (P670) promoters during different stages of epithelial cell differentiation. LCR, long control region.

During HPV infection, viral particles enter the epithelial tissue through microlesions and infect replicating keratinocytes located in the basal layer (Figure 2).[8,22,23] First, the viral L1 protein binds to heparan sulphate proteoglycans (HSPGs) on the surface of the host cell. This interaction induces a conformational change in the viral capsid, exposing the L2 protein, which is then cleaved by furin proteases.[6,24] Subsequently, the virus enters the host cell through endocytosis and undergoes uncoating. The viral genome is then delivered into the nucleus, where the early proteins E1 and E2 induce the replication of low copy number genomes and the maintenance of 50-100 episomal viral DNA copies within each infected basal keratinocyte.[6] The further progression of the productive HPV life cycle depends on the replication and differentiation status of the host keratinocytes.[25] Eventually, the infected host cells migrate from the basal layer to the mid and upper epithelial layers, cease dividing and differentiate into mature keratinocytes. This transition allows HPVs to exploit the cellular machinery for their own replication and survival.[24]

In the mid epithelial layers, the expression of the viral oncoproteins E6 and E7 is induced and thus promotes extensive viral genome amplification as well as continuous cellular proliferation (Figure 2).[23] The E6 oncoprotein plays a role in inhibiting apoptosis (see chapter 1.1.5) and promoting cell survival by targeting and degrading tumor suppressor proteins, such as p53. E7 disrupts the normal cell cycle regulation by binding and inactivating pRb.[21] At a later stage, excessive levels of E2 protein repress the early promoter in oncogenic HPV types, resulting in reduced expression of E6 and E7, which allows for further differentiation of

the host cell.[13,24] In the mid to upper epithelial layers, increased expression of the E4 protein and the late viral proteins L1 and L2 facilitates assembly and release of new virions that can infect other host cells and initiate another productive infection cycle (Figure 2).[8,23] Importantly, the progress and completion of the viral life cycle also depends on the site of infection and the presence of external co-factors such as cytokines and hormones.[25]

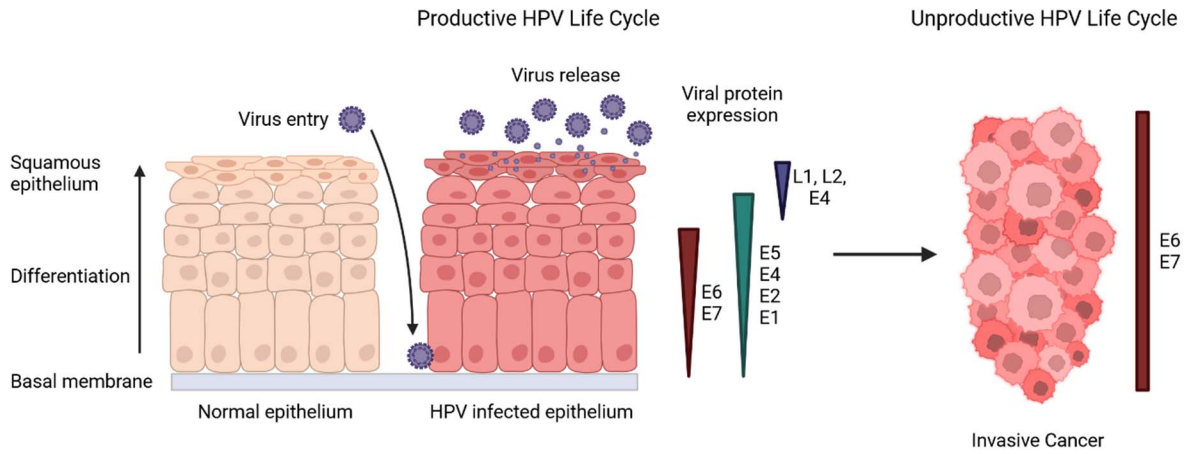

Figure 2. HPV life cycle and progression to invasive cancer.
HPVs enter the epithelium through microlesions and infect keratinocytes located in the basal membrane. During the productive HPV life cycle, the host cell differentiation controls the expression of early (E1, E2, E4, E5, E6, and E7) and late (L1 and L2) genes as well as the viral genome replication. The late viral genes L1 and L2 that regulate assembly and release of virions are expressed in the upper epithelial layer. Progression to invasive cancer is associated with an unproductive HPV life cycle that no longer generates progeny virions. HPV-positive cancer cells constantly express the viral oncoproteins E6 and E7, which drive continuous cell proliferation.

1.1.3 Cervical cancer

The connection between HPV infection and cervical cancer was first postulated and substantiated by Harald zur Hausen and his colleagues[26], a discovery that was acknowledged by the Nobel Prize in Physiology or Medicine in 2008. Up to 99.7% of cervical cancer cases are caused by persistent infections with high-risk HPVs, particularly HPV16 (~ 50-60%) and HPV18 (~ 20%).[22,27]

Cervical cancer is the fourth most prevalent cancer among women worldwide, following breast, colorectal, and lung cancer.[2] In 2020, there were more than 600,000 new cervical cancer diagnoses and roughly 340,000 deaths, with projections indicating a further increase in the coming years.[2,28] The burden of cervical cancer is especially prevalent in low- and middle-income countries, where socio-economic conditions and health care infrastructure affect cancer prevention, screening, and disease management.[2,4] Several cofactors,

including long-term usage of oral contraception, number of childbirths, smoking, vaginal microbiota, and co-infections with *Chlamydia* and Human Immunodeficiency Virus (HIV) can increase the risk of persistent HPV infections and the development of cervical cancer at earlier age.[2,29,30]

1.1.4 Mechanisms of HPV-associated carcinogenesis

Most HPV infections are cleared within a period of 12 – 24 months. This clearance is primarily mediated by cytotoxic T cells, which recognize and eliminate infected cells.[8] However, about 10% of HPV infections persist and pose a risk for the development of cervical cancer.[31] Of note, while a persistent HPV infection is necessary for carcinogenesis, it is not sufficient, as the development of cervical cancer depends on a complex interplay of various cofactors and molecular events.[32] The latency period between HPV infection and the development of cervical cancer can span several decades and most cases of cervical cancers are diagnosed in women between the ages of 45 and 60.[31]

Persistent infections with high-risk HPV types interfere with the normal regulation of cell growth, which leads to the formation of aberrant cells that, if left untreated, can evolve into precancerous lesions and, eventually, progress to invasive cancer.[8] The precancerous lesions, also referred to as cervical intraepithelial neoplasia (CIN), are categorized into three grades, CIN1-3, based on their severity of dysplasia and the risk to progress into severe precancerous forms and invasive cancer.[8,33]

Cervical cancers are classified into two major subtypes based on histomorphological characteristics and their origin. Squamous cell carcinomas originate from ectocervical squamous cells and are responsible for ~ 75% of cervical cancers. Adenocarcinomas, on the other hand, arise from endocervical, mucus producing glandular cells.[28]

Productive high-risk HPV infections can lead to increased cell proliferation in the basal epithelial layers, resulting in the formation of precancerous CIN1 lesions. Further progression to carcinogenesis is rare and associated with an unproductive viral life cycle (Figure 2).[25] In that case, increased expression and activity of the HPV E6 and E7 oncoproteins promote cellular transformation, eventually resulting in high-grade neoplasia (CIN2/CIN3) and invasive cancers of the cervix.[6,24]

In most cases, deregulation of E6/E7 expression is associated with the integration of viral DNA into the host genome.[34,35] The DNA integration often results in a partial loss of the HPV genome, including the *E5* coding sequence. Furthermore, the *E2* ORF gets disrupted, resulting in the inactivation of the transcriptional repressor protein E2. Consequently, this

allows for continuous and increased expression of *E6* and *E7* oncogenes, contributing to disease progression.[36] Moreover, the formation of multiple or tandem repeats of viral integrates can form super-enhancer-like elements that further promote viral oncogene transcription.[37] Notably, HPV16 DNA occasionally resides as episomal DNA and is less frequently integrated (~ 80%) compared to HPV18 DNA (~ 100%), which implies that viral DNA integration and the resulting inactivation of HPV E2 protein are not essential for the development of HPV16-associated cancers.[38]

1.1.5 The viral E6/E7 oncoproteins

The viral E6/E7 oncoproteins of high-risk HPV types are the major regulators of cellular transformation and HPV-induced carcinogenesis.[21] The *E6/E7* genes are transcribed as polycistronic transcripts from the early promoter. Transcription is under control of several transcription factors binding to the URR region, including for instance AP1 and SP1.[39] Alternative splicing within the *E6/E7* ORFs produces multiple different *E6* and *E6/E7* transcripts.[40,41] Depending on the HPV type, E6 and E7 oncoproteins have a size of approximately 150 and 100 amino acids, respectively, and they do not encompass enzymatic activities. Instead, E6/E7 cause direct carcinogenesis by interacting with multiple tumor suppressor proteins and forming complexes with cellular proteins involved in the regulation of cell proliferation, senescence, apoptosis (see chapter 1.2), and genomic stability.[21]

Cervical cancer cells rely on the continuous expression of E6/E7 to maintain the malignant phenotype and are thus referred to as “oncogene-addicted”.[21] The repression of E6 in HPV-positive cervical cancer cells induces apoptosis[42,43], whereas the interference with E6/E7 expression rapidly induces cellular senescence, an irreversible proliferative arrest.[44,45]

E6 and E7 individually possess transforming potential, but their cooperative expression leads to significantly increased transforming activities.[46] The transforming properties of E6/E7 affect virtually all “hallmarks of cancer”, including uncontrolled proliferative signaling, evasion of growth suppressors, resistance to cell death, enabling of replicative immortality, induction of angiogenesis, and activation of tissue invasion and metastasis.[47,48]

One significant mechanism by which high-risk HPV E6 exerts its pro-tumorigenic effects is through the formation of a trimeric complex with p53 and the cellular ubiquitin ligase E6-associated protein (E6AP). This complex facilitates the proteolytic degradation of p53 and thus prevents the induction of apoptosis or cell cycle arrest.[49,50] Additionally, E6 targets cellular proteins containing PDZ (PSD-95/DLG/ZO-1) domains for degradation, including potential tumor suppressor proteins involved in cell polarity regulation such as Dlg, Scribble

and MAGI-1.[51] E6 also stimulates telomerase activity by upregulating human telomerase reverse transcriptase (hTERT) and thus inhibits replicative senescence.[52]

HPV E7 primarily targets the pRb protein and related pocket domain proteins such as p107 and p130, which are crucial regulators of the cell cycle.[53] E7 binds to hypophosphorylated pRb, leading to its degradation via the ubiquitin-proteasome pathway and thereby disrupting the interaction between pRb and the transcription factor E2F.[53] Consequently, the induction of cell cycle-promoting E2F target genes such as *CCNA1* (Cyclin A1) and *CCNE1* (Cyclin E1) is no longer suppressed, leading to unscheduled S-phase entry and sustained cell proliferation.[21,53] Moreover, HPV E7 can interfere with the p53-p21-DREAM pathway by sequestering hypophosphorylated p107 and p130 proteins and thus preventing the formation of the DREAM (dimerization partner, Rb-like, E2F, and multi-vulval class B) transcriptional repressor complex.[54] The inhibition of the DREAM complex promotes uncontrolled expression of cell cycle regulators and cell cycle progression.[54]

In case of uncontrolled cell proliferation, the normal cellular response would involve a p53-mediated cell cycle arrest or the induction of apoptosis. However, the E6-induced proteolytic degradation of p53 protects against pro-senescent and pro-apoptotic signals in HPV-positive cancer cells.[21]

Furthermore, E6 and E7 oncoproteins have been found to impact the cellular microRNA network[55], induce genetic instability in the host cell DNA[56], and deregulate epigenetic reprogramming.[57]

The functions of E6 and E7 and the phenotypic outcomes differ between low-risk and high-risk HPV types and most transforming activities are exclusive for high-risk HPV types, underscoring their oncogenic potential.[58] In low-risk HPV types, E6 lacks the PDZ ligand motif and exhibits weak or no interaction with p53 without inducing p53 degradation. Similarly, only high-risk E7 has the capability to facilitate the degradation of pRb.[58]

Given the pivotal role of the E6 and E7 oncoproteins in HPV-associated carcinogenesis, they represent attractive targets for therapeutic interventions in HPV-associated cancers. Various strategies targeting E6/E7 are studied, including e.g. small interfering RNAs (siRNAs), small molecule inhibitors, peptide aptamers, and immunotherapeutic approaches, which, however, have not been successfully implemented in clinical settings so far.[21]

1.1.6 Prevention of HPV infection and HPV-associated cancer

Prophylactic vaccinations have been proven to be highly effective in preventing the emergence of HPV infections, as well as HPV-related precancerous lesions, and cancers. To date, six prophylactic vaccines are licensed and provide protection against the most prevalent oncogenic high-risk HPV types.[59] These vaccines use recombinantly produced HPV L1 major structural protein, which assembles into virus-like particles (VLPs) and induces the production of neutralizing antibodies.[60,61] Bivalent HPV vaccines (Cervarix, Cecolin, Walrinvax) protect against primary infections with HPV16 and 18; quadrivalent vaccines (Gardasil, Cervavax) against HPV16, 18, 6, and 11; and the nonavalent vaccine (Gardasil 9) contains VLPs against HPV6, 11, 16, 18, 31, 33, 45, 52, and 58.[4,59]

The World Health Organization (WHO) recommends vaccination for girls aged 9–14 before they become sexually active, as well as for teenage boys and older females when feasible.[59] These recommendations aim to provide optimal protection against HPV infections and associated diseases.

However, implementing widespread vaccination programs, particularly in low- and middle-income countries, where most cervical cancers and related deaths occur, presents significant challenges, including logistical constraints and financial barriers.[62,63] To circumvent the loss of vaccine efficacy by interrupted cold chains, ongoing research attempts to generate more thermostable vaccines.[64] Moreover, next-generation vaccines are being developed that utilize a highly conserved epitope of the viral L2 minor structural protein as a basis for immunization and thus provide a broader protection to various HPV types.[63,65]

Unfortunately, prophylactic vaccinations cannot cure existing HPV infections or HPV-induced preneoplastic lesions and cancer. Thus, the development of a therapeutic vaccination against high-risk HPV types is intensely investigated (see chapter 1.1.7).[61]

As the development of cervical cancer often arises more than 10 years after the initial HPV infection, cervical cancer screenings serve as secondary prevention measurements and should be performed at regular intervals. These screenings include the Papanicolaou (Pap) test and/or HPV testing to detect precancerous cellular changes at early stages and thus reduce cervical cancer incidence and mortality.[8,59]

1.1.7 Treatment of cervical cancers

Common treatment strategies for cervical cancers, depending on the stage of cancer progression, include surgery, chemotherapy, radiotherapy or chemoradiotherapy.[28] Among these treatment options, the platinum drug Cisplatin (CDDP, see chapter 1.1.7.1) is widely

utilized and considered highly effective in cervical cancer treatment.[66] Prolonged Cisplatin treatment, however, can lead to the development of drug resistance and reduced treatment efficacy.[67] Therefore, Cisplatin is routinely combined with other chemotherapeutic agents such as Topotecan, Paclitaxel, 5-Fluorouracil and Bleomycin to improve the clinical outcome.[28] Moreover, other platinum-based drugs with lower toxicity profiles, such as Carboplatin, are being investigated as potent alternatives to Cisplatin treatment.[67]

Immunotherapies for cervical cancers are increasingly explored as promising treatment strategies.[68] One notable immunotherapeutic approach is the use of the immune checkpoint inhibitor Pembrolizumab, which targets the programmed cell death protein 1 (PD-1) on lymphocytes. This inhibitor has been approved for the treatment of recurrent and metastatic cervical tumors that are positive for programmed death ligand 1 (PD-L1).[68]

Another emerging and highly personalized approach for cervical cancer treatment is adoptive T cell therapy. This approach comprises the extraction, *ex vivo* expansion and reinfusion of tumor-infiltrating lymphocytes/T cells to efficiently target cancer cells.[68]

Moreover, therapeutic vaccinations are being developed to target HPV-positive precancerous lesions.[69] These therapeutic HPV vaccines deliver HPV-specific antigens, for instance HPV E6/E7 epitopes, to antigen-presenting cells that subsequently activate targeted cytotoxic and helper T cell responses against HPV-infected cells and hence prevent their progression to cancer.[61,69] Several types of therapeutic HPV vaccines, including live vector vaccines, protein or peptide vaccines, nucleic acid vaccines, and cell-based vaccines, are tested in clinical trials. However, no therapeutic vaccine has been licensed so far due to limited clinical success.[61] The investigation of combining different immunotherapies, as well as their integration with existing chemo- or radiotherapy approaches, aims to overcome current treatment limitations and resistance mechanisms.

1.1.7.1 Cisplatin

Cisplatin (cis-diamminedichloroplatinum(II), cis-[$Pt(NH_3)_2Cl_2$]) is a widely used chemo-therapeutic drug for the treatment of cervical cancer. It consists of a platinum core coupled to two chloride and two amine ligands. First synthesized in 1844 by M. Peyrone, it was approved for cancer therapy in 1987 and remains a conventional treatment option for cervical cancers today.[70]

After cellular import, Cisplatin chloride ions are substituted by water molecules, which results in the formation of highly reactive electrophiles.[70] This substitution occurs because intracellular chloride concentrations are lower compared to the extracellular environment.

Cisplatin then binds to the nucleophilic N7 reactive site of DNA purine bases, leading to the generation of both inter- and intrastrand DNA adducts.[71] In a dose-dependent manner, Cisplatin-induced DNA damage results in cell cycle arrest and DNA repair, cellular senescence or apoptosis, the programmed cell death pathway (see chapter 1.2).[72,73]

Severe Cisplatin-induced DNA damage primarily arises from the formation of DNA 1,2-intrastrand d(GpG) and d(ApG) crosslinks, which promote the recruitment of damage recognition proteins, including the Ataxia telangiectasia and Rad3-related (ATR) kinase.[73] ATR phosphorylates Chk1, which in turn activates p53 that plays a central role in the response to Cisplatin.[74,75] Through the transactivation of several target genes such as *p21*$^{Waf1/Cip1}$, *gadd45a*, or pro-apoptotic *bax*, p53 facilitates cell cycle arrest, allowing the cells to repair the DNA lesions or undergo apoptosis.[76,77] Furthermore, p53 induces the expression of specific death receptors, including Fas receptor (FasR) and death receptor 5 (DR5).[78] Hence, Cisplatin treatment can promote apoptosis induction through both the intrinsic and extrinsic apoptosis pathways.[79] Additionally, Cisplatin treatment activates members of the mitogen-activated protein kinase (MAPK) pathway, including extracellular signal-regulated kinases (ERK), c-Jun N-terminal kinases (JNKs), and p38 kinases, which can contribute to the Cisplatin-induced DNA damage response or cell death.[70,73,80]

Cisplatin and other conventional chemotherapeutic drugs lack the selectivity for targeting tumor cells, resulting in damage to healthy proliferating cells as well. Furthermore, Cisplatin-induced nephrotoxicity and the development of Cisplatin resistance constitute major obstacles of cervical cancer therapy.[73,81] Chemoresistance, characterized by an inability to induce apoptosis in tumor cells at clinically feasible drug doses, critically worsens patient survival and constitutes a main cause for tumor recurrence.[73] Cisplatin resistance can be intrinsic or acquired after extended treatment, and Cisplatin-resistant tumor cells often exhibit cross-resistance to other platinum drugs and several unrelated anticancer treatments.[73,82]

Resistance mechanisms to Cisplatin include, for instance, decreased drug uptake or increased drug efflux, drug inactivation and sequestration in the cytoplasm by nucleophilic scavenger proteins (e.g. glutathione (GSH) or metallothioneins), as well as enhanced DNA damage repair or defects in the pro-apoptotic signaling cascade.[83] Notably, it has been shown that only approximately 1% of intracellular Cisplatin binds to nuclear DNA and forms DNA adducts.[84,85] Concurrently, most of the drug is bound and inactivated by cytosolic proteins and thiol-containing molecules or gets sequestered in subcellular organelles such as lysosomes, Golgi and vesicles.[84,85] Importantly, chemoresistance in tumor cells is a complex phenomenon characterized by the interplay of various cooperating mechanisms.

In cervical cancer cells, a key therapeutic resistance mechanism to pro-apoptotic Cisplatin treatment is the inactivation of p53 via E6/E6AP-dependent degradation.[49,86] Moreover, E6/E7 mediate the repression of the pro-apoptotic tumor suppressor Dickkopf-1 (Dkk1), which is a critical determinant for the response of cervical cancer cells to Cisplatin treatment.[87] Investigating the molecular mechanisms, particularly in HPV-positive cancer cells, in response to Cisplatin treatment holds promise for overcoming chemoresistance and improving current treatment strategies.

1.2 Cell death

Cell death is a crucial biological process that is essential for the proper functioning and development of living organisms. In general, cell death can occur through regulated pathways, characterized by structured molecular signaling cascades, or through accidental mechanisms, which occur spontaneously and uncontrolled.[88–90] Over time, various types of cell death pathways have been described, including apoptosis, necrosis, pyroptosis, ferroptosis, entosis, lysosome-dependent cell death, and autophagy-dependent cell death.[90] Importantly, these cell death pathways interact and cross-regulate each other, contributing to the complexity of the overall cell death process.[89,90]

1.2.1 Apoptosis

Apoptosis, a form of programmed cell death, is evolutionary conserved across species and plays a key role in health and disease.[91] Apoptotic cell death is essential during development and for cellular homeostasis, as well as for the clearing of infected cells and cells with irreparable DNA damage.[92] Consequently, deregulation of the apoptotic process can result in severe pathological consequences.[92]

Tumor therapies preferentially induce apoptosis, as it, in contrast to necrosis, does not induce an inflammatory response.[89,92,93] However, cancer cells often evade apoptosis, and upregulate anti-apoptotic proteins, including B-cell lymphoma 2 (BCL-2), BCL-xL, or inhibitor of apoptosis protein (IAP) to support survival.[48]

Apoptosis is characterized by distinct morphological features, including cell and nuclei shrinkage, chromatin condensation, membrane blebbing, and the formation of apoptotic bodies that are subsequently cleared through phagocytosis.[94] Biochemical changes during apoptosis involve the translocation of phosphatidylserine from the inner to outer layer of the cell membrane, DNA fragmentation and caspase activation.[94] Caspases, the major executors of apoptosis signaling, are cysteine-aspartic proteases that cleave a variety of apoptotic

effector proteins, leading to cell death.[95] Caspases are initially expressed as catalytically inactive zymogens and become activated in response to apoptotic stimuli through sequential proteolytic cleavage. During apoptosis, caspases are functionally distinguished as initiator caspases (Caspase 8, 9, 10) and executioner or effector caspases (Caspase 3, 6, 7).[95]

Apoptosis can be induced through the extrinsic and the intrinsic pathway, depending on the apoptotic stimulus (Figure 3).[79,92] The extrinsic or death receptor pathway is activated when extracellular ligands bind to death receptors, such as Fas ligand (FasL) binding to Fas receptor, tumor necrosis factor alpha (TNFα) binding to TNF receptor 1/2 (TNFR1/2), or TNF-related apoptosis-inducing ligand (TRAIL) binding to DR4 or DR5.[96–99] Subsequently, the death receptors oligomerize, recruit adaptor proteins to their cytoplasmic domain (e.g. FADD to Fas/FasR) and induce the formation of a death-inducing signaling complex (DISC) that allows the activation of initiator Caspases 8 and 10.[100] Procaspase 8 and 10 are then activated through autocatalytic cleavage and either directly cleave effector Caspases 3 and 7 or activate the intrinsic apoptosis pathway by cleaving the BH3 interacting domain death agonist (BID) protein, which belongs to the BCL-2 protein family (Figure 3).[101,102]

The intrinsic or mitochondrial pathway is primarily induced via DNA damage, oxidative stress, or nutrient withdrawal.[92] This pathway involves the induction of mitochondrial outer membrane permeabilization (MOMP) and the release of Cytochrome c (Cyt c) into the cytosol which is finely regulated by the expression and interactions of members of the BCL-2 protein family (Figure 3).[103,104] Proteins of the BCL-2 family are subdivided in the pro-apoptotic pore-formers BAX and BAK, pro-apoptotic BCL-2 homology 3 (BH3)-only proteins (e.g. BAD, BID, BIM) and anti-apoptotic factors (e.g. BCL-2 or BCL-xL).[105] The ratio of pro-apoptotic BAX and its anti-apoptotic opponent BCL-2 decisively affects the fate of the cell and the progression of apoptosis.[105] Cellular stressors or DNA damaging agents such as Cisplatin can activate the p53-dependent expression of *bax* or induce BCL-2 cleavage.[77,106] Activation of BAX and BAK allows their oligomerization and the formation of pores in the mitochondrial outer membrane, resulting in MOMP and the release of the pro-apoptotic factors Cyt c, second mitochondria-derived activator of caspase (Smac), Omi/HTR2 and apoptosis inducing factor (AIF) from the mitochondrial intermembrane region into the cytosol.[107–109] Cytosolic Cyt c oligomerizes with apoptotic protease activating factor 1 (APAF1), dATP and Procaspase 9 to form the apoptosome, which enables autoproteolytic cleavage and activation of Caspase 9. This activation subsequently leads to the cleavage of downstream Caspases 3, 6 and 7.[110–112] Smac and Omi/HTR2 interfere with IAPs and prevent their negative regulation of caspase activation.[113,114]

Consequently, both extrinsic and intrinsic apoptosis pathways eventually activate the effector Caspases 3, 6, and 7.[95,115] Among a variety of substrates, these caspases then cleave and

inactivate the poly (ADP-ribose) polymerase (PARP) protein, which is involved in DNA repair and transcriptional regulation, and thus promote DNA fragmentation.[115,116] Accordingly, cleavage of caspases and PARP (resulting in 89 and 24 kDa fragments) are widely recognized as reliable markers for the induction of apoptosis.[111,116,117]

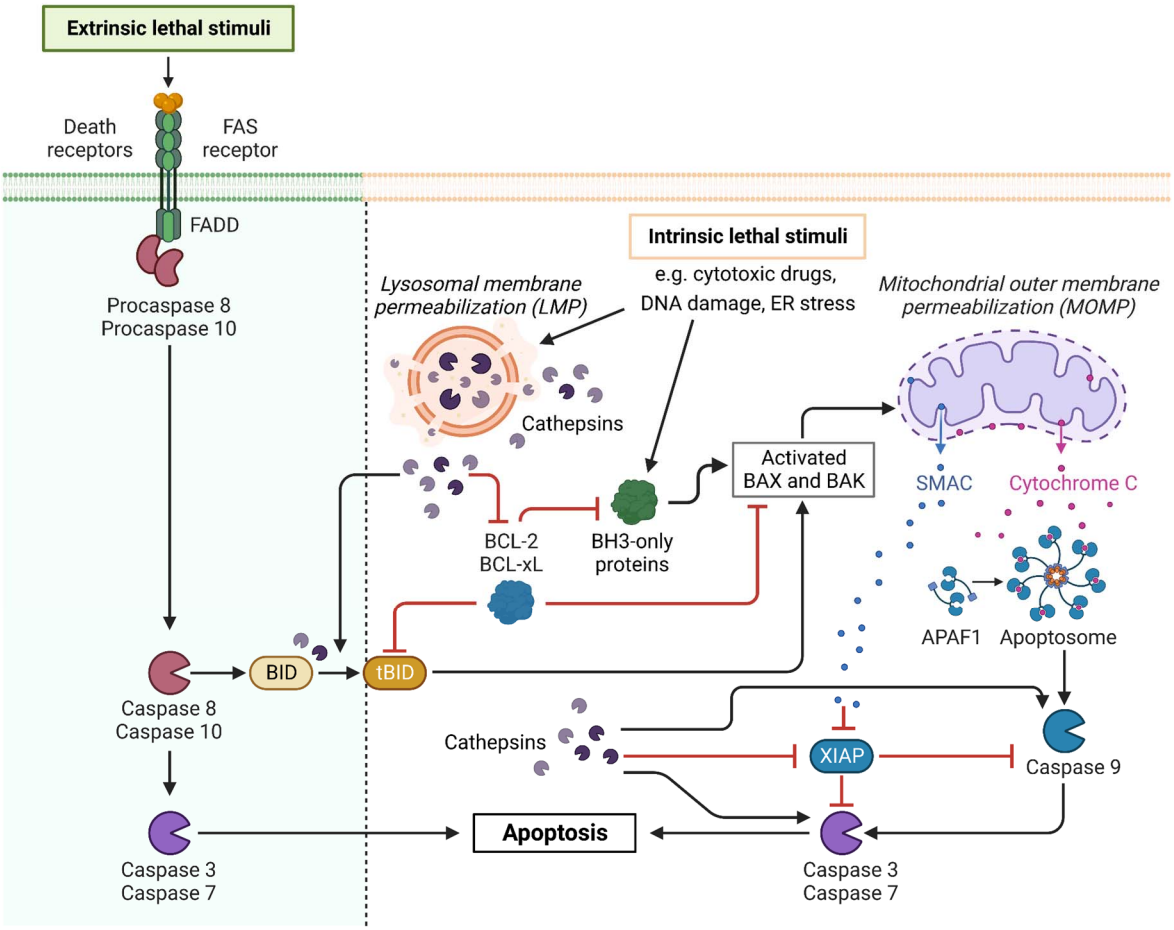

Figure 3. Extrinsic and intrinsic apoptosis pathway.

The extrinsic apoptosis pathway is induced by death ligands, like FasL, binding to death receptors, such as Fas receptor, leading to the formation of an intracellular signaling complex with death receptor adaptor proteins (e.g. FADD). This complex activates Procaspases 8 and 10, which in turn activate executioner Caspases 3 and 7, and trigger apoptosis. The intrinsic apoptosis pathway is induced by the activation of pro-apoptotic BH3-only proteins and the inhibition of anti-apoptotic BCL-2 proteins, for instance by DNA damage or cytotoxic drugs. This pathway involves the recruitment of pore forming proteins BAX and BAK to the mitochondria and the induction of MOMP, leading to the release of Cytochrome c and Smac. The apoptosome, composed of APAF1, Cytochrome c, and Caspase 9, activates Caspase 9, allowing subsequent activation of Caspases 3 and 7, and apoptosis induction. Cytosolic Smac can inhibit X-linked inhibitor of apoptosis (XIAP), which otherwise interferes with the activation of Caspase 3 and 7. The extrinsic and intrinsic apoptosis pathways are interconnected through the Caspase 8-mediated cleavage of BID. The generated truncated BID (tBID) facilitates the recruitment of BAX and BAK to the mitochondrial membrane. Additionally, certain pro-apoptotic stresses can also induce lysosomal membrane permeabilization and the release of lysosomal proteases, such as cathepsins, into the cytosol. Cathepsins can stimulate the apoptosis cascade by cleaving BID, BCL-2 homologues, XIAP or procaspases.

1.2.2 Role of BID in apoptosis signaling

BID plays a crucial role in the apoptosis signaling, connecting the extrinsic, death-receptor-initiated apoptosis and the intrinsic, mitochondrial apoptosis pathways.[101,118,119] As a member of the BH3-only family, BID interacts with and inhibits anti-apoptotic BCL-2 family members.[105] Of note, *bid* expression is transcriptionally regulated by p53 and is induced in response to DNA damage.[120]

During apoptosis, BID gets activated, primarily through cleavage by Caspase 8 (Figure 3).[101,121] The truncated BID (tBID) protein translocates to and inserts into the mitochondrial membrane, where it recruits inactive, cytosolic BAX.[107,122,123] Subsequently, tBID triggers a conformational change in BAX, allowing its oligomerization and its insertion into the outer mitochondrial membrane, resulting in the release of Cyt c.[107,122,123] Recently, tBID was shown to promote MOMP also independently of BAX and BAK.[124] In addition, BID is targeted and cleaved by other intracellular proteases in response to cellular stress, for instance by Caspases 10, 2 and 3, granzymes, calpains or cathepsins that are leaking into the cytosol after lysosomal damage.[125–131] Interestingly, full-length BID may also translocate to mitochondria and exhibit pro-apoptotic functions without undergoing proteolytic activation, for instance during anoikis, a form of cell death triggered by the disruption of cell-matrix-interactions.[132]

In cervical cancer cells, BID is essential for Fas/CD95 and TRAIL-induced apoptosis but is also involved in DNA damage-induced apoptosis by Etoposide, Oxaliplatin and Doxorubicin.[133] Therefore, abnormal expression or activation of BID within cancer cells can affect the apoptosis signaling and subsequently influence the efficacy of chemotherapy.

1.3 Lysosome biology and lysosomal functions in cancer cells

Lysosomes are membrane-bound organelles that contain more than 60 different hydrolytic enzymes (e.g. proteases, lipases, glycosidases, phosphatases, nucleases, and sulfatases) with the ability to break down diverse biomolecules including proteins, lipids, carbohydrates, and nucleic acids.[134] The acidic lysosomal lumen with pH 4.5–5 ensures optimal enzyme activity and is generated by the ATP-dependent activity of the vacuolar H^+ ATPase (V-ATPase) proton pump on the lysosomal transmembrane.[135,136]

Lysosomes are essential for the maintenance of cellular homeostasis and the catabolism of cargo from endo- or phagocytosis, as well as for the degradation of damaged proteins and organelles during autophagy (see chapter 1.4).[134] Furthermore, lysosomes are important signaling hubs, for instance for the nutrient sensing mechanistic target of rapamycin (mTOR)

complex 1 (mTORC1) and participate in cell growth and energy metabolism.[137] Additionally, lysosomes are involved in plasma membrane repair, cellular stress responses, several cell death pathways, and in the defense against invading pathogens.[134]

Lysosomal enzymes are synthesized as precursor proteins at the rough endoplasmic reticulum (ER) and undergo a complex trafficking and sorting process through the Golgi apparatus, the *trans*-Golgi network and transport vesicles to reach the lysosomes (Figure 4).[138] This trafficking involves the mannose-6-phosphate (M6P) pathway.[138] Mechanistically, M6P residues are added to the lysosomal precursor enzymes in the Golgi, involving the catalytic activities of N-acetylglucosaminyl-1-phosphotransferase (GNPTAB) and uncovering enzyme (UCE).[139–141] The M6P-tagged precursor enzymes are recognized by M6P receptors (MPR), either by the cation-dependent CD-MPR (46 kDa) or the cation-independent CI-MPR/IGF2R (300 kDa). The MPRs are located in the *trans*-Golgi network and in endosomes and ensure the vesicular transport to the lysosomes.[138,142] Both MPRs have distinct and shared M6P-containing targets and are essential for the complete targeting of all lysosomal enzymes.[143] Several lysosomal proteins are proteolytically cleaved in the acidic environment of the endosomes, and are then processed into their mature, active forms within the lysosomes.[144]

Lysosomal dysfunctions caused by genetic mutations, reduced lysosomal enzyme activities, impaired acidification or defective lysosomal membrane integrity are linked to several malignancies, including cancer (see chapter 1.3.1-1.3.2).[145–147] Therefore, lysosomes are increasingly investigated as therapeutic targets in cancer cells.[147–150]

1.3.1 Cathepsins

Cathepsins are a group of important lysosomal proteases that belong to the papain family.[151] Based on their catalytic sites, cathepsins are classified as serine (Cathepsins A and G), cysteine (Cathepsins B, C, F, H, K, L, O, S, V, X, W) and aspartic (Cathepsins D and E) proteases.[151,152] Among these, Cathepsin B (CTSB), Cathepsin L (CTSL) and Cathepsin D (CTSD) are the most abundant lysosomal proteases.[151]

Cathepsins are synthesized as immature, inactive proenzymes, which are subsequently sorted to the lysosomes via the M6P pathway. Within the lysosomes, they undergo processing to their mature, active forms (Figure 4).[138] The final activation of cathepsins in the lysosomes is either an auto-catalytic process (e.g. for CTSB, H, L, S, K) or trans-catalytic with the assistance of other lysosomal proteases (e.g. for CTSC, D, X).[151]

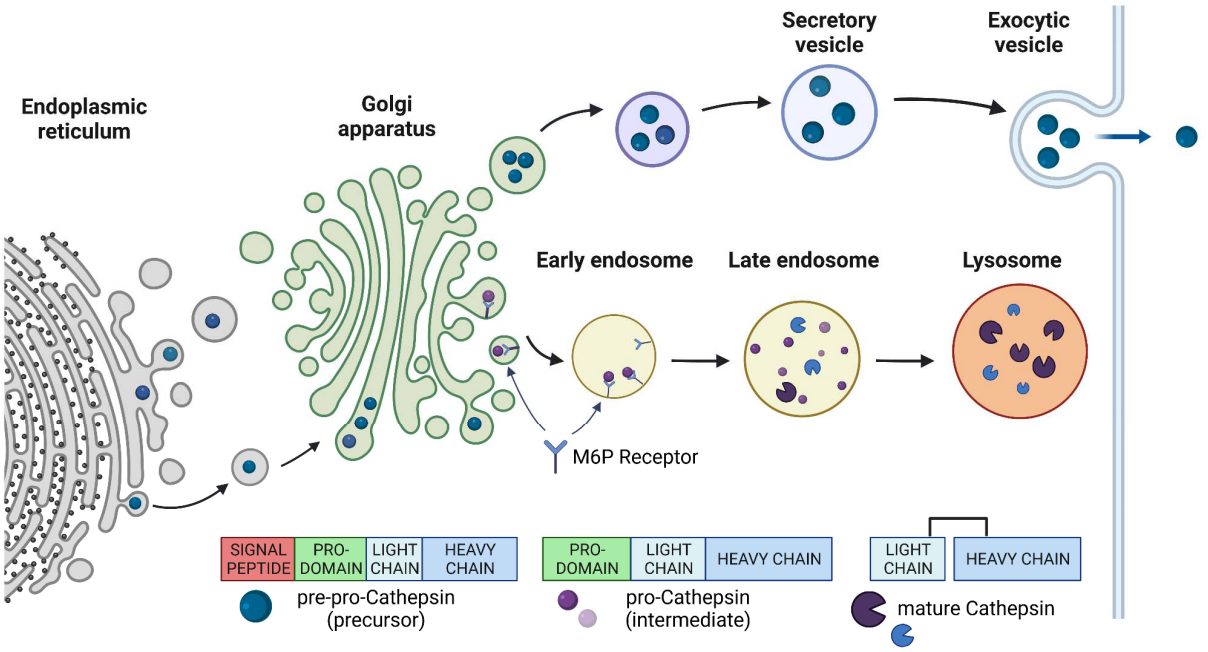

Figure 4. Transport and maturation process of cathepsins.

Cathepsins are synthesized in the endoplasmic reticulum as inactive pre-pro-cathepsins, consisting of signal peptide, prodomain, light chain, and heavy chain. Removal of the signal peptide generates pro-cathepsin intermediates, which are tagged with mannose-6-phosphate (M6P) residues and bind to M6P receptors in the *trans*-Golgi network. Pro-cathepsins are then transported to early and late endosomes, dissociate from the M6P receptor, and are processed in the acidic environment of the endosomes. In the lysosome, cathepsins are cleaved, either auto- or trans-catalytically, into their active, double-chain form. Precursor cathepsins can also be released via secretory vesicles into the extracellular space.

Alterations in the lysosomal pH can critically influence the activation and function of cathepsins. Interestingly, even though cathepsins are most active at lysosomal pH of 4–5, several cathepsins have been shown to exert their proteolytic activity also at higher pH, allowing them to function also outside of the endo-/lysosomal compartments.[151,153,154] In addition to the pH-dependent regulation, cathepsin activities are also controlled by endogenous protein inhibitors such as stefins, cystatins, and kininogens. These inhibitors reversibly regulate cathepsin activities, particularly when small amounts of lysosomal enzymes leak into the cytosol.[151,152]

Lysosomal cathepsins are crucially involved in various cellular processes, including protein turnover, autophagy, and cellular homeostasis. Additionally, depending on the cathepsin type and the cellular context, cathepsins can exhibit diverse physiological and pathological functions when they localize to different cellular compartments such as the nucleus, mitochondria, or cytoplasm, or when they are secreted into the extracellular space.[151,152] For instance, secreted cathepsins are involved in the degradation of extracellular matrix (ECM) components, which facilitates tumor invasion and metastasis into surrounding tissues.[155]

Intracellular cathepsins, on the other hand, can modulate immune responses and antigen processing, mediate inflammatory responses via inflammasome activation, regulate chemokine activity, promote angiogenesis, and participate in apoptosis signaling.[151] Thus, abnormal cathepsin localization, expression, and activity levels have been linked to pathological changes and contribute, among others, to cancer progression.[151,155,156]

1.3.2 The role of lysosomes and cathepsins in cell death

Lysosomal stress and lysosomal membrane permeabilization (LMP) can trigger the induction of several cell death pathways, including apoptosis, lysosome dependent cell death (LDCD), necrosis, pyroptosis, and ferroptosis.[148,150] Upon LMP, lysosomal content, including hydrolytic enzymes, is released into the cytosol. The severity of lysosomal rupture determines the cellular fate.[148] While minor LMP can be compensated by endolysosomal damage-response mechanisms, moderate LMP leads to an increased release of lysosomal enzymes and the induction of controlled cell death pathways.[150,157] Complete lysosome rupture results in uncontrolled necrosis.[148]

Apoptotic stimuli by certain chemotherapeutic drugs can induce LMP, leading to the release of cathepsins into the cytoplasm.[148,150,158] The released cytosolic cathepsins, for instance Cathepsins B, D or L, can trigger and enhance pro-apoptotic signaling by cleaving procaspases, BID, or BCL-2 homologues, and thereby promoting the release of mitochondrial Cyt c (Figure 3).[125,126,158–160]

As cathepsins released during LMP can facilitate both caspase-dependent apoptosis as well as caspase-independent LDCD or necrosis, their role in cell death regulation is complex and critically depends on the cellular context, the types of cathepsins involved and the LMP-inducing stimulus.[158–161]

1.4 Autophagy

Autophagy is a cellular process that is essential for maintaining cellular homeostasis by degrading and recycling unnecessary or damaged proteins and organelles through the lysosomal pathway.[162] The recycled biomolecules can be used for metabolic processes and new biosynthesis.[162] Various stress conditions, including nutrient starvation, oxidative and heat stress, increase cellular autophagy levels to allow adaptation and survival.[163] Thereby, the regulation of mTOR and AMP activated protein kinase (AMPK) signaling is critical, as active mTORC1 inhibits early steps of autophagy, while active AMPK promotes autophagy.[164] Multiple forms of autophagy that are regulated by distinct molecular

mechanisms can be distinguished, including for instance macroautophagy, microautophagy, and chaperone-mediated autophagy.[162]

Macroautophagy, which will be referred to as ‘autophagy’ hereafter, is characterized by the formation of a double-membrane structure, the autophagosome, which engulfs cellular contents. Subsequently, the autophagosome fuses with the lysosome to degrade its cargo.[163] Mechanistically, autophagy is characterized by sequential processes of (step i) initiation, (step ii) nucleation, (step iii) phagophore expansion and autophagosome maturation, (step iv) autophagosome-lysosome fusion, (step v) cargo degradation and amino acid/peptide generation.[163,165] During the entire process, autophagy-related genes (ATGs) tightly control the proceeding of the distinct autophagy steps.[165]

Upon mTORC1 inactivation, the Unc-51-like kinase 1 (ULK1) complex is activated (step i) and recruits components of the class III phosphatidylinositol 3-kinase (PI3K) complex to the phagophore assembly site. The class III PI3K complex then induces phosphatidylinositol 3-phosphate (PI3P) synthesis at the ER for the formation of the phagophore membrane (step ii). Subsequently, two ubiquitin-like conjugation systems, the ATG12-ATG5-ATG16 complex and the ATG8 system (also known as microtubule-associated light chain 3, LC3) control the elongation of the phagophore (step iii). During autophagosome maturation, LC3 gets cleaved by ATG4, generating LC3-I, and is conjugated to phosphatidylethanolamine in the phagophore membrane, forming LC3-II. LC3-II then sequesters autophagic cargo by recognizing autophagic receptors, for instance p62/SQSTM1, before the autophagosomal membrane is sealed and fused with lysosomes to autophagolysosomes (step iv). Lysosomal hydrolases degrade the autophagic cargo and the recovered amino acids, fatty acids etc. are released into the cytosol and recycled for novel biosynthesis (step v).[163,165]

In the context of cancer, autophagy can exert both pro- and antitumorigenic functions, depending on the cellular context.[166,167] During the early stages of cancer, autophagy can suppress tumorigenesis. In established cancers, however, autophagy facilitates survival of tumor cells in response to metabolic or therapeutic stress.[166,167] Given the significance of autophagy in cancer, there is increasing interest in targeting and modulating autophagy as a therapeutic strategy for cancer patients. Studies have shown promising synergistic effects when combining autophagy modulation with chemotherapeutic agents in different types of cancer.[166,168] Autophagy inhibition alleviates tumor growth and sensitizes cancer cells to cytotoxic treatment.[168] However, the dual role of autophagy also implies therapeutic limitations that need to be carefully considered and evaluated. Thus, investigations of autophagy modulation in combination with chemotherapeutic agents provide valuable new insights for cancer treatment strategies.[166,168]

1.5 Tumor hypoxia

A main feature of the tumor microenvironment in solid cancers is the presence of tumor hypoxia.[169–171] Hypoxic tumor subregions are characterized by low oxygen partial pressure ranging from < 0.1 mm Hg (anoxia) to 15 mm Hg, which corresponds to an oxygen concentration below 2%.[171–173]

It is important to note that most *in vitro* research conducted under standard cell culture conditions at 20–21% O_2 ("normoxia") does not accurately reflect the physiological oxygen levels in organs. For example, in the healthy uterine cervix, the median oxygen levels range from 5–6% ("physoxia"), while cervical cancers exhibit a median oxygen concentration of only 1.2%.[173]

Two major forms of tumor hypoxia are distinguished: chronic hypoxia and cycling hypoxia (cycH) (Figure 5).[169] Chronic hypoxia arises after prolonged oxygen deficit lasting multiple hours to days. Due to diffusion limitations, cancer cells that are not in spatial proximity to blood vessels (distance > 70 µm) receive insufficient nutrients and oxygen.[169,170] Cycling hypoxia, on the other hand, results from perfusion limitations of poorly structured, and often functionally impaired tumor microvessels.[169,174,175] Periodic occlusions of these vessels, for instance by blood cell aggregates, followed by subsequent reperfusions, expose nearby tumor cells to repetitive cycles of hypoxia (H) and reoxygenation (R) (H-R cycles). The H-R cycles vary in duration and frequency and can range from minutes to days.[175,176]

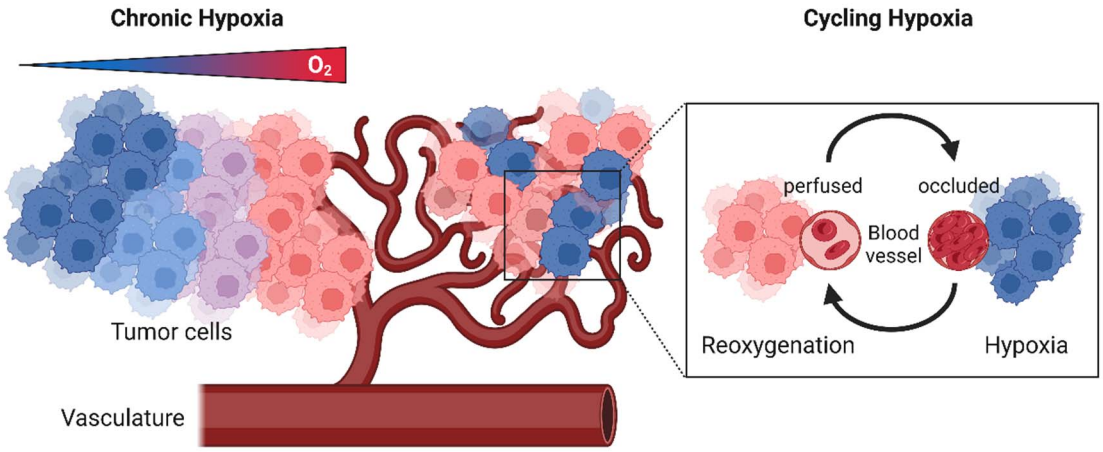

Figure 5. Chronic and cycling hypoxia are two types of tumor hypoxia.
Left: Chronic hypoxia is caused by diffusion limitations. Tumor cells with enlarged distances (> 70 µm) from blood vessels receive insufficient oxygen and become hypoxic. Right: Cycling hypoxia results from repetitive perfusion limitations of blood vessels, e.g. by red blood cell aggregates. Nearby tumor cells are exposed to fluctuating cycles of hypoxia and reoxygenation. Red: oxygenated tumor cells, blue: hypoxic tumor cells.

In response to limited oxygen supply, tumor cells undergo various adaptive changes in cellular processes. These adaptations include metabolic reprogramming and a switch from oxygen-dependent oxidative phosphorylation to increased anaerobic glycolysis[177], the stimulation of angiogenesis[178], as well as increased invasion and metastasis[179]. Moreover, hypoxia increases genomic instability[180], downregulates DNA repair mechanisms[180], suppresses apoptosis[181] and senescence[182], and contributes to an immunosuppressive tumor microenvironment.[183] These adaptations ultimately contribute to the selection of a more aggressive and therapy-resistant tumor cell subpopulation.

1.5.1 Hypoxia-induced alterations of cellular pathways

1.5.1.1 Hypoxia-inducible factors (HIFs)

HIFs are master regulators of many hypoxia-induced changes in gene expression. They are heterodimeric transcription factors composed of a stably expressed HIF-β subunit and an oxygen-regulated α subunit, HIF-1α, HIF-2α, or HIF-3α.[184] The genes encoding HIF-α subunits are constantly transcribed and translated but are stabilized only under hypoxic conditions.[185] Under normoxia, prolyl hydroxylases (PHDs) and the von-Hippel-Lindau (VHL) tumor suppressor protein, that function as E3 ubiquitin ligase complex, facilitate hydroxylation and subsequent ubiquitination and proteolytic degradation of HIF-α subunits, respectively.[184–186] In addition, factor-inhibiting HIF-1 (FIH1) hydroxylates an asparagine residue of HIF-1, hindering the recruitment of transcriptional coactivators.[187,188]

Under hypoxic conditions, the lack of oxygen and cellular metabolites, particularly iron and α-ketoglutarate, impede the activity of FIH1 and PHD and prevent HIF-α hydroxylation and degradation.[186,188] Consequently, HIF-α and HIF-β subunits dimerize and translocate into the nucleus, where they form a complex with the coactivators CREB-binding protein (CBP) and p300.[185] The HIF complexes then bind to hypoxia responsive elements (HREs) with the consensus sequence 5′ RCGTG 3′ and induce the transcription of target genes.[189] HIFs regulate the expression of more than a hundred target genes that are involved in glucose transport, metabolism, and angiogenesis, among others.[185,190] Under certain circumstances, HIF-α expression and stabilization can occur also via oxygen-independent mechanisms, for instance by oncogenic signaling, genetic alterations of the *VHL* gene or by mutations in the Wnt/β-catenin signaling pathway.[185]

Among the HIF-α subunits, HIF-1α and HIF-2α are the main mediators of the HIF transcriptional program. Despite their structural and functional similarities, HIF-1α and HIF-2α can exhibit distinct but complementary transcriptional regulations upon binding to the same HRE.[191] The divergence in target gene regulation can be attributed to differences in time- and

oxygen-dependent stabilization kinetics as well as interactions with transcription factors and coregulators.[192,193] While HIF-1α predominantly governs metabolic reprogramming in response to acute hypoxic stress, HIF-2α is stabilized at higher relative O_2 concentrations (~ 5%) and rather influences extracellular remodeling and angiogenesis.[191,194]

1.5.1.2 N-myc downstream regulated gene 1 (NDRG1)

NDRG1 is ubiquitously induced in response to cellular stress conditions such as hypoxia, DNA damage, hormone responses, cellular growth arrest, and cellular differentiation in various human tissues and cancers.[195] NDRG1 is a highly conserved, predominantly cytosolic protein with a molecular weight of 43 kDa. The protein belongs to the α/β hydrolase superfamily, however, it does not possess hydrolytic catalytic activity.[196]

The expression of NDRG1 is regulated at the transcriptional, post-transcriptional, and translational level.[195,197] Multiple effectors are known to influence intracellular NDRG1 levels, including e.g. N-myc and c-myc.[198] Hypoxic upregulation of NDRG1 expression can be induced by the HIF-1 complex binding to one of the three HREs upstream of the NDRG1 promoter or by HIF-independent mechanisms, for instance via EGR1 or AP1.[199–202] Moreover, other factors including p53, PTEN, iron depletion and heavy metal ions can promote transcriptional upregulation of NDRG1.[203–206] Post-translationally, NDRG1 is phosphorylated at multiple serine and threonine residues by serum/glucocorticoid regulated kinase 1 (SGK1), which primes for phosphorylation by glycogen synthase kinase (GSK-3β).[207,208] Additionally, NDRG1 has potential phosphorylation sites for calmodulin kinase 2, protein kinase A, and protein kinase C.[209,210] In addition to its predominantly cytoplasmic localization, NDRG1 can also localize to the nucleus, the plasma membrane and adherens junctions.[197] Phosphorylation, localization, and direct binding of effector molecules determine the function of NDRG1; however, its specific mechanism of action remains elusive.[211–213]

The role of NDRG1 in different tumors is strongly dependent on the specific cancer type. In brain, breast, pancreas, colorectal, and prostate cancers, NDRG1 possesses anti-oncogenic functions and acts as metastasis suppressor.[214] Anti-oncogenic NDRG1 activity is exerted by interference with various signaling pathways including the nuclear factor kappa-light-chain-enhancer of activated B cells (NF-κB) pathway, the PI3K/AKT/mTOR signaling, the Ras/Raf/MEK/ERK pathway, the transforming growth factor-β (TGF-β) network as well as Wnt signaling.[215]

In contrast, in liver, kidney, ovarian, and cervical cancers, NDRG1 expression has been linked to poor prognosis, increased invasion and tumor growth *in vitro* and *in vivo*.[216–219]

In cervical cancer, elevated levels of NDRG1 have been associated with enhanced angiogenesis and resistance to chemoradiotherapy.[217,220] Given the multitude of cancer cell type-specific functions, further in-depth research on NDRG1 in cervical cancer is required.

1.5.2 Hypoxia and cancer therapy

Tumor hypoxia critically influences tumor development, angiogenesis, and metastasis. Furthermore, hypoxic tumors exhibit increased resistance to chemo- and radiotherapy and are associated with poor clinical prognosis.[169,171] The hypoxia-linked therapy resistance can be attributed to several factors. Firstly, many chemotherapeutic drugs require molecular oxygen for their efficacy, making them less effective under hypoxic conditions.[221] Secondly, inadequate tumor vascularization can hinder the proper delivery of drugs to hypoxic cells and the upregulation of drug efflux transporters under hypoxia further diminishes intracellular concentrations as well as the effectiveness of chemotherapeutic agents.[221] Thirdly, due to their low proliferation rates, cells under hypoxia are less susceptible to chemotherapeutic drugs that commonly target highly proliferative cells.[221] Furthermore, hypoxia has a radioprotective effect and prevents radiotherapy-induced DNA damage, as the permanent fixation of DNA lesions is dependent on oxygen. Consequently, cells under hypoxia require 2.5–3 times higher radiation doses compared to cells under normoxia to achieve comparable therapeutic effects.[222]

The challenges associated with treating hypoxic tumor cells have led to the development of hypoxia-activated prodrugs and small molecule inhibitors specifically targeting hypoxia-induced molecular targets.[223] These approaches aim to overcome the limitations posed by tumor hypoxia and improve the efficacy of cancer treatments.

1.5.3 Hypoxia in HPV-positive cancers

In cervical cancers with a median oxygen concentration of 1.2%, tumor hypoxia is a significant challenge for tumor therapy and negatively affects patient prognosis.[169] In addition to general cellular adaptations to a hypoxic tumor environment, HPV-positive cancer cells exposed to hypoxia induce unique alterations regarding the virus/host cell crosstalk.[224,225]

Under chronic hypoxia (1% O_2, 24 h), HPV-positive cancer cells strongly repress the viral *E6/E7* oncogene expression, a phenomenon that can be reversed through reoxygenation.[225] Hypoxic repression of *E6/E7* expression requires the hypoxia-induced activation of the PI3K/AKT signaling pathway (Figure 6).[226] The upstream activators of AKT, namely PI3K and mTORC2, phosphorylate both isoforms of AKT, AKT1 and AKT2. Consequently,

phosphorylated AKT mediates the repression of HPV *E6/E7* oncogenes under hypoxic conditions, which occurs, at least in part, at the transcriptional level.[226] Of note, unphysiologically high medium glucose concentrations (4.5 g/L) can counteract the downregulation of HPV E6/E7 under chronic hypoxia.[225]

In contrast to experimental silencing of E6/E7 under normoxia, e.g. by RNA interference (RNAi), the repression of E6/E7 under chronic hypoxia does not lead to a reconstitution of p53 and does not induce cellular senescence.[225] Instead, the cells enter a state of dormancy characterized by a temporary growth arrest, which can be overcome by reoxygenation.[225] These observed phenotypic differences can be attributed, in part, to impaired mTORC1 signaling under chronic hypoxia. Intact mTORC1 signaling is crucial for the "geroconversion" of transiently arrested cells into irreversibly arrested senescent cells.[182,227] Thus, hypoxic inhibition of mTORC1 signaling allows HPV-positive cancer cells to evade efficient senescence induction and provides resistance to pro-senescent chemotherapies (Figure 6).[224,225]

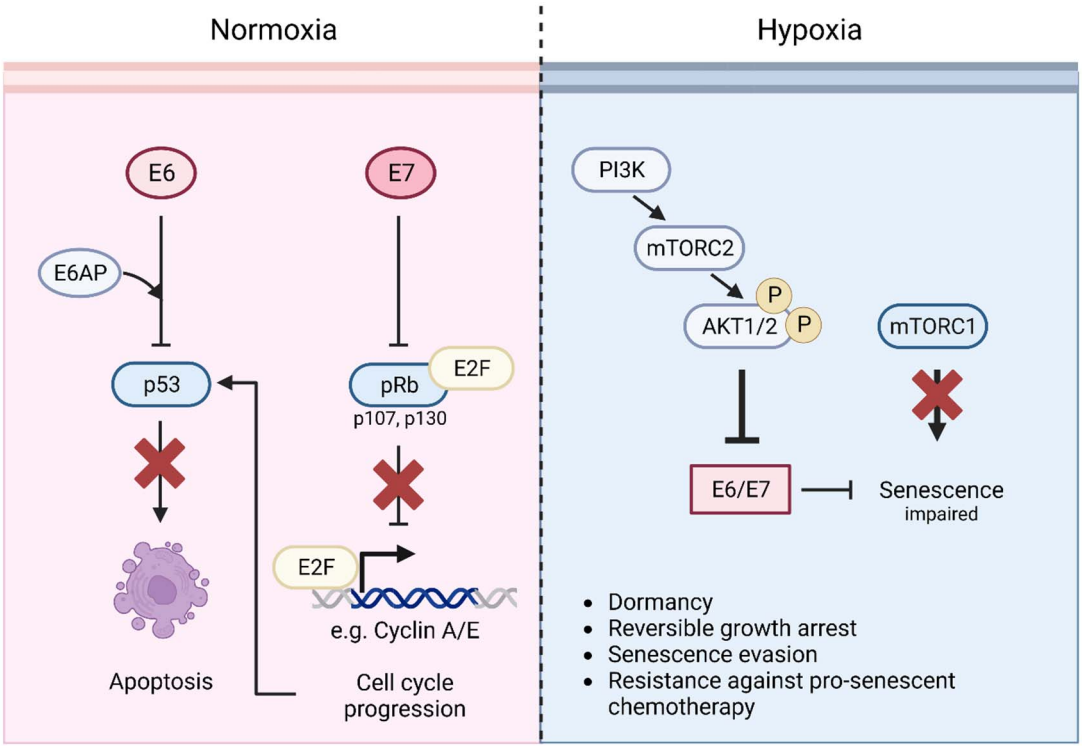

Figure 6. Virus/host cell crosstalk in HPV-positive cancer cells under normoxia and chronic hypoxia.
Under normoxia (21% O_2), continuous expression of HPV E6/E7 oncoproteins drives the malignant phenotype of HPV-positive cervical cancer cells. HPV E7 targets pRb and related pocket proteins p107 and p130, leading to their proteasomal degradation. Consequently, E2F transcription factors are released and activate the transcription of cell cycle promoting genes, such as Cyclin A/E, allowing sustained cell cycle progression. Simultaneously, HPV E6, in combination with E6-associated protein (E6AP), induces the proteasomal degradation of p53 and thereby protects against pro-apoptotic stimuli. In contrast, under chronic hypoxia (1% O_2), the *E6/E7* oncogene expression is repressed via the PI3K/mTORC2/AKT pathway. Upon E6/E7 repression, hypoxic cells induce a dormant state and reversibly inhibit cell proliferation. Hypoxic impairment of mTORC1 signaling allows HPV-positive cervical cancer cells to evade senescence induction.

The hypoxia-induced changes in HPV-positive cancer cells thus could have a substantial impact on their clinical behavior and particularly on their response to specific antiviral approaches. In addition to the general immunosuppressive effects of hypoxia, the repression of E6/E7 oncoproteins could pose a challenge for immunotherapeutic approaches targeting E6/E7-derived peptides as the presentation of viral antigens on the cellular surface might be impeded.[21,224] Moreover, the hypoxia-mediated suppression of viral oncogenes could protect hypoxic HPV-positive cancer cells from potential E6/E7 inhibitors. Furthermore, the reversible growth arrest of cervical cancer cells under hypoxia raises the possibility that dormant hypoxic tumor cells may favor tumor recurrence after reoxygenation, for instance after therapeutically induced tumor shrinkage and access to improved oxygenation.[21,224,225] Hence, further investigations of hypoxia-induced molecular changes in HPV-positive cancer cells are required to improve our insights into the process of HPV-associated carcinogenesis and to possibly provide a basis for future therapeutic strategies.

1.5.4 Cycling hypoxia

In hypoxic tumor regions, cancer cells are exposed to both chronic hypoxia and cycH (Figure 5).[169,174,228] However, the effects of cycH and continuous oxygen fluctuations on cancer cells are much less investigated compared to chronic hypoxia. In a xenograft mouse model analyzing HPV16-positive cervical cancer cells (SiHa), the presence and spatiotemporal characteristics of cycH were evidenced and highlight the therapeutic relevance of cycH for cervical cancer.[228]

1.5.4.1 Kinetics of cycH in tumors

The kinetics and distribution of cycH within solid tumors are complex. Fluctuations of oxygen supply are attributed to changes in erythrocyte flow, perfusion limitations, as well as the formation of new vascular networks.[175] Consequently, the frequency and duration of hypoxic cycles can range from two to five cycles per hour to slow fluctuations over multiple hours or days.[175] CycH occurs in networks of microvessels and both short-term and long-term cycH coincide in tumor entities.[176,229] Variations in blood flow and resulting differences in oxygen fluctuation magnitudes are dependent on tumor type, sites of tumor growth as well as tumor histology.[229,230] For instance, connective tissue surrounding microvessels may stabilize blood flow and oxygen partial pressure and protect tumor tissue from extensive cycH.[231] Thus, cervical cancer xenografts with higher fractions of connective tissue-associated blood vessels show reduced oxygen fluctuation frequency and relative amplitude in comparison to melanoma xenografts with low connective tissue fractions.[231]

The countless variations in cycH parameters pose a challenge to accurately mimic cycH *in vitro,* compare existing studies, and draw universal conclusions.[232]

1.5.4.2 CycH-associated cellular changes

There is increasing evidence suggesting that cycH and chronic hypoxia have distinct effects on gene regulatory networks and signaling pathways.[175,230,232,233] Specifically, the reoxygenation periods during cycH activate processes that go beyond the adaptation to chronic hypoxia. For instance, it is widely accepted that upon reperfusion of hypoxic tumor regions, cells can restore signaling pathways related to cell proliferation and ATP-consuming processes, like protein synthesis.[175] Furthermore, cycH reoxygenation phases can promote the generation of reactive oxygen species (ROS) production (up to 100-fold higher than basal levels), leading to increased oxidative stress and DNA damage compared to chronic hypoxia, which eventually selects for a more stress-resistant surviving cell subpopulation.[175,234–238]

Interestingly, cycH also has characteristic and distinct effects on HIFs compared to chronic hypoxia. HIF-1α is increasingly stabilized during hypoxic phases of cycH after repeated H-R cycles, exceeding the corresponding levels observed under chronic hypoxia, even though it is completely degraded during each cycH reoxygenation period.[236,239–241] The cycH-induced HIF-1α stabilization is likely attributed to post-translational modifications or ROS-dependent mechanisms.[236,239,240,242]

Phenotypically, cycH has been linked to proangiogenic effects, the selection of cancer stem cells, enhanced epithelial-mesenchymal transition (EMT), cancer cell migration, invasion and metastasis, as well as tumor-promoting inflammation.[239,240,243–245] Furthermore, cycH is attributed to increased chemo- and particularly radioresistance of endothelial cells and several cancer cell lines.[236,239,246–249] It is important to note that the responses to cycH are likely dependent on the cell type, the duration and number of H-R cycles, and the oxygen concentrations applied. Nonetheless, cancer cells under cycH appear to constitute a unique subset of cells that may be associated with a more aggressive malignant phenotype and increased therapy resistance, even compared to chronic hypoxia.[175,230,232] Consequently, cells exposed to cycH may contribute to rapid tumor repopulation and tumor growth between treatments.[175,230,232]

1.6 Research objectives

Tumor hypoxia critically determines the behavior of cancer cells, including their response to chemo- and radiotherapy. In HPV-positive cancer cells, chronic hypoxia leads to distinct effects on the virus/host cell crosstalk, resulting in E6/E7 repression, and allows their evasion from pro-senescent chemotherapy. CycH is a second major form of hypoxia, which is much less investigated, but may be associated with particularly pronounced therapy resistance.

The aim of this thesis is to explore the so far unknown effects of cycH on the phenotype and the virus/host cell interactions in HPV-positive cervical cancer cells, addressing the following questions:

(1) Does cycH affect expression and function of the viral *E6* and *E7* oncogenes? Investigations will include comparative analyses of HPV-positive cervical cancer cells cultivated under cycH versus normoxia, physoxia, and chronic hypoxia, regarding (i) the effects on E6/E7 expression at the protein and transcript level, (ii) the regulation of critical cellular targets (e.g. p53, pRb) for HPV-induced cell transformation, and (iii) the effects of cycH on cell proliferation and cell cycle regulation.

(2) What are global effects of cycH in HPV-positive cancer cells? Quantitative proteome analyses will be performed to characterize cycH-linked alterations of the protein composition in HPV-positive cervical cancer cells, compared to normoxia, physoxia and chronic hypoxia. This approach will be followed by detailed functional analyses of factors, which may show substantial differences in their expression levels under cycH compared to physoxia.

(3) Do cervical cancer cells under cycH differentially respond to radio- and chemotherapy compared to treatment under normoxia, physoxia and chronic hypoxia? Here, the response to γ-irradiation, pro-senescent chemotherapy with Etoposide as well as pro-apoptotic chemotherapy with Cisplatin, the key chemotherapeutic drug used for cervical cancer treatment, will be investigated under different oxygen conditions.

(4) If cycH increases the resistance to pro-apoptotic Cisplatin treatment, it will be attempted (i) to decipher the underlying molecular mechanism by modifying expression (e.g. by RNAi) or function (e.g. by small molecule inhibitors) of factors, which are critical for their enhanced therapy resistance and (ii) to re-sensitize cervical cancer cells to Cisplatin.

Overall, it is hoped that these investigations will provide first insights into the phenotypic effects of cycH in cervical cancer cells and may serve as a basis for the development of strategies against a cell population, which could be particularly problematic for cancer therapy.

CHAPTER 2

RESULTS

2 Results

2.1 Virus/host cell crosstalk in HPV-positive cervical cancer cells under cycH

2.1.1 HPV oncogene expression is maintained under cycH

The expression of the hypoxia-regulated HIF-1α and HIF-2α proteins, as well as the HPV E6/E7 oncoproteins, was analyzed in cervical cancer cells under different oxygen conditions. HPV16-positive SiHa and CaSki cells and HPV18-positive HeLa cells were exposed for 24 h to 21% O_2 (normoxia), 5.5% O_2 (physoxia), 1% O_2 (chronic hypoxia) or cycH, consisting of H-R cycles of 1 h at 1% O_2 (hypoxic phase, H phase) and 1 h at 5.5% O_2 (reoxygenation phase, R phase) to mimic the *in vivo* oxygen conditions of cervical cancers during cycH as close as possible (Figure 7A).

Incubation under cycH induced a marked stabilization of HIF-1α and HIF-2α protein levels during the H phases of cycH in all tested cell lines (Figure 7B). In SiHa and HeLa cells, HIF-1α protein levels under cycH exceeded the corresponding levels under physoxia and chronic hypoxia, which is consistent with previous studies in other cellular models.[236,239,241] The levels of HIF-2α were most pronounced during the H phase of cycH in HeLa and CaSki cells (Figure 7B). However, during the R phase of cycH, HIF-1α and HIF-2α protein levels visibly declined in all cell lines (Figure 7B). This finding indicates that HIF-α subunits are rapidly stabilized in H phases of cycH followed by a quick oxygen-dependent degradation in R phases of cycH. Thereby, HIF-1 and HIF-2 target genes could be intermittently activated in H phases of cycH and allow adaptation to the fluctuations in oxygen supply.

Intriguingly and in striking contrast to the repression of HPV E6/E7 oncoprotein levels under chronic hypoxia, that was described before[225], E6 and E7 protein levels were largely retained in SiHa, CaSki and HeLa cervical cancer cells under cycH, both in the H and R phases (Figure 7B). Additionally, there were no significant changes in HPV *E6/E7* expression under cycH at the transcriptional level in SiHa and HeLa cells, in contrast to the strong downregulation observed under chronic hypoxia (Figure 7C). These observations indicate that the cellular phenotype of HPV-positive cervical cancer cells induced under cycH differs not only from normoxia and physoxia, but also from chronic hypoxia.

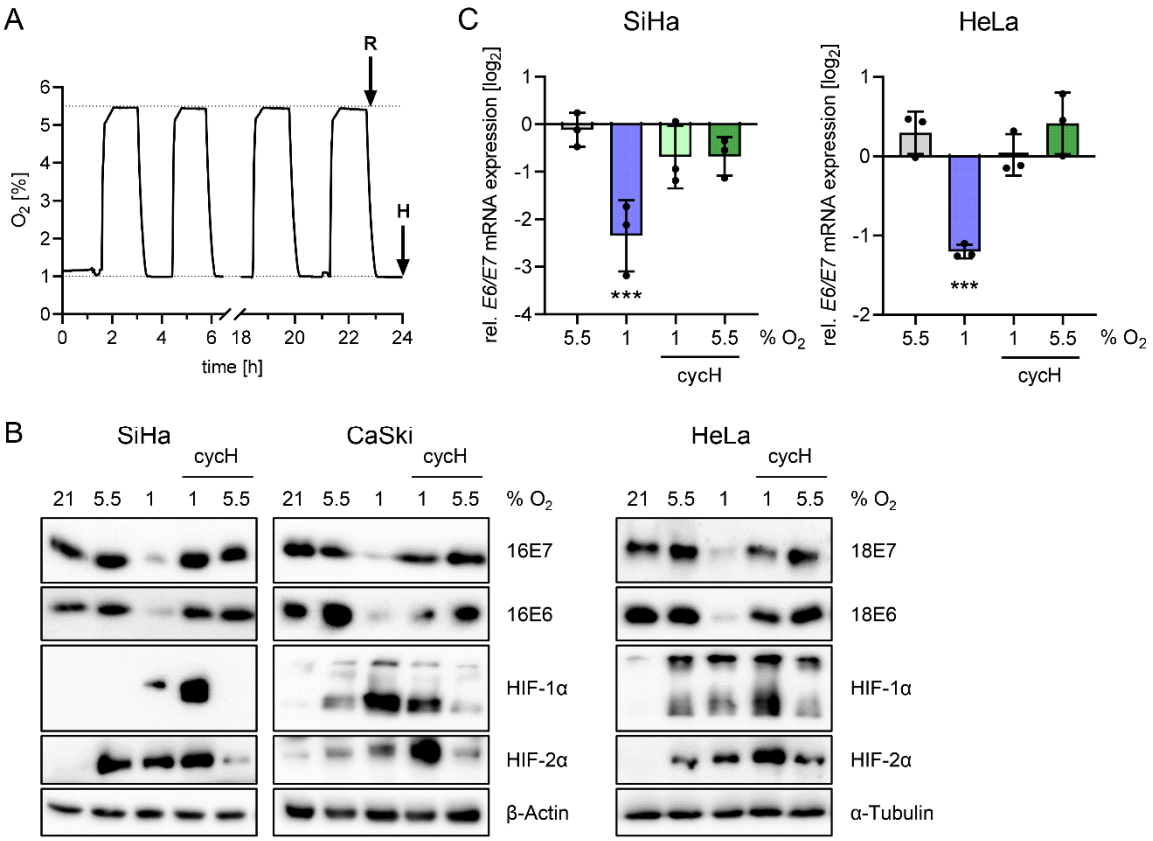

Figure 7. HPV oncogene expression is largely maintained under cycH.

(A) Treatment scheme for cycling hypoxia (cycH) incubations. Cells were exposed to repetitive cycles of 1 h at 1% O_2 (H phase) and 1 h at 5.5% O_2 (R phase). Cells were harvested after 24 h at the end of the H and the R phase, as indicated by arrows, if not stated otherwise. (B) Immunoblot analyses of HPV E6, HPV E7, HIF-1α and HIF-2α protein levels in HPV16-positive SiHa and CaSki and HPV18-positive HeLa cells incubated under 21% O_2, 5.5% O_2, 1% O_2 or cycH for 24 h. β-Actin, α-Tubulin, representative loading controls. (C) qRT-PCR analyses of *E6/E7* mRNA levels in SiHa and HeLa cells cultured under 21% O_2, 5.5% O_2, 1% O_2 or cycH for 24 h. Individual data points as well as mean expression levels relative to the expression under normoxia are shown (log2). Error bars depict standard deviation from biological replicates (n = 3) and asterisks indicate statistically significant changes as determined by one-way ANOVA (***, $p < 0.001$).

2.1.2 E6/E7 retain their transforming activities under cycH

To functionally characterize the sustained expression of the HPV oncogenes under cycH, RNAi-mediated gene silencing targeting all *E6/E7* transcript classes was performed.[43] Immediately after transient siRNA transfection, SiHa and HeLa cells were exposed to cycH and harvested after 48 h or 72 h, respectively.

Similar to the observations under normoxia, repression of *E6/E7* under cycH led to an increase in p53 levels and its downstream effector p21, as well as a decrease in phosphorylated pRb levels and its downstream target E2F1 (Figure 8). Hence, I could

evidence that, under cycH, the HPV E6 and E7 proteins retain their well-characterized effects on the critical transformation targets p53 and pRb.[44,50] This observed maintenance of viral oncogene expression, which also remains functionally active, represents a significant difference between cycH and chronic hypoxia in cervical cancer cells.

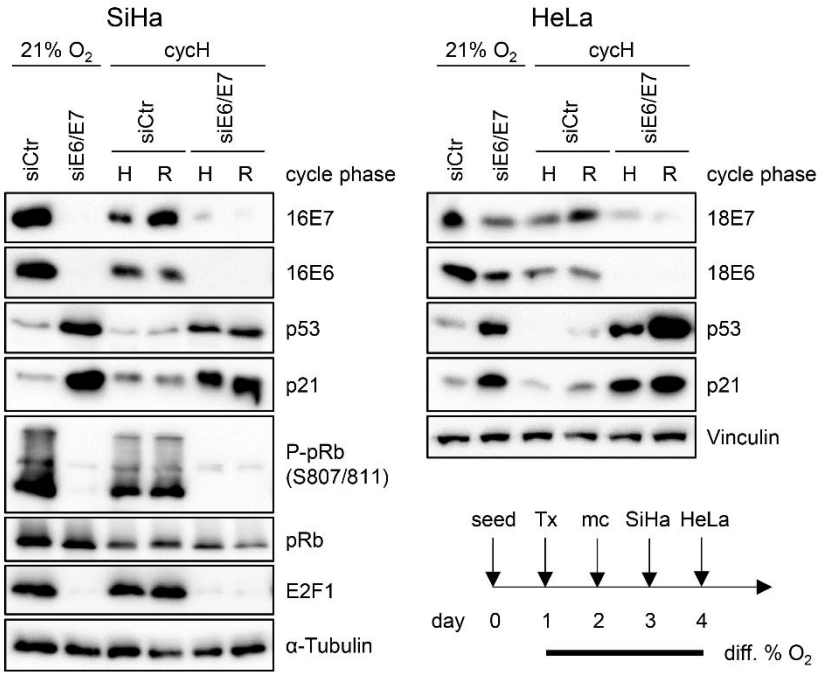

Figure 8. E6/E7 retain key transforming activities under cycH.

SiHa and HeLa cells were transfected with E6/E7-targeting siRNAs (si16E6/E7 or si18E6/E7, respectively) or control siRNA (siCtr) under 21% O_2 or under cycH and harvested 48 h (SiHa) or 72 h (HeLa) post-transfection. Cells exposed to cycH were harvested at the end of the H and R phases, respectively. Immunoblot analyses show HPV E6, HPV E7, p53, p21, phosphorylated (P-)pRb, pRb and E2F1 protein levels. α-Tubulin and Vinculin, representative loading controls. Tx, transfection; mc, medium change; diff., different.

2.1.3 Cervical cancer cell proliferation is reduced under cycH

Next, I analyzed the cellular proliferation and cell cycle distribution of SiHa and HeLa cells cultivated under normoxia, physoxia, chronic hypoxia or cycH for up to 72 h (Figure 9A and 9B). Under normoxia and physoxia, both cell lines showed comparable and continuous proliferation. In line with previous studies[225], chronic hypoxia inhibited the proliferation of HPV-positive cervical cancer cells, coinciding with the repression of the viral *E6/E7* oncogenes (Figure 9A). Interestingly, incubation under cycH also induced a cellular growth arrest after 48 h in SiHa and HeLa cells that was, however, somewhat delayed compared to cultivation under chronic hypoxia (Figure 9A). Notably, a delayed downregulation of HPV E7 protein levels was observed in SiHa cells after 72 h under cycH, which correlated with the proliferative arrest (Figure 9C).

Cell cycle analyses revealed a largely comparable cell cycle distribution after 72 h under chronic hypoxia and cycH in SiHa cells, characterized by a considerable reduction of cells in S phase compared to normoxia and physoxia (Figure 9B, upper panel). In HeLa cells, only chronic hypoxia led to a strong decrease in the cell population in S phase. Intriguingly, however, both chronic hypoxia and cycH caused an increase of HeLa cells in G2/M phase compared to normoxia and physoxia, suggesting a G2/M phase arrest under both hypoxic conditions (Figure 9B, lower panel). These findings indicate that after prolonged incubation for 72 h, cervical cancer cells under cycH eventually exhibit a phenotype similar to cells under chronic hypoxia in terms of proliferation and cell cycle distribution.

However, the dynamics of HIF-1α expression and the activity of the mTOR pathway, which are critically involved in hypoxic adaptation and cell growth[250,251], differ noticeably between chronic hypoxia and cycH, even after prolonged treatment. Under chronic hypoxia, HIF-1α levels were most pronounced after 24 h and subsequently decreased, while under cycH, HIF-1α stabilization in the H phases progressively increased over the monitored time course of 72 h (Figure 9C). Furthermore, the activation of mTORC1 downstream targets eukaryotic translation initiation factor 4E binding protein 1 (4E-BP1), p70S6 kinase (p70S6K), and the ribosomal protein S6 was inhibited under chronic hypoxia as evidenced by their reduced phosphorylation after 48 h, consistent with previous studies.[225,252] Similarly, a reduction in activated mTORC1 targets was observed in the H phases of cycH after 48 h. In contrast, increased levels of phosphorylated (P)-p70S6K, P-S6 and P-4E-BP1 were detected in each R phase of cycH, suggesting a rapid repression and activation of mTORC1 activity during the H-R phases of cycH (Figure 9C). The reduced levels of phosphorylated mTORC1 targets after 48 – 72 h under normoxia and physoxia were most probably due to nutrient limitations resulting from sustained cell proliferation of these cells (Figure 9A and 9C).

Taken together, prolonged cultivation of cervical cancer cells under cycH attenuates proliferation, which coincides with a delayed reduction in HPV oncoprotein levels. Moreover, compared to chronic hypoxia and physoxia, cycH differentially affects HIF-1α and mTORC1 pathways, reflected by increased HIF-1α stabilization in the H phases of cycH and a cycH phase-dependent activation of mTORC1 targets. Given that HIF-1α and mTOR signaling are crucial for the cellular response to oxygen and nutrient availability[250,251], respectively, these observed changes under cycH may contribute to the adaptive mechanisms of cervical cancer cells in response to fluctuating oxygen levels.

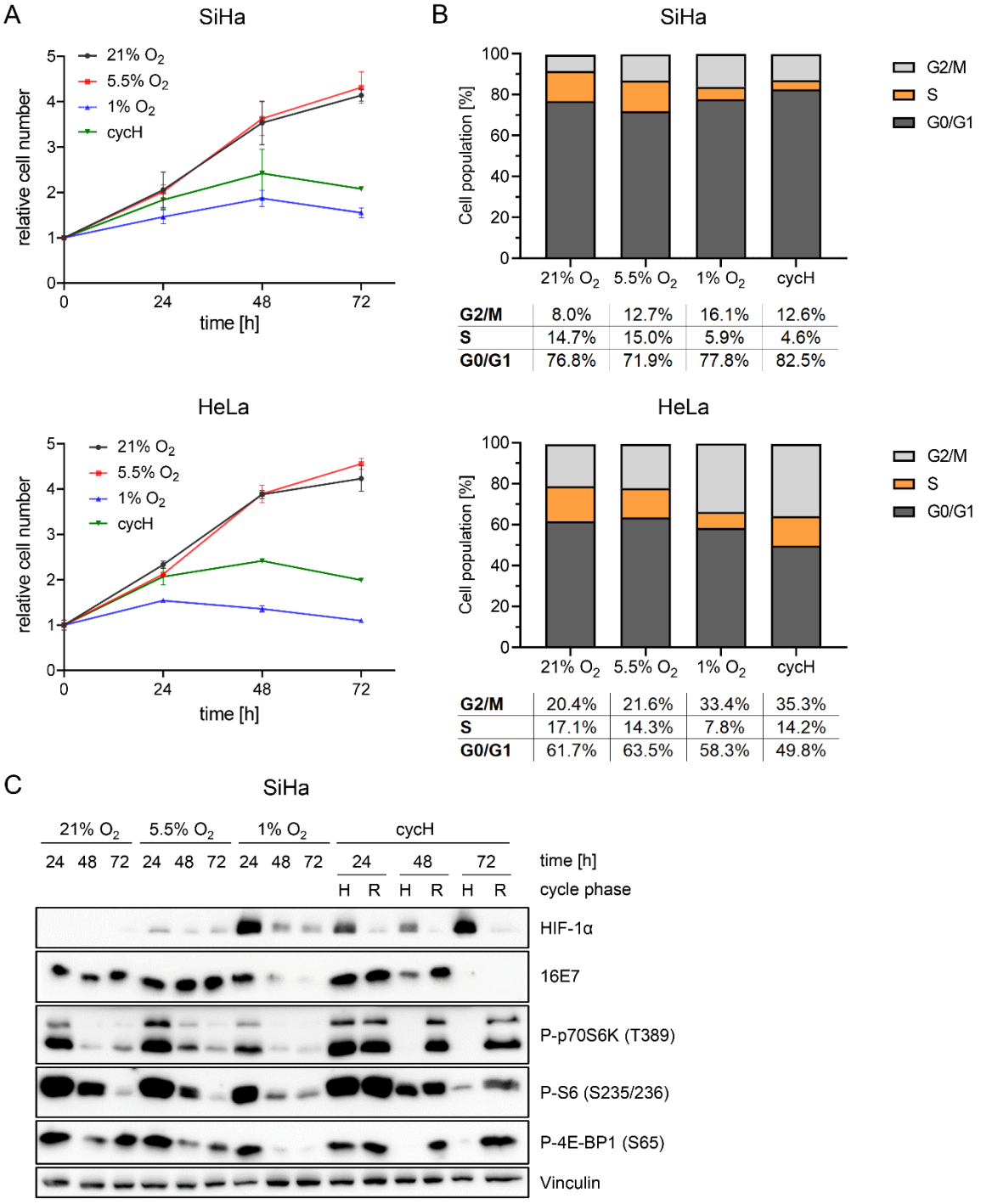

Figure 9. CycH induces a cellular growth arrest.

(A) Proliferation of SiHa and HeLa cells grown under 21% O_2, 5.5% O_2, 1% O_2 or cycH. The initial cell counts (time point 0) are set at 1.0. Relative cell counts at the indicated time points are depicted with standard deviations of biological replicates (SiHa n = 3, HeLa n = 2). (B) Corresponding cell cycle analyses of SiHa and HeLa cells cultivated under different oxygen conditions for 72 h. The percentages of cell populations in G0/G1, S and G2/M phases, respectively, are depicted. (C) Time kinetics of HPV16-positive SiHa cells cultured for 72 h under 21% O_2, 5.5% O_2, 1% O_2 or cycH. Immunoblot analyses of HIF-1α, HPV16 E7, phosphorylated (P-)p70S6K (T389), P-S6 (S235/236) and P-4E-BP1 (S65) protein levels are shown. Vinculin, representative loading control.

2.2 Stress granules are formed under chronic hypoxia but not under cycH

A potential adaptation to various environmental stress stimuli, e.g. by hypoxia, oxidative or heat-shock stress, and viral infections, is the formation of stress granules (SGs).[253,254] SGs are dynamic, membrane-less structures composed of proteins and mRNA molecules that assemble in the cytoplasm in response to stress-induced translational inhibition.[253,255] Interestingly, HIF-1α and mTOR signaling, which both show differential regulation under cycH compared to normoxia, physoxia or chronic hypoxia, have been implicated in SG formation.[256,257] SGs formed under hypoxia act as storage sites for mRNAs, allowing cells to quickly adapt to hypoxic conditions and resume protein synthesis upon reoxygenation when SGs disassemble.[258] Additionally, SG formation may enhance drug resistance.[258] Previous studies have suggested that cycH promotes dynamic assembly and disaggregation of SGs, enabling the storage of HIF-1 regulated transcripts, energy preservation, and recovery from oxidative insults.[237,256]

Therefore, I investigated SG formation under different oxygen conditions in SiHa cervical cancer cells. Sodium arsenite (Ars) treatment causes severe oxidative stress and induces pronounced SG formation under normoxia[254], as detected in immunofluorescence staining for eukaryotic translation initiation factor 3 subunit B (eIF3B), a component of the preinitiation complex and a reliable SG marker (Figure 10).[254] Consistent with other studies, SiHa cells cultured under chronic hypoxia for 48 h showed an increased emergence of SGs compared to cells under normoxia.[258] Strikingly, however, no SG formation was observed under cycH, neither during the hypoxic nor the reoxygenation phase (Figure 10). This finding suggests that the hypoxic insult under cycH is not sufficient to induce translational inhibition required for SG formation. It is possible that the duration of the (hypoxic) cycle phases may play a pivotal role in SG assembly. Collectively, the presented data provide no evidence that the cycH conditions used in this study facilitate SG formation.

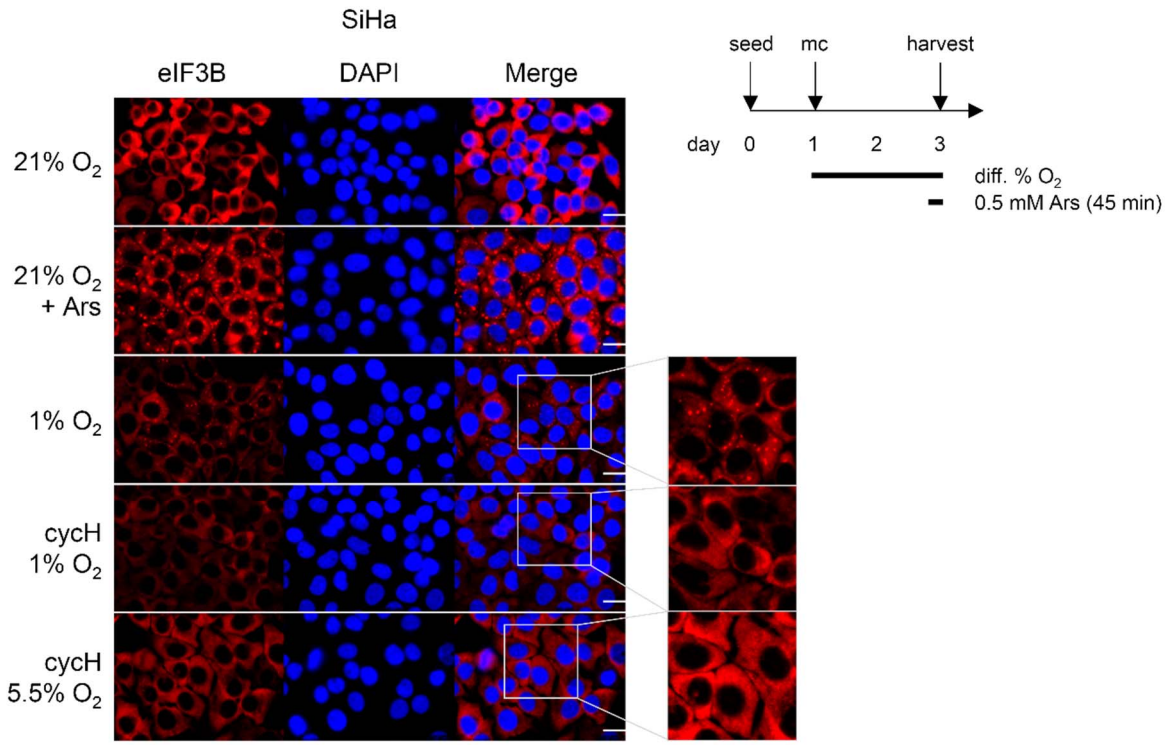

Figure 10. Stress granules are formed under chronic hypoxia but not under cycH.
SiHa cells cultivated under 21% O_2, 1% O_2 or cycH for 48 h were stained for the SG marker eIF3B and analyzed by fluorescence microscopy. Normoxic cells treated for 45 min with 0.5 mM sodium arsenite (Ars) served as positive control for SG formation. Nuclei are counterstained with DAPI. For better visualization, eIF3B-stained image sections of cells under chronic hypoxia and cycH are further magnified and displayed with adjusted brightness. Representative images of three independent experiments are shown. Scale bar: 20 µm. mc, medium change; diff, different.

2.3 The effects of cycH on therapy responses of cervical cancer cells

2.3.1 Cycle phase of cycH determines the sensitivity of cervical cancer cells to radiotherapy

Next, I investigated the response of cervical cancer cells to anticancer therapies under different oxygen conditions. Radiotherapy plays an important role for the treatment of advanced cervical carcinoma.[28] However, hypoxic tumor cells constitute a particularly radioresistant cell population because the lack of oxygen hampers the fixation of radiation-induced DNA damage.[169] Previously, several studies have shown that cycH can further enhance the radioresistance of certain cancer cells compared to chronic hypoxia.[236,239,249] Thus, I tested the response of HPV-positive HeLa cervical cancer cells to γ-irradiation under different oxygen conditions, including cycH for the first time. HeLa cells were cultivated under normoxia, physoxia, chronic hypoxia, or cycH for 24 h followed by

irradiation under their respective oxygen conditions. Subsequently, the cells were replated at defined cell numbers for clonogenic survival assays under normoxia (Figure 11).

Upon irradiation with 6 Gy, HeLa cells cultivated under chronic hypoxia or in the H phase of cycH exhibited strongly increased colony formation capacity compared to cells irradiated under normoxia, physoxia, or in the R phase of cycH (Figure 11). This finding highlights the crucial role of oxygen concentration during irradiation in determining the cellular response of cervical cancer cells to radiotherapy. Low oxygen concentrations, as present under chronic hypoxia or in the H phase of cycH, impede the fixation of radiation-induced DNA damage, while higher oxygen concentrations render cells more susceptible to radiation-induced DNA damage, proliferative arrest, and cell death.[259] Consequently, cycH affects the response of cervical cancer cells to radiotherapy depending on the oxygen concentrations of the respective H-R cycle phase.

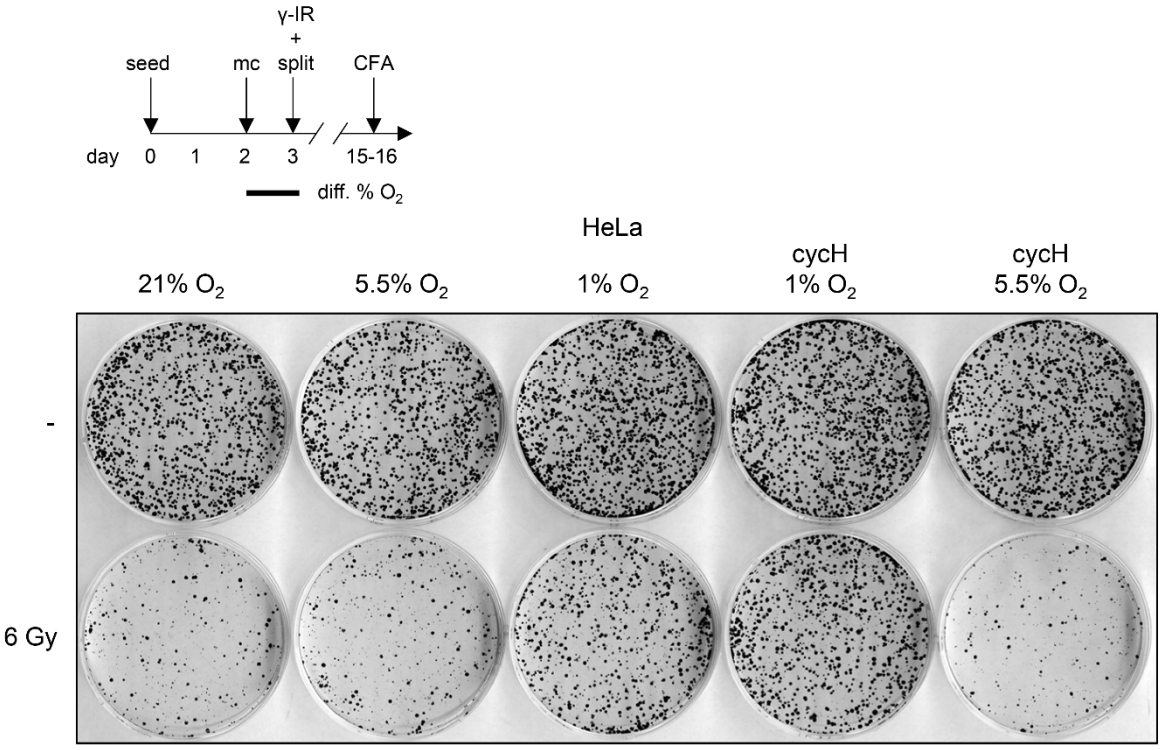

Figure 11. Chronic hypoxia and H phase of cycH protect against γ-irradiation.

Clonogenic survival of HeLa cervical cancer cells after γ-irradiation (γ-IR) treatment under different (diff.) oxygen conditions. HeLa cells cultivated under 21% O_2, 5.5% O_2, 1% O_2 or cycH for 24 h were irradiated with 6 Gy under the respective oxygen conditions. Cells exposed to cycH were irradiated either in the H (1% O_2) or in the R (5.5% O_2) phase. After irradiation, 5000 cells were replated and cultured under normoxia. Colony formation assays (CFAs) after radiation treatment were fixed and stained 12-13 days after replating. Representative CFAs of three independent experiments are shown. mc, medium change.

2.3.2 Cervical cancer cells under cycH can evade senescence induction despite remaining mTOR activity

Several chemotherapeutic drugs are able to induce cellular senescence, an irreversible growth arrest.[260–262] Previous work of our group has shown that the induction of senescence upon treatment with the topoisomerase II inhibitor Etoposide is differentially regulated in HPV-positive cancer cells treated under normoxia or chronic hypoxia in that the hypoxic impairment of the mTOR signaling pathway allows the cells to evade from efficient senescence induction.[225] Active mTOR signaling is better maintained under cycH compared to chronic hypoxia, as evidenced by the presence of the phosphorylated mTORC1 targets p70S6K, S6, and 4E-BP1, especially in the R phases of cycH, in SiHa and HeLa cells (Figure 9C; Figure 12A).

Based on these differences in mTOR activity, I investigated the response of HPV-positive cancer cells to pro-senescent chemotherapy under cycH in more detail. SiHa and HeLa cells were treated with Etoposide under different oxygen conditions and monitored for typical morphological signs of senescence and their colony formation capacity upon drug release and reoxygenation. Of note, Etoposide treatment of cells under physoxia, chronic hypoxia or cycH was conducted after 18 h preincubation under the respective oxygen conditions (Figure 12B).

SiHa and HeLa cells under normoxia and physoxia efficiently induced senescence in response to Etoposide treatment, reflected by the presence of enlarged and flattened senescent cells staining positive for the well-established senescence marker senescence-associated β-Galactosidase (SA-β-Gal) (Figure 12C). In contrast, many cells treated under chronic hypoxia lacked the phenotypic characteristics of cellular senescence, consistent with previous observations.[225] Interestingly, when treated under cycH, SiHa and HeLa cells showed slightly more enlarged SA-β-Gal-positive cells compared to cells treated under chronic hypoxia. However, a substantial number of cells treated with Etoposide under cycH also managed to evade senescence induction (Figure 12C).

These findings were further supported by colony formation assays of SiHa and HeLa cells following pro-senescent chemotherapy under different oxygen conditions. Since senescence represents an irreversible cell growth arrest[263], Etoposide-treated cells under normoxia and physoxia exhibited a strongly reduced colony formation capacity upon drug release and recultivation under standard cell culture conditions. In contrast, the colony formation capacities of SiHa and HeLa cells treated under chronic hypoxia or cycH were markedly increased compared to cells treated under normoxia or physoxia, in line with the notion that they evade senescence induction (Figure 12C).

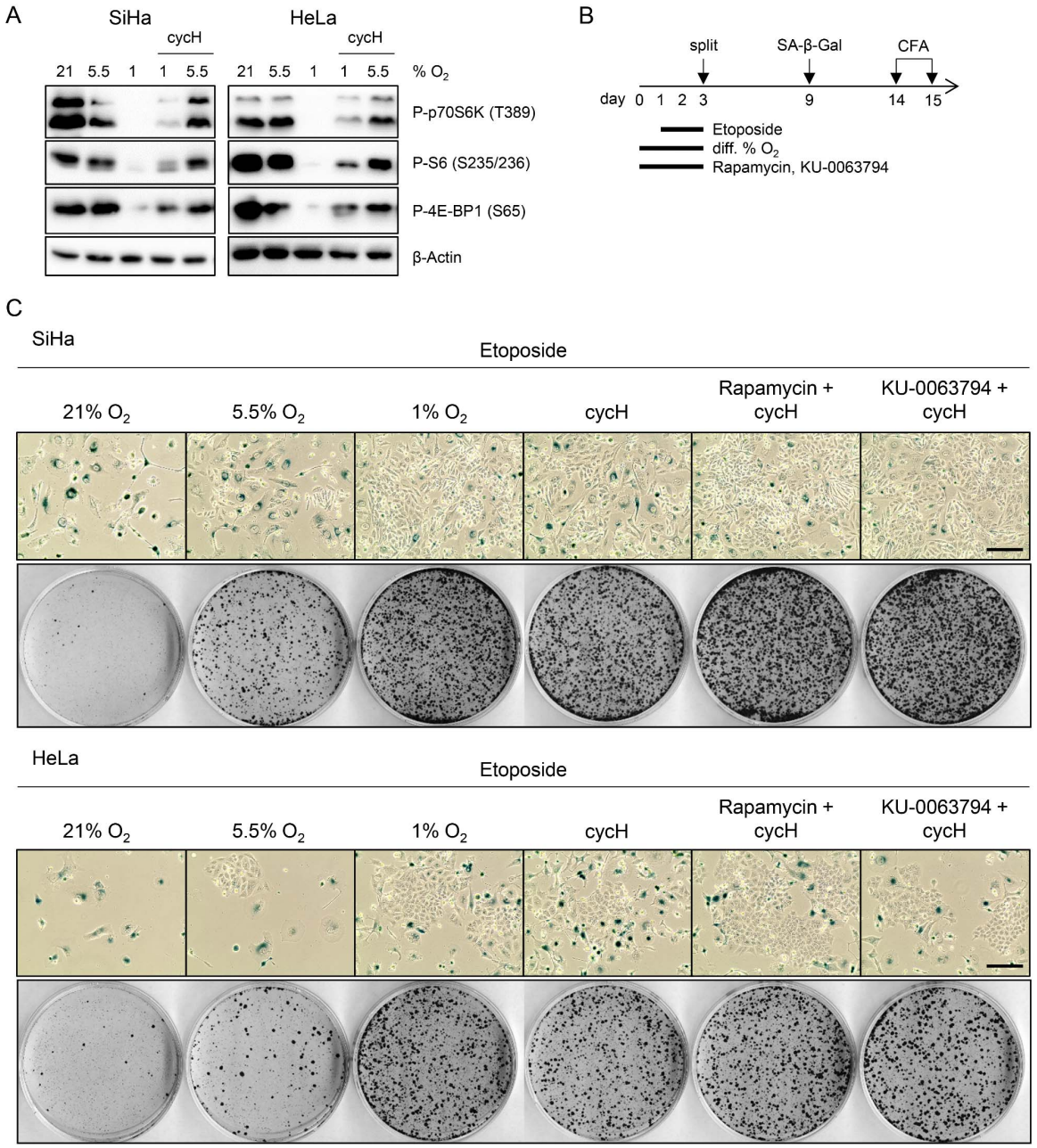

Figure 12. Cervical cancer cells under cycH can evade Etoposide-induced senescence.

(A) Immunoblot analyses of phosphorylated (P-)p70S6K (T389), P-S6 (S235/236) and P-4E-BP1 (S65) protein levels in HPV16-positive SiHa and HPV18-positive HeLa cells cultured for 24 h under 21% O_2, 5.5% O_2, 1% O_2 or cycH. β-Actin, representative loading control. (B) Treatment protocol for Figure 12C. Cells were treated for 48 h with 20 µM (SiHa) or 15 µM (HeLa) Etoposide under different (diff.) O_2 concentrations, as indicated. Cells under cycH were treated with Etoposide in the absence or presence of the mTOR inhibitors Rapamycin (50 nM) or KU-0063794 (5 µM). Subsequently, cells were split at defined cell numbers for senescence assays (SA-β-Gal staining) and CFAs and cultured under normoxia in drug-free medium. (C) Senescence assays (SA-β-Gal staining, blue) and corresponding CFAs of SiHa and HeLa cells treated as described in subfigure B. Scale bar: 200 µm. Representative results of three independent experiments are shown.

To investigate the potential influence of remaining mTOR activity under cycH on the response of cervical cancer cells to pro-senescent chemotherapy, I combined Etoposide treatment with chemical mTOR inhibitors, namely Rapamycin (mTORC1 inhibitor) or KU-0063794 (mTORC1/mTORC2 inhibitor). Co-treatment with either mTOR inhibitor slightly reduced the number of SA-β-Gal-positive cells following Etoposide treatment under cycH, and only marginally increased the outgrowth of SiHa and HeLa cells in colony formation assays (Figure 12C).

Collectively, these findings indicate that the partial reduction of mTOR activity under cycH is sufficient to enable HPV-positive cervical cancer cells to escape efficient senescence induction upon Etoposide treatment. Consequently, Etoposide-treated cells under cycH exhibited a similar capacity to evade pro-senescent chemotherapy as cells treated under chronic hypoxia.

2.3.3 CycH leads to increased resistance of cervical cancer cells to Cisplatin-induced apoptosis

For the treatment of advanced cervical carcinomas, chemotherapy with the pro-apoptotic drug Cisplatin (CDDP) plays a central role.[66] As cycH has been associated with a more aggressive cellular phenotype and increased resistance to chemotherapy[175,247,248], I next investigated the sensitivity of HPV-positive cervical cancer cells to pro-apoptotic Cisplatin treatment under different oxygen concentrations.

In line with its pro-apoptotic potential[73], Cisplatin treatment under normoxia and physoxia led to strong cleavage of the apoptosis markers poly(ADP-ribose) polymerase (PARP) and Caspase 9 in SiHa, HeLa and CaSki cells (Figure 13A). In comparison, both apoptosis markers were moderately reduced after Cisplatin treatment under chronic hypoxia and further diminished under cycH in all tested cell lines. These findings imply a particularly reduced sensitivity to pro-apoptotic Cisplatin treatment under cycH. Additionally, Cisplatin treatment repressed HPV E7 protein levels under normoxia, as expected[264], but also under physoxia and cycH in SiHa and HeLa cells (Figure 13A). Under chronic hypoxia, E7 expression was downregulated *per se* and could not be further reduced by the DNA damaging agent.

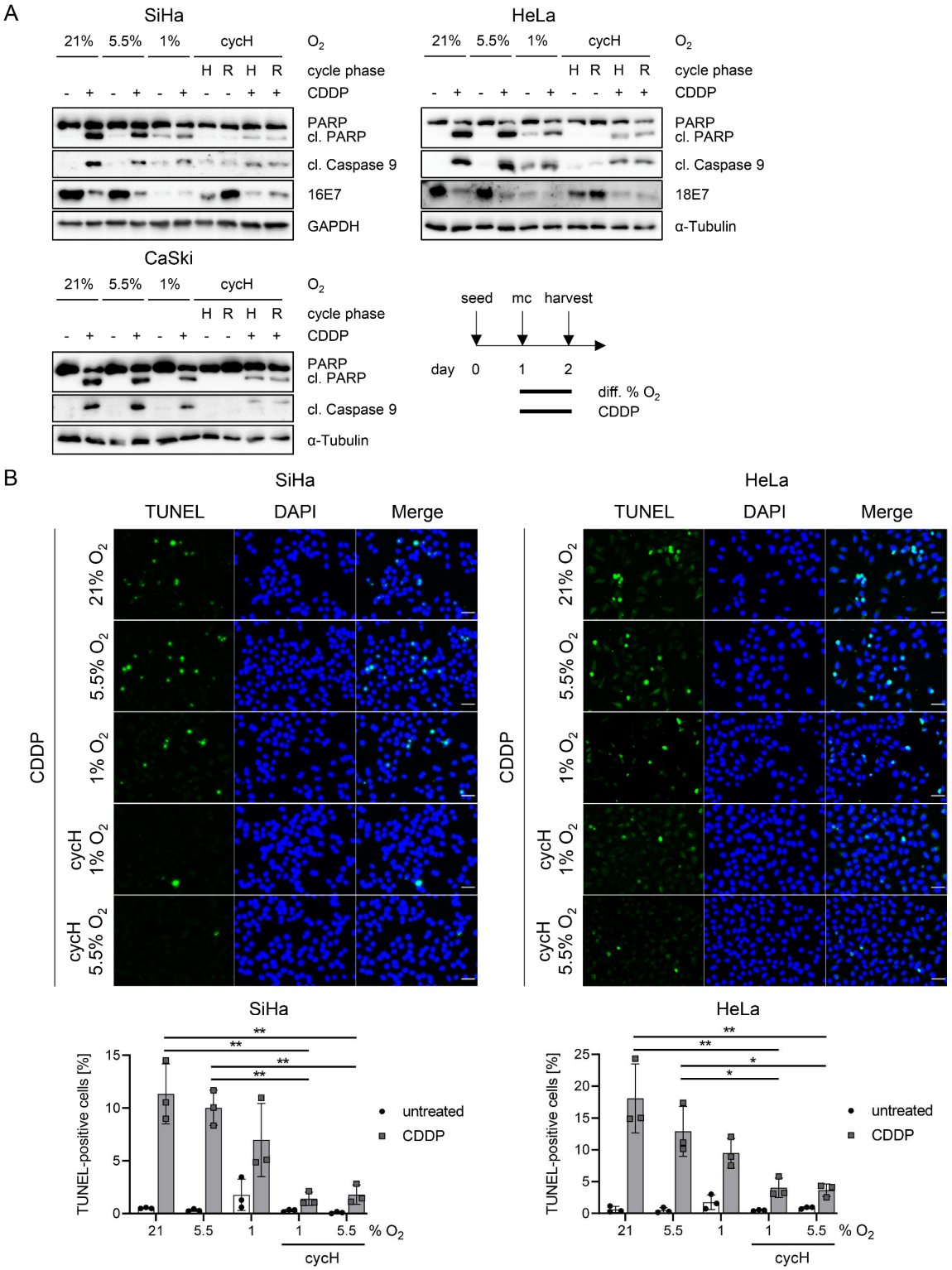

Figure 13. Cervical cancer cells under cycH show increased resistance to Cisplatin-induced apoptosis. (A) SiHa, HeLa and CaSki cells were cultivated under 21% O_2, 5.5% O_2, 1% O_2 or cycH and treated for 24 h with 30 µM (SiHa) or 15 µM (HeLa, CaSki) CDDP, as indicated. Protein levels of PARP, cleaved (cl.) PARP, cl. Caspase 9, and HPV E7 were analyzed by immunoblots. GAPDH and α-Tubulin, representative loading controls. mc, medium change; diff, different. (B) Corresponding TUNEL analyses of SiHa and HeLa cells upon treatment with 30 µM or 15 µM CDDP, respectively, under different O_2 conditions. Scale bar: 50 µm (upper panel). The percentage of TUNEL-positive cells was calculated relative to the total number of DAPI-stained cells (lower panel). Mean values with standard deviations are shown (n = 15 fields of view with ≥ 50 cells from three independent experiments). Asterisks indicate statistical significance as determined by one-way ANOVA (*, $p < 0.05$; **, $p < 0.01$).

Further analyses using TUNEL assays were performed to quantify late-stage apoptotic cells following Cisplatin treatment. These TUNEL analyses corroborate the enhanced chemotherapy resistance of cervical cancer cells under cycH as the percentages of TUNEL-positive cells were significantly reduced in Cisplatin-treated SiHa and HeLa cells in both cycH phases, compared to normoxia, physoxia and chronic hypoxia (Figure 13B).

Overall, these findings show that cervical cancer cells under cycH are more resistant to pro-apoptotic Cisplatin treatment, not only compared to cells under normoxia or physoxia, but also to cells under chronic hypoxia.

To further investigate the cellular fate of Cisplatin-treated cervical cancer cells under different oxygen conditions, SiHa and HeLa cells were split after drug treatment and cultivated under normoxic conditions for subsequent senescence assays. Consistent with the effective induction of apoptosis after Cisplatin treatment in SiHa and HeLa cells under normoxia, physoxia, and chronic hypoxia, only few cells survived and stained positive for the senescence marker SA-β-Gal (Figure 14). In contrast, a substantial proportion of cells treated under cycH, rather than undergoing apoptosis, interestingly switched to a senescent phenotype, as evidenced by increased SA-β-Gal-positive staining (Figure 14). These findings further support the increased resistance of HPV-positive cervical cancer cells under cycH to pro-apoptotic chemotherapy compared to cells under normoxia, physoxia or chronic hypoxia.

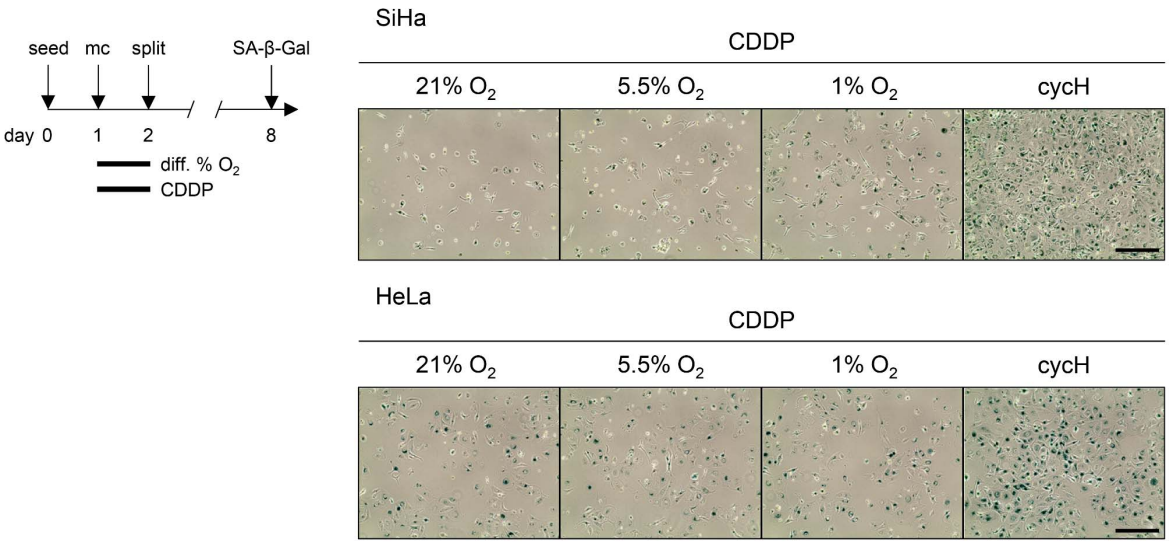

Figure 14. Cisplatin treatment under cycH induces a senescent phenotype.

SiHa and HeLa cells were treated for 24 h with 30 µM (SiHa) or 15 µM (HeLa) CDDP under 21% O_2, 5.5% O_2, 1% O_2 or cycH. Cells were then split, incubated under normoxia in drug-free medium and stained for SA-β-Gal activity. Scale bar: 400 µm. Representative results of three independent experiments are shown. mc, medium change; diff, different.

2.4 Proteome changes in SiHa cells under different oxygen conditions

To gain further insights into the cellular changes under different oxygen conditions that may contribute to the therapy response of cervical cancer cells, I compared the proteomes of HPV16-positive SiHa cells cultivated for 24 h under 21% O_2, 5.5% O_2, 1% O_2, or cycH. In collaboration with Dr. Bianca Kuhn & Prof. Dr. Jeroen Krijgsveld (DKFZ Heidelberg), I performed tandem mass tag (TMT) mass spectrometry (MS)-based quantitative proteome analyses.

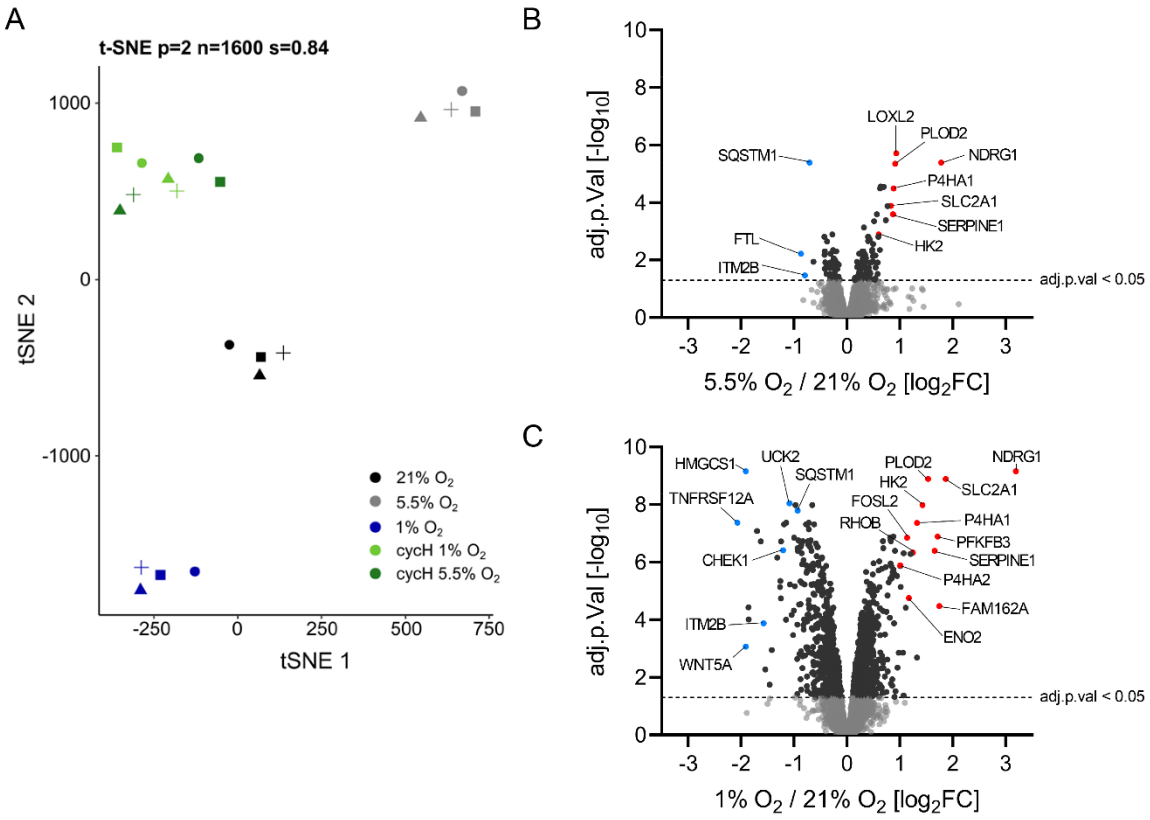

Figure 15. Proteome analysis of SiHa cervical cancer cells under different oxygen conditions.
Mass spectrometry-based proteome analyses of SiHa cells cultivated for 24 h under 21% O_2, 5.5% O_2, 1% O_2 or cycH (harvested in the H phase (1% O_2) and in the R phase (5.5% O_2)). (A) Clustering is visualized by t-SNE analysis of four biological replicates (different symbols) after batch correction. n = total iterations; s = silhouette score. (B) Differential expression analysis using Limma moderated t-statistics for the comparison of changes in the proteome of cells grown for 24 h under physoxia (5.5% O_2) compared to normoxia (21% O_2), in four biological replicates each. Volcano plot displaying log_2 fold change (log_2FC) ratios of protein expression (x-axis) and adjusted (adj.) p-values ($-log_{10}$) (y-axis). Grey color of dots indicates non-significantly changing protein levels, black color indicates significantly changing protein levels, with a p-value adjusted for multiple testing according to Benjamini-Hochberg, *adj. $p \leq 0.05$ (horizontal dashed line). Selected proteins showing significant up- (red) or downregulation (blue) between groups are labeled. (C) Proteome changes of SiHa cells cultivated under chronic hypoxia (1% O_2) versus 21% O_2 for 24 h, analyzed and displayed as described in subfigure B.

The t-distributed Stochastic Neighbor Embedding (t-SNE) analysis, which is based on a dimensionality reduction algorithm and clusters complex protein expression data into a 2D mapping[265], revealed that the proteomes of SiHa cells cultivated under normoxia, physoxia, chronic hypoxia and cycH can be clearly distinguished (Figure 15A). On average, approximately 4700 proteins were detected and their levels were compared among the different treatment groups.

2.4.1 Proteomic differences between physoxia and normoxia in SiHa cells

2.4.1.1 Hypoxia-associated factors can be upregulated under physoxia vs. normoxia

As a first interesting observation, I found that there were few but significant differences between the proteomes of SiHa cells under physoxia (5.5% O_2) and normoxia (21% O_2) (Figure 15B). This finding is of importance because standard *in vitro* cell culture is conducted at 21% O_2, which does not accurately reflect the physiological oxygen levels of the uterine cervix (refer to chapter 1.5).[173]

Under physoxia, the levels of 96 proteins were significantly increased compared to normoxia (adj. p-value < 0.05), but only a few proteins exhibited a strong upregulation (Figure 15B; $\log_2$FC > 0.58). Among the upregulated factors, the NDRG1 protein, which is increasingly linked to tumorigenesis[195], showed the highest increase in its protein levels under physoxia compared to normoxia ($\log_2$FC +1.779). Interestingly, the significantly upregulated proteins under physoxia compared to normoxia, including LOXL2, PLOD2, P4HA1, SLC2A1, SERPINE1, and HK2 are primarily associated with the adaptation to oxygen-deprived conditions[266–269] and are also significantly upregulated in cells under chronic hypoxia compared to normoxia (Figure 15C). Of note, chronic hypoxia induced more extensive proteome changes compared to cells under normoxia than observed under physoxia (Figure 15B and 15C).

The levels of exemplary hypoxia-regulated proteins in cervical cancer cells under different oxygen conditions were visualized in a heat map in pairwise comparisons to normoxia or physoxia (Figure 16A). Interestingly, there is a noticeable overlap of similarly up- and downregulated proteins under physoxia and chronic hypoxia vs. normoxia, respectively (Figure 16A and 16B). In fact, 79 out of 96 significantly upregulated proteins and 42 out of 47 significantly downregulated proteins under physoxia vs. normoxia ($p < 0.05$) were also significantly regulated under chronic hypoxia compared to normoxia (Figure 16B).

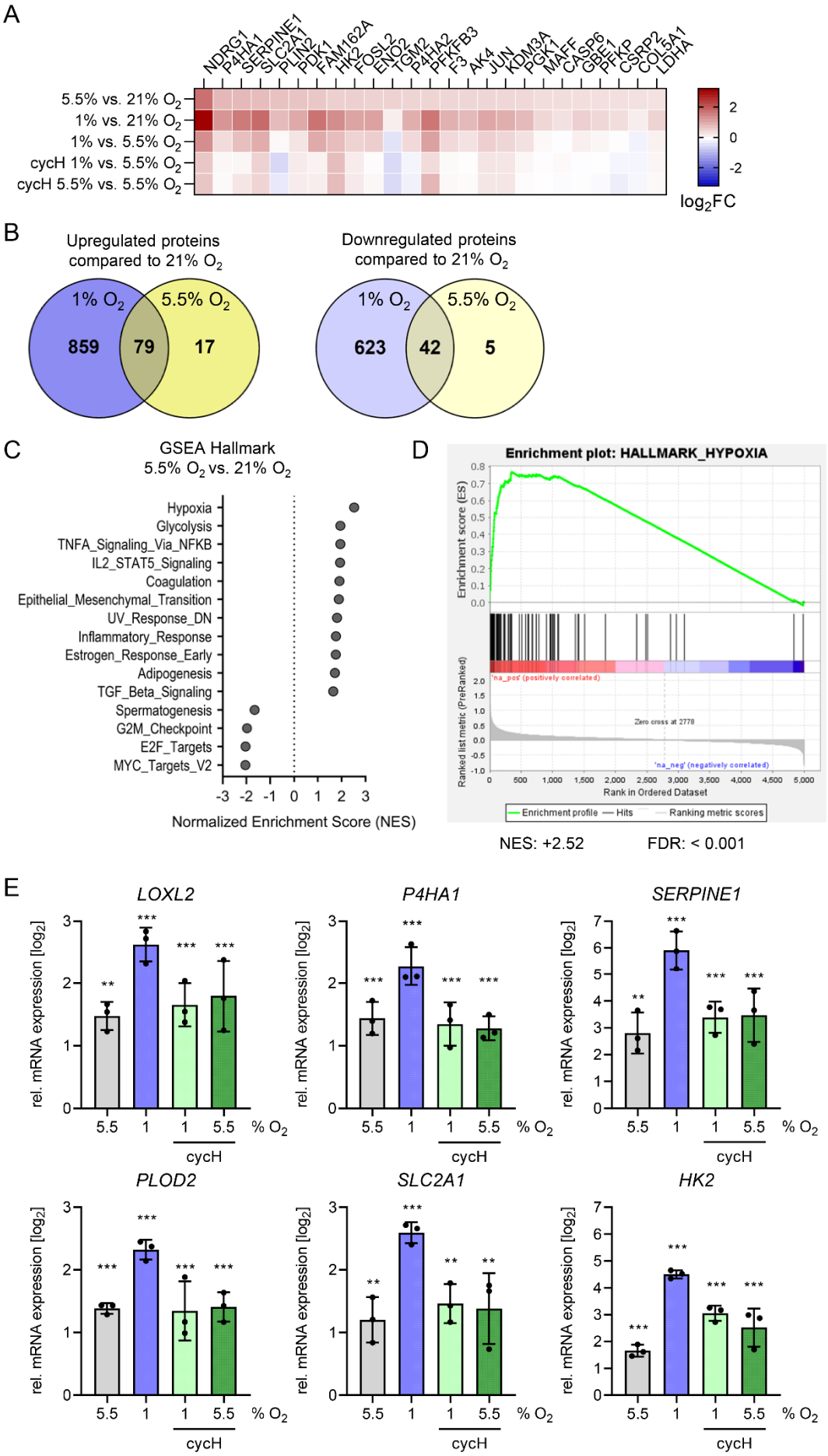

Figure 16. *See figure legend on the next page*.

Figure 16. Physoxia can promote the expression of hypoxia-linked genes.

(A) Heatmap depicting average log_2 fold changes (log_2FC) of representative hypoxia-regulated proteins under physoxia (5.5% O_2) and chronic hypoxia (1% O_2) in pairwise comparisons to normoxia (21% O_2), as well as under chronic hypoxia and cycH (both H and R phases) in pairwise comparison to physoxia (5.5% O_2). Color code indicates upregulation (red) and downregulation (blue). (B) *Left panel*: Venn diagram depicting the overlap between the significantly upregulated proteins under 5.5% O_2 or under 1% O_2 vs. 21% O_2 ($p \leq 0.05$, no cutoff for log_2FC). *Right panel*: Venn diagram depicting the overlap between the significantly downregulated proteins under 5.5% O_2 or 1% O_2 vs. 21% O_2. (C) Gene set enrichment analysis (GSEA) performed for SiHa cells cultivated under 5.5% O_2 vs. 21% O_2. Average log2FC values (n = 4) of all proteins detected in the proteome analyses were used as input for preranked GSEA with 1000 permutations. "Hallmark" gene sets that show significant positive or negative enrichment under 5.5% O_2 vs. 21% O_2 are shown by their normalized enrichment scores (NES) ($p \leq 0.05$). (D) Enrichment plot of the positively enriched gene set "Hallmark_Hypoxia" under 5.5% O_2 vs. 21% O_2. FDR, false discovery rate. (E) qRT-PCR analyses of *LOXL2, P4HA1, SERPINE1, PLOD2, SLC2A1,* and *HK2* mRNA levels in SiHa cells cultivated under 21% O_2, 5.5% O_2, 1% O_2 or cycH for 24 h. Mean expression levels relative (rel.) to the expression under 21% O_2 are displayed (log_2FC). Standard deviations of biological replicates (n = 3) are shown and asterisks denote statistically significant changes determined by one-way ANOVA (**, $p < 0.01$; ***, $p < 0.001$).

Consistent with these observations, gene set enrichment analysis (GSEA) using the molecular signatures database (MSigDB) revealed a significant positive enrichment of the Hallmark gene set "Hypoxia" under physoxia vs. normoxia, with a normalized enrichment score of +2.52 (Figure 16C and 16D). Concomitantly, other hallmark gene sets such as "Glycolysis", "TNFα signaling via NFκB", and "Epithelial Mesenchymal Transition" were positively enriched under physoxia compared to normoxia, while "G2M Checkpoint", "E2F Targets", and "Myc Targets" were downregulated (Figure 16C). To validate the upregulation of hypoxia-induced genes indicated by the proteome analyses, mRNA levels of *LOXL2, P4HA1, PLOD2, SLC2A1, HK2,* and *SERPINE1* were determined in SiHa cells under physoxia, chronic hypoxia, and cycH relative to expression levels under normoxia. These analyses demonstrated a gradual increase in the expression of these genes with descending oxygen concentrations (Figure 16E). Interestingly, most hypoxia-associated transcripts, except for *HK2*, exhibited a comparable increase under physoxia and cycH, irrespective of the cycH H-R phases, compared to expression levels under normoxia (Figure 16E).

Collectively, these results corroborate that physoxia induces a cellular phenotype that is distinct from standard cell culture conditions (normoxia).

2.4.1.2 Physoxia upregulates the hypoxia-related factor NDRG1

Next, I analyzed the regulation of NDRG1, which exhibited the strongest induction in the proteome analysis of SiHa cells under physoxia compared to normoxia, in more detail. NDRG1 has been reported to play a critical oncogenic role in the progression of cervical cancer, however, many of its functions remain poorly understood.[218,219]

Compared to normoxia, I observed a significant upregulation of *NDRG1* in SiHa cells under physoxia, chronic hypoxia, and cycH at the transcript level (Figure 17A). Further, immunoblot analyses confirmed the upregulation of NDRG1 protein levels in SiHa cells (Figure 17B) and showed that this regulatory phenomenon is also conserved in other cervical cancer cells, such as CaSki and HeLa cells (Figure 17C). Moreover, NDRG1 protein and mRNA expression levels were also significantly increased under physoxia compared to normoxia in HPV-negative cells, such as A549 lung cancer cells or HCT116 colorectal cancer cells (Figure 17D and 17E). In A549 cells, similar to the regulation observed in SiHa, CaSki and HeLa cells, incubation under chronic hypoxia further increased NDRG1 levels compared to physoxia. In HCT116 cells, however, both physoxia and chronic hypoxia equally increased NDRG1 protein and transcript levels (Figure 17D and 17E). Hence, the observed physoxia-induced upregulation of NDRG1 expression levels is not limited to HPV-positive cervical cancer cells and may have broader implications in other cell types.

Furthermore, I investigated the subcellular localization of NDRG1, which is a main determinant for its interaction with other cellular factors[197,213], in SiHa cells under normoxia, physoxia or chronic hypoxia. Consistent with the immunoblot analysis (Figure 17B), NDRG1 was virtually undetectable in SiHa cells under normoxia as observed by immunofluorescence (Figure 17F). Notably, a remarkable increase in cytoplasmic NDRG1 staining was observed under physoxia and chronic hypoxia (Figure 17F). In addition, few cells under chronic hypoxia also exhibited nuclear NDRG1 staining (Figure 17F), as previously reported for human trophoblasts.[212] Subcellular fractionation and immunoblot analyses of SiHa cells confirmed the predominantly cytoplasmic localization of NDRG1 protein under physoxia and chronic hypoxia (Figure 17G). Furthermore, a clear enrichment of NDRG1 levels at the organelles and at the plasma membrane was detected under chronic hypoxia, which was less pronounced or absent under physoxia (Figure 17G). These findings raise the possibility that, based on the differences in subcellular localization, NDRG1 could potentially exhibit distinct functions under physoxia and chronic hypoxia.

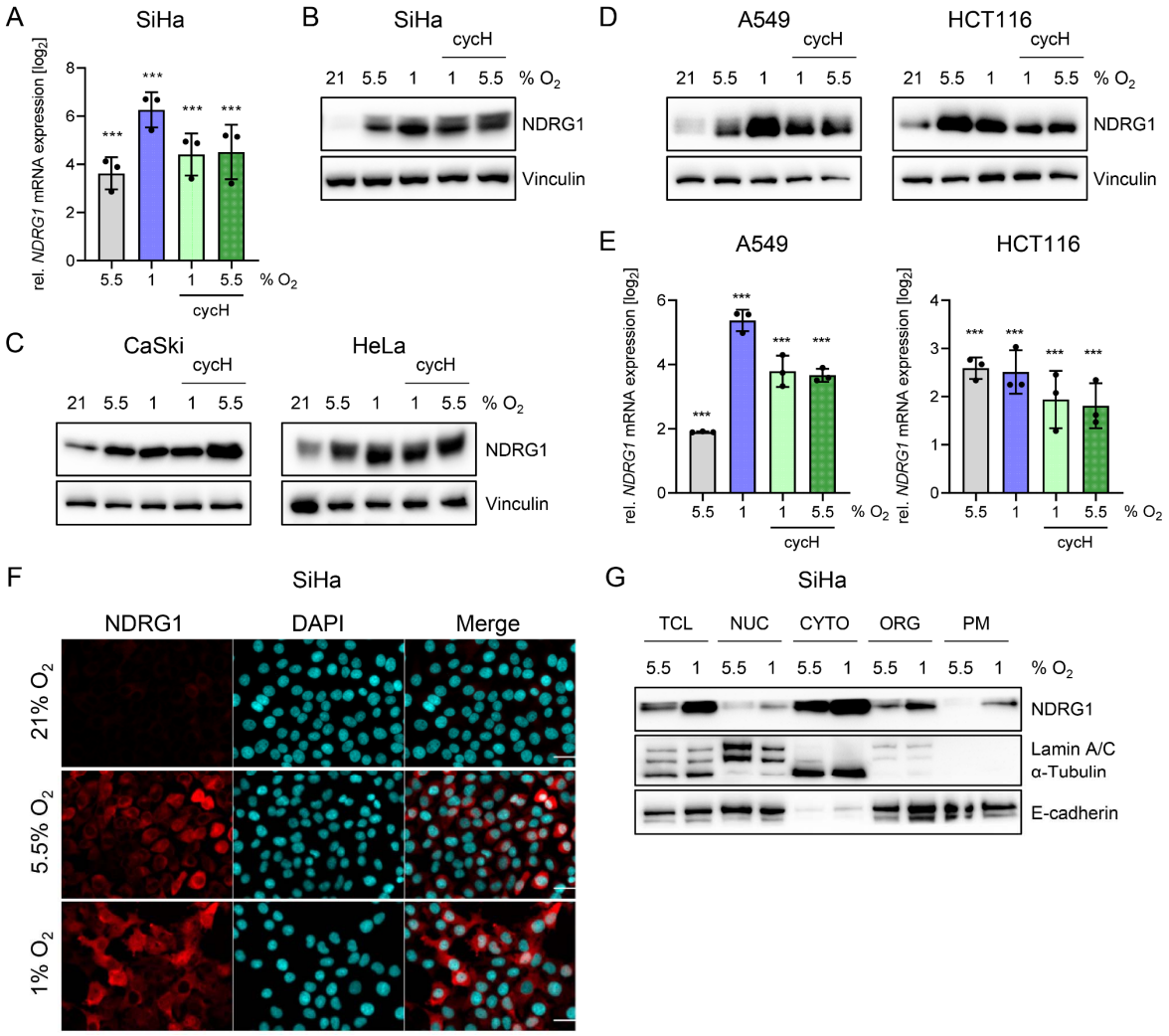

Figure 17. Physoxia and chronic hypoxia increase cellular NDRG1 levels.

(A) qRT-PCR analyses of *NDRG1* levels in SiHa cells incubated under 21% O_2, 5.5% O_2, 1% O_2 or cycH for 24 h. Individual data points as well as mean expression levels relative (rel.) to the expression under 21% O_2 are shown (log_2FC). Standard deviations of biological replicates (n = 3) are depicted, and asterisks indicate statistically significant changes as determined by one-way ANOVA (***, $p < 0.001$). (B) Analysis of NDRG1 protein levels by immunoblot in SiHa cells under different oxygen conditions. (C) Immunoblot analyses of NDRG1 levels in CaSki and HeLa cells under different oxygen conditions. (D) Immunoblot analyses of NDRG1 levels in HPV-negative A549 lung cancer cells and HCT116 colorectal cancer cells. Vinculin, loading control. (E) Corresponding *NDRG1* mRNA levels under different oxygen conditions determined by qRT-PCR in A549 and HCT116 cells presented as described in subfigure A. (F) Immunofluorescence analysis of intracellular localization of NDRG1 in SiHa cells after incubation under 21% O_2, 5.5% O_2 and 1% O_2 for 24 h. Nuclei are stained with DAPI. Representative images of three independent experiments are shown. Scale bar: 30 µm. (G) Subcellular fractionation of SiHa cells cultured under 5.5% O_2 or 1% O_2 for 24 h. Immunoblot analyses of NDRG1 in the total cell lysate (TCL), nucleus (NUC), cytoplasm (CYTO), organelle (ORG) and plasma membrane (PM) fraction are shown. As controls for the individual fractions, Lamin A/C (nucleus), α-Tubulin (cytoplasm) and E-cadherin (membrane) were used.

2.4.1.3 The regulation of NDRG1 expression and phosphorylation is largely comparable under physoxia and chronic hypoxia in cervical cancer cells

The hypoxia-mediated upregulation of NDRG1 levels can occur via HIF-1 dependent or HIF-1 independent mechanisms, e.g. involving Egr1 or AP1.[200–202] To investigate the mechanism of the physoxia-induced increase in NDRG1 levels in cervical cancer cells, I silenced the expression of HIF-1α and HIF-2α, individually or in combination, via RNAi. Interestingly, only the combined silencing of HIF-1α and HIF-2α efficiently prevented the upregulation of both total and T346-phosphorylated NDRG1 protein levels under physoxia in SiHa and HeLa cells. In contrast, individual knockdown of either HIF-1α or HIF-2α did not significantly reduce NDRG1 protein levels under physoxia compared to control siRNA-transfected cells, if at all (Figure 18A). These findings indicate that NDRG1 is a HIF-1α/HIF-2α regulated factor, and its expression is efficiently induced by HIF activities under physoxia.

Furthermore, I analyzed and compared the phosphorylation of NDRG1 under physoxia and chronic hypoxia in SiHa and HeLa cells. Phosphorylation of NDRG1 at Thr346 by SGK1 primes for subsequent phosphorylation by GSK-3β[207] and is potentially required for critical NDRG1 functions, including its interference with NFκB signaling.[208] Hence, I investigated the effects of different chemical inhibitors targeting components of the mTORC2-PDK1-SGK1 axis, mTORC1 or AKT signaling, and the effects of unphysiologically high glucose concentrations (4.5 g/L) on NDRG1 phosphorylation under physoxia and chronic hypoxia. Treatments with the mTORC1/mTORC2 inhibitor KU-0063794, the PDK1 inhibitor GSK2334470 and the SGK1 inhibitor efficiently reduced P-NDRG1 (T346) levels under both physoxia and chronic hypoxia in SiHa and HeLa cells (Figure 18B). By contrast, treatments with the selective mTORC1 inhibitor Rapamycin, the AKT inhibitor VIII or incubation under high glucose concentrations had no decreasing effect on P-NDRG1 (T346) levels (Figure 18B). These results indicate that the mTORC2-PDK1-SGK1 axis is critically involved in the phosphorylation of NDRG1 at Thr346, in line with previous studies[207,270], and that this regulation occurs not only under chronic hypoxia but also under physiological oxygen concentrations.

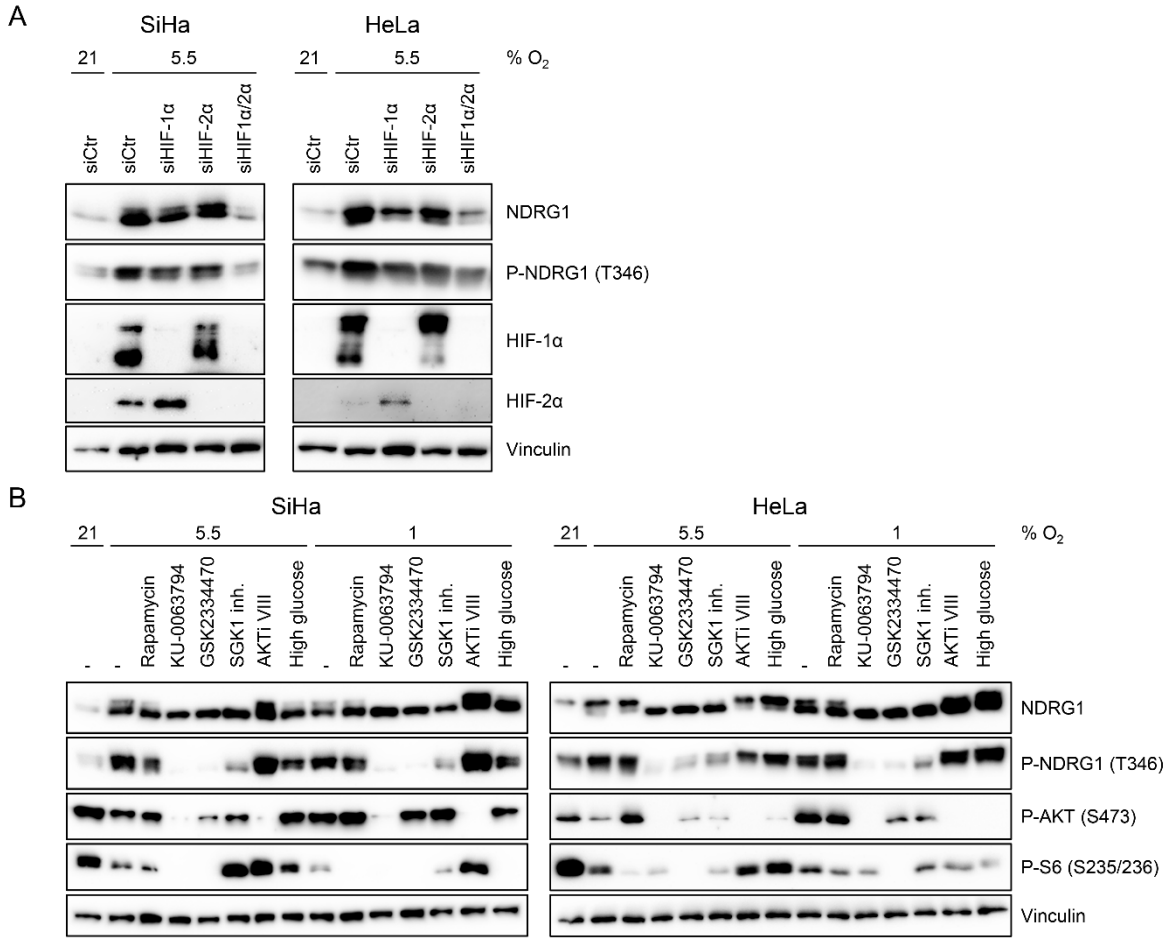

Figure 18. The regulation of NDRG1 expression and phosphorylation is largely comparable under physoxia and chronic hypoxia.

(A) SiHa and HeLa cells were transfected with control siRNA (siCtr) or siRNAs targeting HIF-1α and HIF-2α, alone or in combination, and cultured for 24 h under 5.5% O_2. Cells under normoxia (21% O_2) transfected with siCtr served as control. Immunoblot analyses of NDRG1, phosphorylated (P-)NDRG1 (T346), HIF-1α and HIF-2α are shown. Vinculin, representative loading control. (B) SiHa and HeLa cells were treated with 50 nM Rapamycin, 5 µM KU-0063794, 5 µM GSK2334470, 20 µM SGK1 inhibitor (inh.), 10 µM AKTi VIII, high glucose (4.5 g/L glucose) or DMSO as solvent control (-) under 21% O_2, 5.5% O_2 or 1% O_2 for 24 h. Immunoblot analyses of NDRG1, P-NDRG1 (T346), P-AKT (S473) and P-S6 (S235/236) are shown. Vinculin, representative loading control.

In conclusion, these findings demonstrate that the regulation of both total and T346-phosphorylated NDRG1 protein levels is comparable in cervical cancer cells under physoxia and chronic hypoxia. Moreover, once the biological activities of NDRG1 are better characterized[195,214], it will be interesting to investigate whether its increased expression under physoxia compared to normoxia may differentially affect the phenotype of cervical cancer cells. Of note, these NDRG1 activities would not be detectable under the normoxic conditions of standard cell culture.

2.4.2 CycH is characterized by a unique proteome signature and downregulation of luminal lysosomal proteins

SiHa cells under cycH exhibit a unique proteome signature and can be clearly distinguished from the other tested oxygen conditions (Figure 15A). Given the profound effects of cycH on the phenotype of HPV-positive cervical cancer cells and their therapeutic response, as shown earlier, these proteome changes may help to reveal the underlying molecular mechanisms.

In differential expression analyses, using a threshold of $log_2FC \geq 0.58$ or ≤ 0.58 and an adjusted p-value of ≤ 0.05, the levels of 43 proteins were significantly changed under cycH (as depicted for the H phase) compared to physoxia (Figure 19A). Strikingly, I found that the levels of several luminal lysosomal proteins (marked in orange) were significantly reduced under cycH compared to physoxia, including Legumain (LGMN), Alpha-L-fucosidase 1 (FUCA1), Hexosaminidase subunit A and B (HEXA and HEXB), Gamma-glutamyl hydrolase (GGH) and members of the cathepsin (CTS) family, whereas the levels of Lysosome-associated membrane glycoproteins 1 and 2 (LAMP1 and LAMP2, marked in purple) remained largely unaffected (Figure 19A). Interestingly, the levels of luminal lysosomal proteins were also downregulated under chronic hypoxia (1% O_2) compared to physoxia, although largely not as pronounced as observed under cycH (Figure 19B and 19C).

In line with these results, GSEA using MSigDB revealed that lysosome-associated gene sets were significantly negatively enriched under cycH (H phase) compared to physoxia (Figure 19D), including the gene set “KEGG_LYSOSOME” (NES: -2.34; FDR q value < 0.001) (Figure 19E). Additionally, several gene sets related to vascular transport, active transmembrane transporter activity, and iron uptake and transport were positively enriched under cycH (H phase) compared to physoxia (Figure 19D).

In summary, these findings uncover pronounced differences in global protein expression under cycH compared to physoxia and chronic hypoxia. Strikingly, cycH induces a significant downregulation of luminal lysosomal proteins in SiHa cervical cancer cells, which I further analyzed in the following.

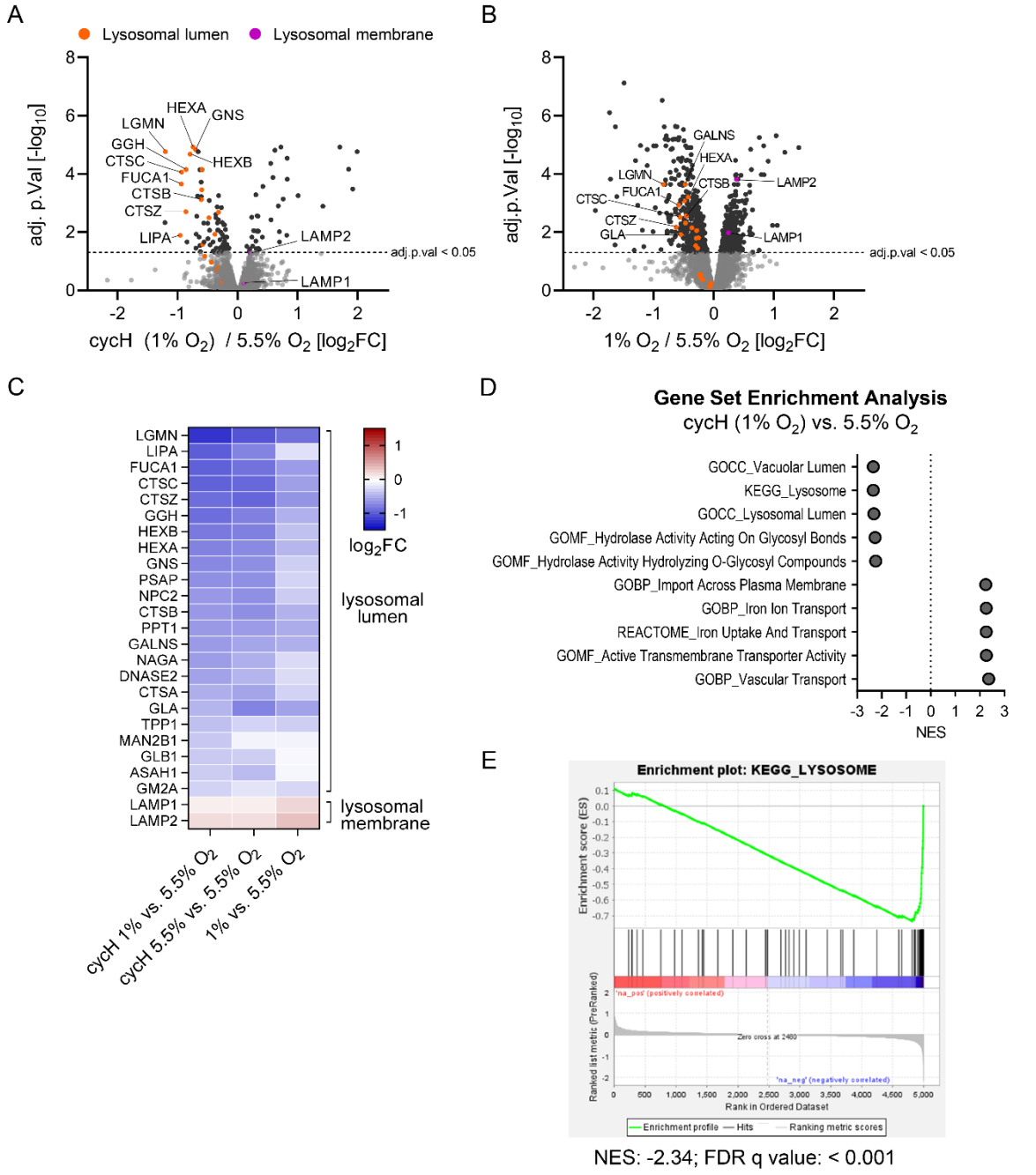

Figure 19. CycH has a unique proteomic signature that is characterized by a significant downregulation of luminal lysosomal proteins.

(A) Proteome changes in SiHa cells cultivated for 24 h under cycH (H phase) compared to 5.5% O_2, quantified by mass spectrometry (n = 4). Volcano plot displaying log_2 fold change (log_2FC) ratios of protein levels (x-axis) and adjusted (adj.) p-value ($-log_{10}$) (y-axis). LIMMA analysis with Benjamini Hochberg correction was performed and cutoff for significance was set to adj. p-value ≤ 0.05 (horizontal dashed line). Grey color of dots indicates non-significantly changing protein levels, black color indicates significantly changing protein levels. Selected hits are highlighted and categorized by color code. (B) Proteome changes in SiHa cells cultivated for 24 h under chronic hypoxia (1% O_2) compared to 5.5% O_2, detected and analyzed as described in subfigure A. (C) Heat map showing log_2FC values of lysosome-associated proteins that contribute to the negative core enrichment of the gene set „KEGG_LYSOSOME“ under cycH vs. 5.5% O_2. Changes in protein expression under cycH (H and R phases) and chronic hypoxia are shown in pairwise comparisons to 5.5% O_2.

Figure 19. Continued (D) GSEA comparing SiHa cells cultivated under cycH (H phase) vs. 5.5% O_2. Average log2FC values (n = 4) of all proteins were used as input for preranked GSEA with 1000 permutations. Top five ranks of positively and negatively enriched gene sets are shown with their normalized enrichment score (NES; P < 0.05). Gene Ontology (GO) annotations: CC, Cellular Component; MF, Molecular Function; BP, Biological Process. (E) Enrichment plot of the gene set "KEGG_LYSOSOME". FDR, false discovery rate.

2.5 Effects of cycH on lysosomal pathways in cervical cancer cells

2.5.1 The levels and total enzymatic activities of mature CTSB and CTSL are reduced under chronic hypoxia and cycH

To further elucidate the potential consequences of the reduced luminal lysosomal protein levels in HPV-positive cervical cancer cells under cycH compared to physoxia, I focused on cathepsins, particularly on Cathepsin B (CTSB) and Cathepsin L (CTSL). Cathepsins are synthesized as immature, inactive proenzymes and are sorted to the lysosomes, where they are processed into their mature, active forms.[138] Notably, cathepsins not only play a crucial role in lysosomal catabolism, but have also been associated with the regulation of apoptosis[148,151,156], which may be interesting in view of my findings that cycH is linked to increased resistance towards the pro-apoptotic effects of Cisplatin.

Incubation of SiHa and HeLa cells under chronic hypoxia or cycH only slightly affected the transcript levels of *CTSB* and *CTSL*, if at all, compared to normoxia (Figure 20A). Strikingly, however, compared to either normoxia or particularly physoxia, the levels of the mature protein forms of both CTSB and CTSL were strongly reduced under chronic hypoxia and in both cycH H-R phases (Figure 20B). Interestingly, the decrease in mature CTSL protein levels under cycH was also detected in HPV-negative HCT116 colorectal cancer cells and, to a smaller extent, in A549 lung cancer cells (Figure 20C). These results suggest that cycH reduces the levels of mature cathepsins across cell lines of different tumor entities, independent of their HPV status.

To test whether the reduction of the mature cathepsin protein levels under cycH is reflected by changes in cathepsin activities, I measured the activities of CTSB and CTSL in cells cultivated under different oxygen conditions using fluorescently labeled substrates. Cells under normoxia treated with protease inhibitors (PI) served as negative control. In line with the decrease in mature cathepsin protein levels, the total activities of CTSB and CTSL were strongly reduced in SiHa and HeLa cells under chronic hypoxia and cycH, compared to the enzyme activity under physoxia (Figure 21). In HeLa cells, the total CTSB and CTSL activities were also reduced under normoxia compared to physoxia (Figure 21). These findings indicate that chronic hypoxia and cycH can negatively affect the proteolytic function of cathepsins in cervical cancer cells.

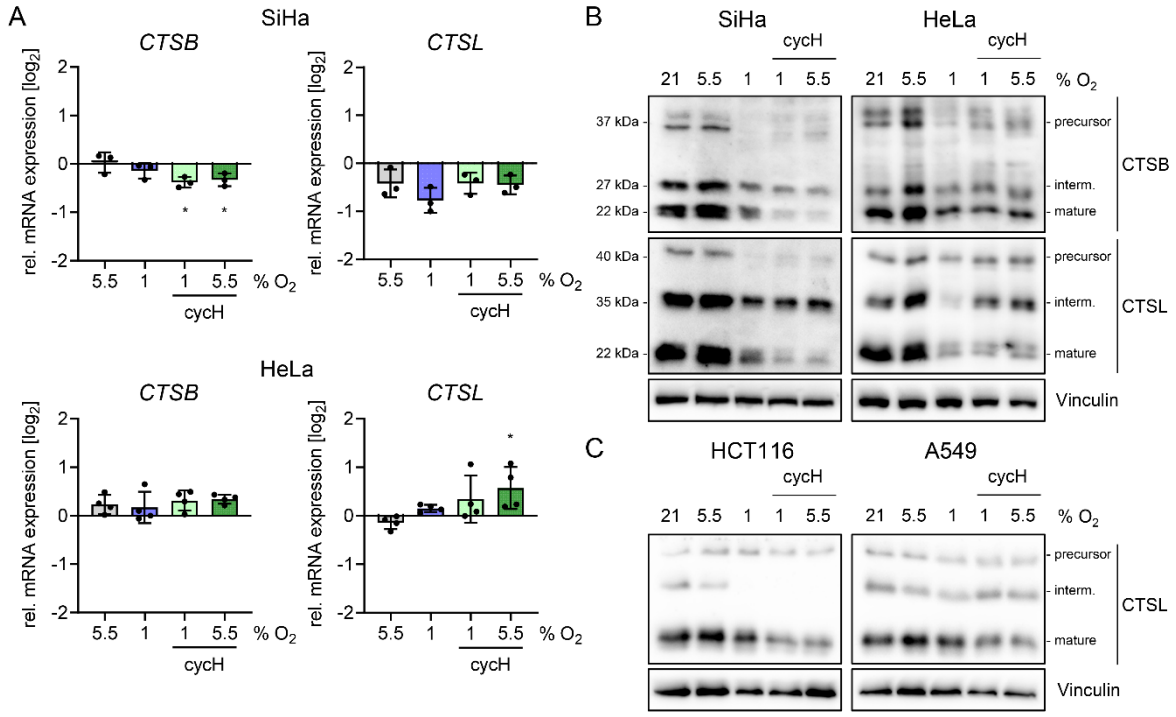

Figure 20. The levels of mature lysosomal cathepsins are reduced under cycH.

(A) Cathepsin B (*CTSB*) and Cathepsin L (*CTSL*) transcript levels determined by qRT-PCR in SiHa and HeLa cells cultivated under 21% O_2, 5.5% O_2, 1% O_2 or cycH for 24 h. Individual data points and mean expression levels are shown relative to the expression under 21% O_2 (log_2). Error bars represent standard deviations of biological replicates (n = 3). Asterisks indicate statistical significance as determined by one-way ANOVA (*, $p < 0.05$). (B) Corresponding immunoblot analyses of CTSB and CTSL in SiHa and HeLa cell lysates under different oxygen conditions. (C) CTSL protein levels in HCT116 and A549 cells cultivated under 21% O_2, 5.5% O_2, 1% O_2 or cycH for 24 h. Interm., intermediate cathepsin precursor. Vinculin, representative loading control.

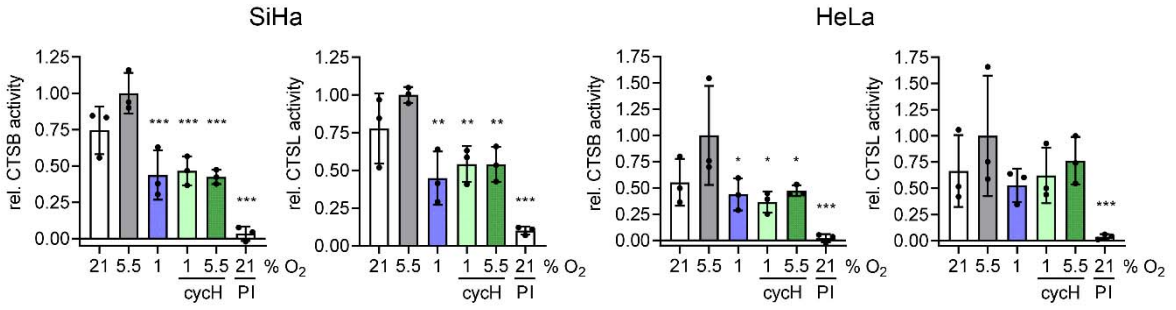

Figure 21. Chronic hypoxia and cycH reduce the total enzymatic activity of cathepsins in cervical cancer cells.

Enzymatic activities of CTSB and CTSL in SiHa and HeLa cells after 24 h under 21% O_2, 5.5% O_2, 1% O_2 or cycH. Cells under normoxia treated with protease inhibitors (PI) were used as negative control. Mean activity levels relative to the enzyme activity under 5.5% O_2 (set to 1.0) are shown. Error bars represent standard deviations of 3 independent experiments. Asterisks indicate statistical significance as determined by one-way ANOVA (*, $p < 0.05$; **, $p < 0.01$; ***, $p < 0.001$).

As *CTSB* and *CTSL* transcript levels were largely unaffected under chronic hypoxia and cycH, other reasons for the reduction in mature luminal lysosomal enzymes include for instance aberrant trafficking of lysosomal precursors and subsequent secretion into the extracellular space.[138] To investigate whether different oxygen conditions affect the trafficking of lysosomal enzymes from Golgi to lysosomes, I investigated the secretion of cathepsin precursors into the extracellular space. Notably, immature CTSB and CTSL proenzymes were particularly enriched in the supernatant of SiHa and HeLa cervical cancer cells under cycH and to less extent under chronic hypoxia (Figure 22). These results raise the possibility that both chronic hypoxia and cycH interfere with the proper trafficking of lysosomal enzymes, as observed for CTSB and CTSL.

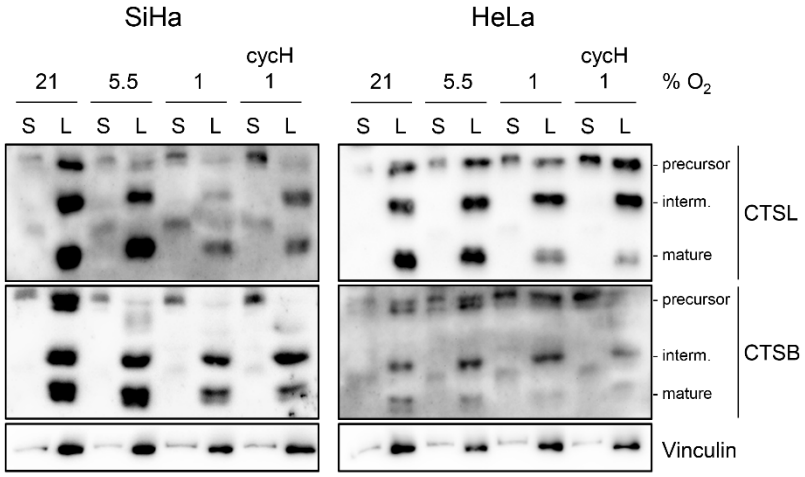

Figure 22. Levels of extracellular, immature cathepsins are increased in cervical cancer cells under cycH and chronic hypoxia.

Protein levels of CTSB and CTSL in SiHa and HeLa cells cultivated for 24 h under different O_2 conditions, analyzed by immunoblot. Secretion of immature cathepsin precursors was assessed in cellular supernatants. Interm., intermediate cathepsin precursor; S, supernatant; L, lysate. Vinculin, representative loading control.

Using CTSL as an example, I examined its protein levels in SiHa and HeLa cells under different oxygen conditions over time to gain further understanding of its regulation during prolonged oxygen deprivation. Under chronic hypoxia and cycH, CTSL protein levels progressively decreased and became barely detectable after 48 to 72 h in both cell lines, which is in strong contrast to the sustained CTSL protein expression under physoxia (Figure 23A).

To evaluate whether the downregulation of CTSL protein levels under chronic hypoxia and cycH could be related to the increased glycolysis rates and limited glucose availability under hypoxia, I cultivated SiHa and HeLa cells in media containing different glucose concentrations. Strikingly, glucose withdrawal (0 g/L glucose) reduced CTSL protein levels under all tested oxygen conditions compared to physiologic serum glucose concentrations (1 g/L) (Figure 23B). In contrast, unphysiologically high concentrations of glucose (4.5 g/L) strongly increased the levels of precursor, intermediate and mature forms of CTSL protein under both chronic hypoxia and cycH (Figure 23B).

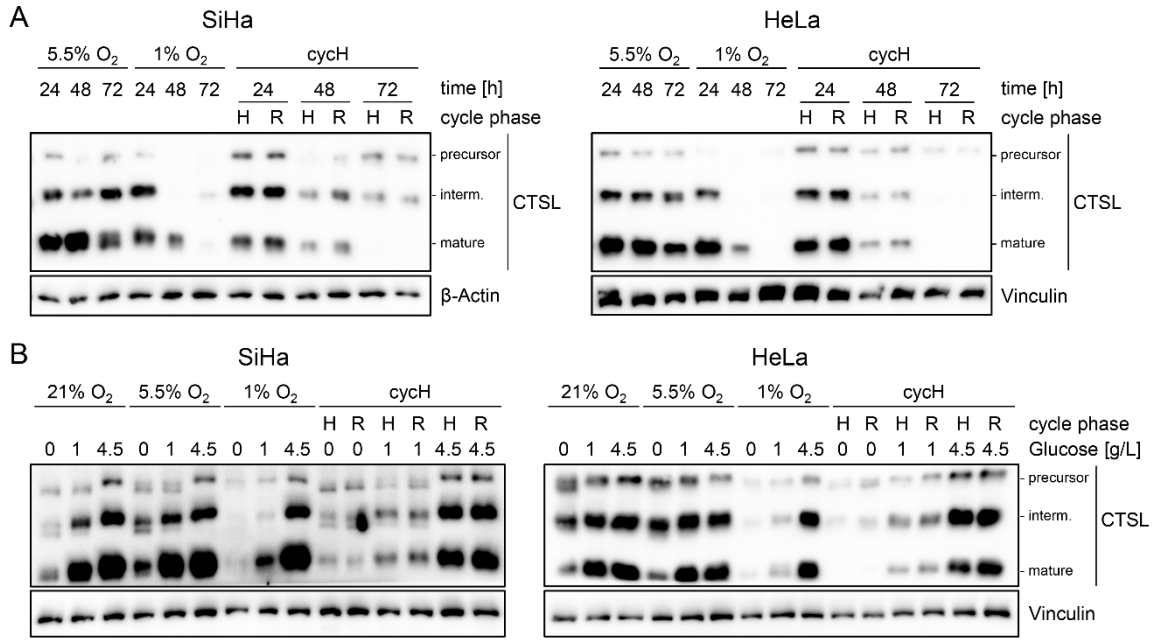

Figure 23. The downregulation of CTSL under chronic hypoxia and cycH is time- and glucose-dependent.

(A) Immunoblot analyses of CTSL protein levels in SiHa and HeLa cells cultivated under 5.5% O_2, 1% O_2 or cycH for 24 h, 48 h, and 72 h. (B) Immunoblot analyses of CTSL protein levels in SiHa and HeLa cells cultivated under different O_2 conditions in the presence of the indicated amounts of glucose for 24 h. Interm., intermediate cathepsin precursor. Vinculin and β-Actin, loading controls.

In summary, both chronic hypoxia and cycH, as compared to normoxia and physoxia, reduced the levels of mature cathepsin proteins and the total cathepsin enzymatic activity in HPV-positive cervical cancer cells. In addition, the levels of extracellular, immature cathepsins increased under both hypoxia forms. Furthermore, the downregulation of cathepsin protein levels under chronic hypoxia and cycH, as demonstrated for CTSL, is time- and glucose-dependent, which is particularly relevant when considering the oxygen- and glucose-deprived environment in solid tumors.

2.5.2 Cisplatin-induced apoptosis in cervical cancer cells involves lysosomal membrane permeabilization and the release of cathepsins into the cytoplasm

In addition to their key role in autophagy and the proteolytic degradation of lysosomal contents, cathepsins are involved in the regulation of cell death, depending on the cathepsin type and the cellular context.[158] Upon lysosomal membrane permeabilization, cathepsins can be released into the cytoplasm and trigger pro-apoptotic signaling by cleaving procaspases, BID or BCL-2 homologues.[158,160] Therefore, I investigated whether the hypoxia-linked reduction of mature and active CTSB and CTSL, which both have been described to possess pro-apoptotic potential[125,160], may contribute to the increased resistance of HPV-positive cervical cancer cells to pro-apoptotic chemotherapy with Cisplatin, particularly under cycH.

To examine the release of potentially pro-apoptotic cathepsins from lysosomes into the cytoplasm, I performed subcellular fractionation of Cisplatin-treated SiHa and HeLa cells.

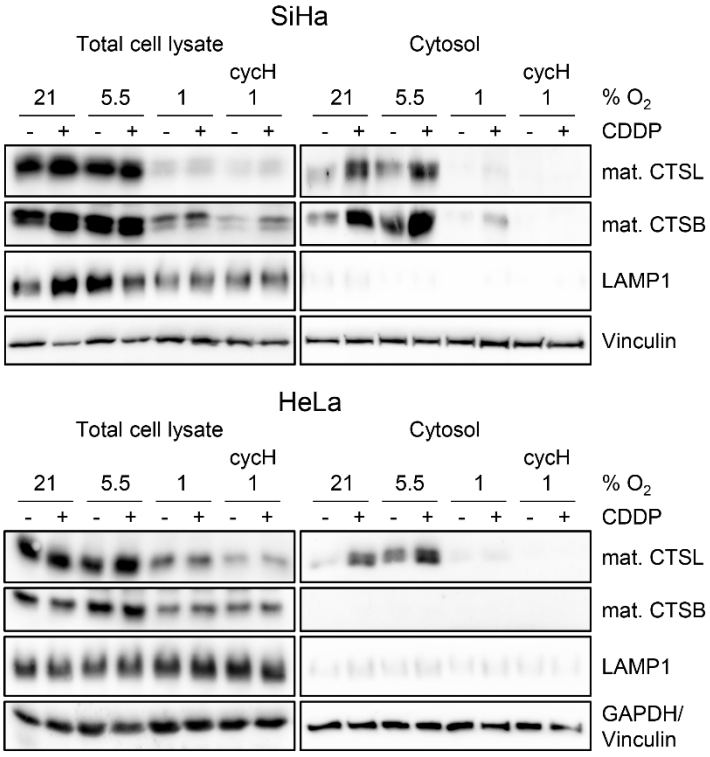

Figure 24. The cytosolic release of cathepsins in response to Cisplatin treatment is impaired under chronic hypoxia and cycH.

Immunoblot analyses of mature (mat.) CTSL and CTSB in total cell lysates (left panels) and cytosolic fractions (right panels) of SiHa and HeLa cells treated for 24 h with 30 µM (SiHa) or 15 µM (HeLa) CDDP under different oxygen conditions. Analysis of the lysosomal membrane marker LAMP1 shows that the cytosol is efficiently depleted of lysosomes. Vinculin, representative loading controls; GAPDH, loading control for HeLa total cell lysate.

Cisplatin treatment did not critically affect the levels of mature CTSL or CTSB protein in the total cellular lysate of SiHa and HeLa cells under any of the tested oxygen concentrations (Figure 24, left panels). However, Cisplatin-treated SiHa cells under normoxia and physoxia exhibited increased levels of mature CTSL and CTSB in their cytoplasm compared to untreated cells (Figure 24, right panels). This was equally shown for mature CTSL in HeLa cells, whereas no mature CTSB was detected in the cytosolic fraction of this cell line. Interestingly, the Cisplatin-induced increase of cytosolic mature CTSL and CTSB was strongly impaired or undetectable in cells under chronic hypoxia or cycH (Figure 24, right panels), indicating that the release of potentially pro-apoptotic cathepsins into the cytosol is strongly impeded.

2.5.3 Lack of evidence that the Cisplatin response of cervical cancer cells is dependent on lysosomal protease activity

Based on the striking differences observed in the cytoplasmic release of mature CTSL and CTSB upon Cisplatin treatment under different oxygen conditions, I assessed whether the activity of lysosomal proteases influences the response of HPV-positive cancer cells to Cisplatin. To inhibit cellular cysteine cathepsin activities, I applied the cysteine protease inhibitor E64 or the CTSB inhibitor CA-074-Me. E64 irreversibly inhibits several cysteine proteases including CTSB, CTSL and CTSK, papain, actinidin, calpain and others.[271] CA-074-Me is a potent CTSB inhibitor but also reduces CTSL activity to some extent.[272] By applying 10 µM E64 and 1 µM CA-074-Me, CTSB activity and CTSL activity were efficiently inhibited in SiHa or HeLa cells, respectively (Figure 25A), confirming their functionality in cervical cancer cells under the experimental conditions.

Next, SiHa and HeLa cells were pre-treated with E64 or CA-074-Me for 4 h under normoxia, physoxia, chronic hypoxia or cycH before being exposed to pro-apoptotic concentrations of Cisplatin (Figure 25B). Notably, the combination of E64 or CA-074-Me with Cisplatin did not appreciably change the levels of the apoptosis marker cl. PARP in SiHa or HeLa cells under any of the tested oxygen conditions (Figure 25C). These findings indicate that the differences in cysteine protease activities, particularly of CTSL and CTSB, are not responsible for the differential response of cervical cancer cells to pro-apoptotic Cisplatin treatment under different oxygen conditions.

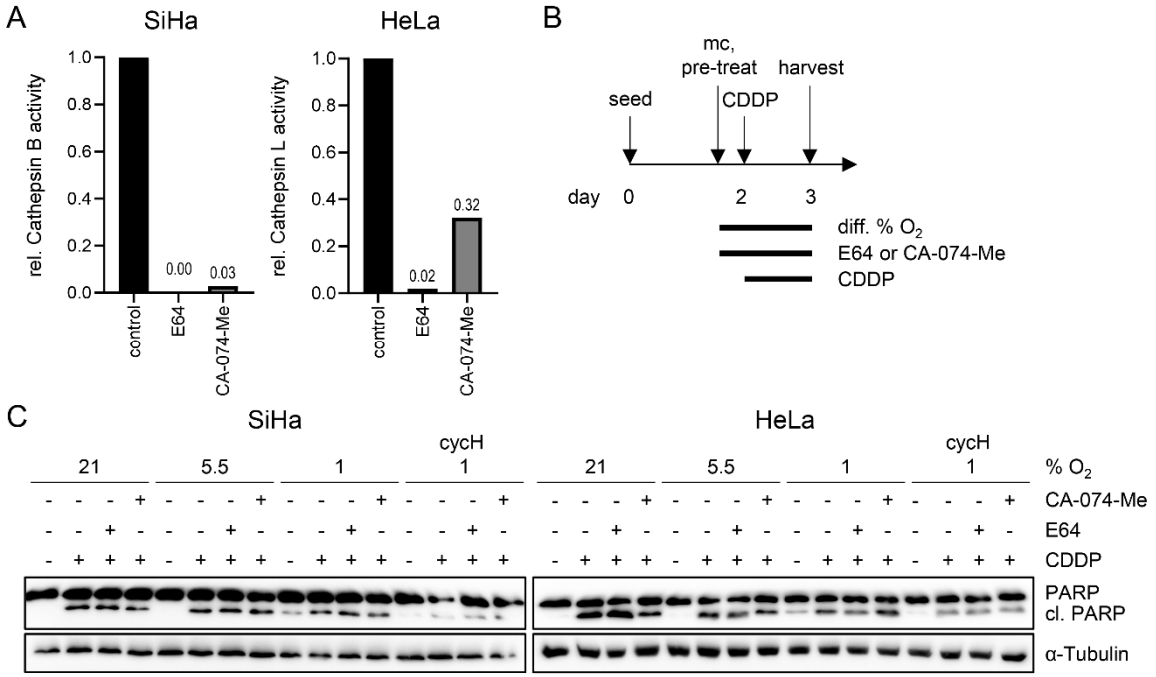

Figure 25. Cathepsin activity does not affect Cisplatin-induced apoptosis.

(A) Enzymatic activity of CTSB in SiHa cells and of CTSL in HeLa cells after 24 h treatment with 10 µM E64 or 1 µM CA-074-Me under 21% O_2, compared to control (-) (set to 1.0) (B) Scheme for combination treatment with protease inhibitors and CDDP used in subfigure C. mc, medium change; diff, different. (C) SiHa and HeLa cells under 21% O_2, 5.5% O_2, 1% O_2 or cycH were pre-treated for 4 h with 10 µM E64, 1 µM CA-074-Me or DMSO as solvent control (-) before being exposed to 30 µM (SiHa) or 15 µM (HeLa) CDDP for 24 h. Levels of PARP and cl. PARP were analyzed by immunoblot. α-Tubulin, representative loading control.

2.5.4 CycH reduces autophagic flux in HPV-positive cervical cancer cells

The decrease in active lysosomal enzymes observed in cervical cancer cells under chronic hypoxia and cycH also potentially affects other important lysosomal functions that could critically influence the cellular phenotype and the response to pro-apoptotic chemotherapy. Lysosomes play an important role in cellular signaling cascades and are pivotally involved in autophagy to maintain energy homeostasis.[134]

Interestingly, I observed an increased accumulation of the autophagosomal marker protein LC3B-II in cervical cancer cells under cycH compared to normoxia, physoxia or chronic hypoxia (Figure 26A). Consistent with this, SiHa cells cultivated under cycH displayed a visibly increased amount of LC3B puncta, some of which colocalize with LAMP1, compared to cells under physoxia or chronic hypoxia (Figure 26B).

To further investigate the impact of cycH on autophagic flux in cervical cancer cells, I treated SiHa and HeLa cells with the autophagy inhibitor Bafilomycin A1 (BafA1). BafA1 is a potent inhibitor of the lysosomal proton pump V-ATPase and interferes with lysosomal

acidification, which was also evidenced by the significant decline of CTSL protein levels (Figure 26C).[273] BafA1 treatment resulted in a noticeable accumulation of LC3B-II protein in both SiHa and HeLa cells under normoxia and physoxia, indicating active autophagic flux (Figure 26C). Under chronic hypoxia, only a slight increase of LC3B-II levels was detected upon BafA1 treatment, indicating a reduced autophagic flux (Figure 26C). Strikingly, the levels of LC3B-II, which were already considerably elevated under cycH, did not further increase after BafA1 treatment, implying a strong reduction of autophagic flux under cycH (Figure 26C). Accompanying immunofluorescence analyses in HeLa cells confirmed the increase in LC3B puncta formation after BafA1 treatment under normoxia and, to less extent, under chronic hypoxia. Under cycH, LC3B staining was already pronounced in solvent control treated cells and only showed marginal increase after BafA1-mediated autophagy inhibition (Figure 26D).

Starvation of cells, for instance by cultivating them in amino acid and serum-free medium such as Earle's Balanced Salt Solution (EBSS), potently induces autophagy.[274] To analyze whether the decreased autophagic flux under cycH can be reinduced, HeLa cells under normoxia, chronic hypoxia or cycH were grown in EBSS for 4 h and simultaneously exposed to BafA1 or Chloroquine (CQ). CQ is another established autophagy inhibitor that increases the lysosomal pH and inhibits the fusion of autophagosomes and lysosomes.[275] Interestingly, EBSS-induced starvation increased CTSL protein levels under all tested oxygen conditions, although to slightly different extents (Figure 26E). Moreover, EBSS-induced starvation at most slightly increased the autophagic flux under normoxia, as indicated by the analysis of LC3B-II levels after combined EBSS and BafA1 treatment compared to BafA1 treatment alone (Figure 26E). This finding indicates that the ‘basal’ autophagy levels in HeLa cells under normoxia are relatively high. Under chronic hypoxia, simultaneous treatment with EBSS and BafA1 visibly increased LC3B-II levels compared to BafA1 treatment alone (Figure 26E). Interestingly, EBSS treatment under cycH visibly reduced LC3B-II levels and restored autophagic flux as evidenced by a marked increase in LC3B-II levels after co-treatment with EBSS and BafA1 or CQ (Figure 26E).

Taken together, these results suggest that autophagic flux is reduced in cervical cancer cells under hypoxic conditions compared to normoxia or physoxia. Interestingly, cervical cancer cells under cycH are characterized by a particular accumulation of autophagosome-associated LC3B protein. However, in response to amino acid and serum starvation, autophagic flux can be reinitated under cycH as well as under chronic hypoxia.

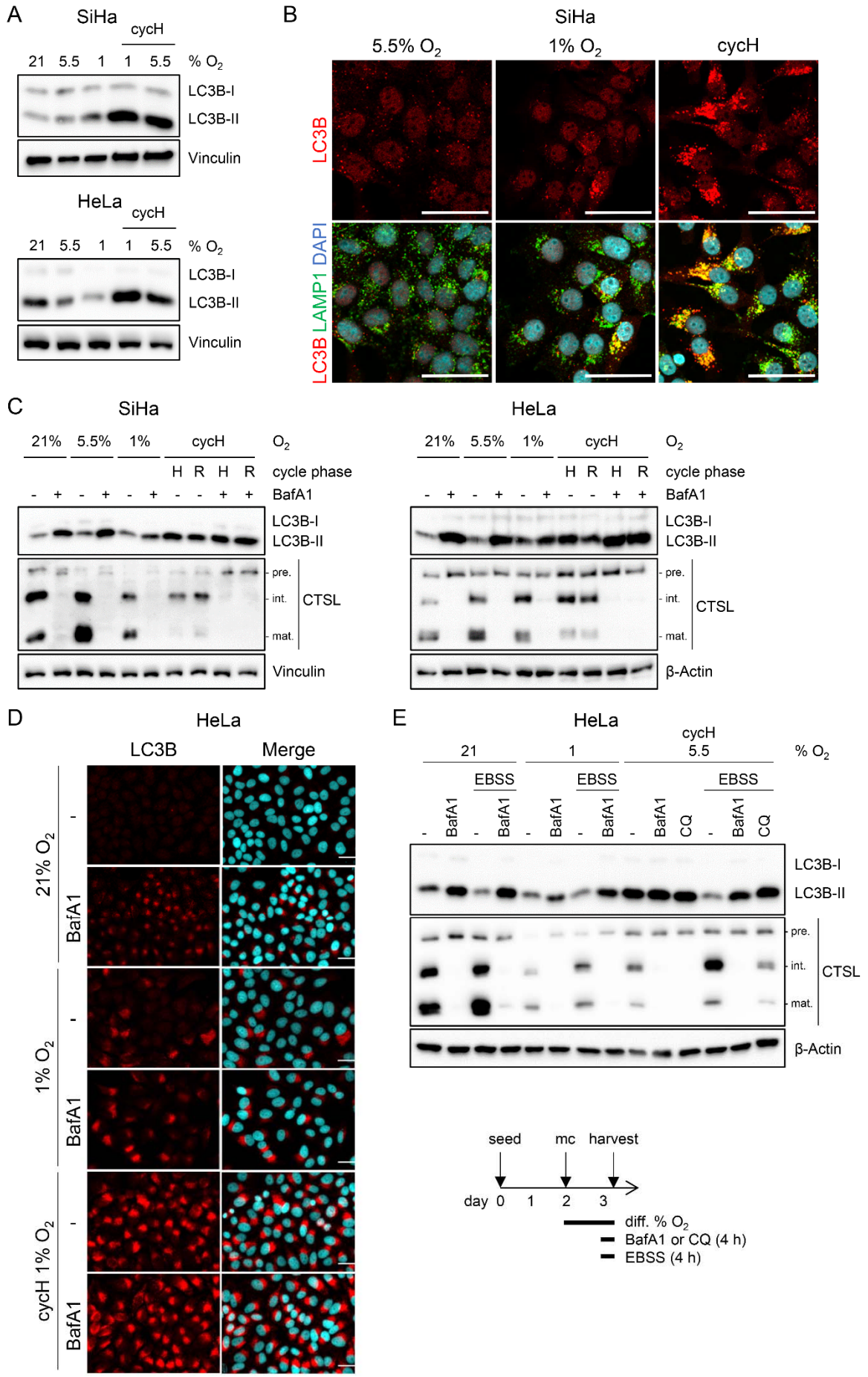

Figure 26. *See figure legend on the next page.*

Figure 26. Autophagic flux is reduced under cycH but can be restored upon amino acid and serum starvation.

(A) Immunoblot analyses of LC3B protein levels in SiHa and HeLa cells cultivated under 21% O_2, 5.5% O_2, 1% O_2 or cycH for 24 h. (B) LC3B (red) and LAMP1 (green) co-staining in SiHa cells after 72 h cultivation under 5.5% O_2, 1% O_2 or cycH, analyzed by immunofluorescence. Nuclei are counterstained with DAPI. Scale bars: 50 µm. (C) LC3B and CTSL protein levels in SiHa and HeLa cells cultured under different oxygen conditions for 24 h, analyzed by immunoblot. Cells were treated with DMSO (-) or 100 nM BafA1 for 4 h before harvesting. Cells under cycH were harvested in both the H or R phases. (D) Immunofluorescence analyses of LC3B in HeLa cells treated with 100 nM BafA1 under 21% O_2, 1% O_2 or cycH as described in subfigure C. Nuclei are stained with DAPI. Scale bar: 50 µm. (E) HeLa cells were cultured under 21% O_2, 1% O_2 or cycH for 24 h and treated as depicted in the experimental workflow (lower panel). Cells were treated with DMSO (-), 100 nM BafA1 or 50 µM Chloroquine (CQ) and incubated in EBSS for 4 h before harvesting, as indicated. Pre, precursor; Int., intermediate; mat. mature cathepsin form; mc, medium change; diff, different. Vinculin and β-Actin, loading controls.

2.5.5 Acidic vesicular organelles accumulate under chronic hypoxia and cycH

To investigate the effects of cycH on acidic vesicles in more detail, I performed acridine orange (AO) stainings. AO is an acidotropic dye that emits green fluorescence when it intercalates into DNA and red fluorescence when it is trapped in acidic vesicular organelles (AVOs) such as endosomes and autolysosomes.[276,277]

SiHa and HeLa cells cultivated under normoxia, physoxia, chronic hypoxia or cycH were stained with AO and analyzed by flow cytometry or fluorescence microscopy (Figure 27). Intriguingly, flow cytometry analyses revealed a noticeable increase in the mean red fluorescence intensity in SiHa cells under chronic hypoxia or cycH compared to normoxia and physoxia (Figure 27A, left panel). The mean green fluorescence intensity, however, remained relatively consistent across the different oxygen conditions (Figure 27A, right panel). These findings were supported by corresponding microscopy analyses that also showed enhanced staining of red fluorescent AVOs in SiHa cells under chronic hypoxia and cycH in comparison to normoxia and physoxia (Figure 27B). Similar results were observed in HeLa cells (Figure 27C and 27D).

These findings suggest that cervical cancer cells under chronic hypoxia and cycH exhibit an increase in the number and/or the volume of AVOs, including endosomes and lysosomes, as compared to cells under normoxia and physoxia. Interestingly, previous studies have shown that a deficiency in luminal lysosomal enzyme activity and a reduction in autophagic flux can lead to the accumulation of acidic vesicles.[278,279] This result thus supports the notion that lysosomal and autophagic processes may be impaired in cervical cancer cells exposed to hypoxic conditions.

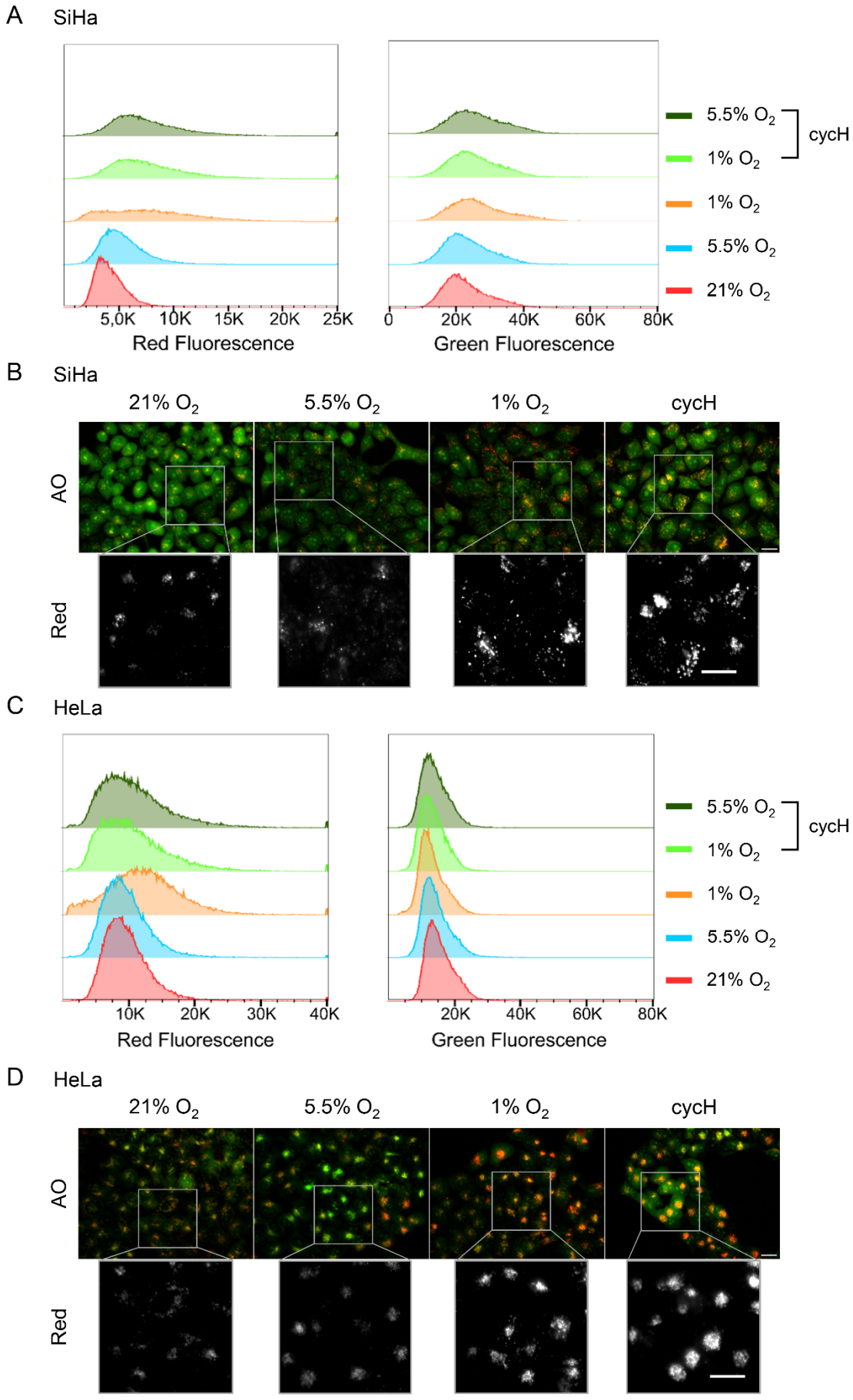

Figure 27. *See figure legend on the next page.*

Figure 27. Acidic vesicular organelles accumulate under chronic hypoxia and cycH.
SiHa and HeLa cells were cultivated under 21% O_2, 5.5% O_2, 1% O_2 or cycH for 24 h. Subsequently, cells were stained with AO for 15 min and analyzed directly by flow cytometry or fluorescence microscopy. (A) Flow cytometry analysis of AO-stained SiHa cells under different oxygen conditions. Histograms depict the fluorescence intensity values of red fluorescence (~ 680 nm, acidic organelles) and green fluorescence (~ 530 nm, nucleic acids). (B) Corresponding fluorescence microscopy of AO-stained SiHa cells. For better visualization of acidic vesicles, red channel images of AO-stained cells were further magnified and displayed in grey scale. Scale bar: 50 µm. (C) Flow cytometry analysis and (D) Fluorescence microscopy of AO-stained HeLa cells, as further detailed in subfigures A and B. Representative images of three independent experiments are shown.

2.5.6 Autophagy inhibitors can sensitize cervical cancer cells to Cisplatin treatment

The regulation of lysosomal function and autophagy in cancer cells recently gained the attention of the scientific community as promising therapeutic targets and autophagy modulators are increasingly explored as chemosensitizers in cancer therapy.[166] Therefore, I next tested whether the interference with autophagy, either by chemical inhibition using CQ or by genetic silencing of Autophagy protein 5 (ATG5), affects the response of HPV-positive cervical cancer cells to Cisplatin under different oxygen conditions.

The combination of prolonged CQ treatment and Cisplatin effectively inhibited autophagic flux, reduced the levels of mature CTSL and increased the levels of LC3B-II under all oxygen conditions in both SiHa and HeLa cells (Figure 28). Furthermore, the co-treatment of CQ and Cisplatin strongly increased the levels of the apoptosis markers cl. PARP and cl. Caspase 9 under normoxia and physoxia in SiHa and HeLa cells compared to Cisplatin treatment alone (Figure 28). Notably, the levels of cleaved apoptosis markers were also elevated to a large extent in cells co-treated with CQ and Cisplatin under chronic hypoxia or cycH (Figure 28).

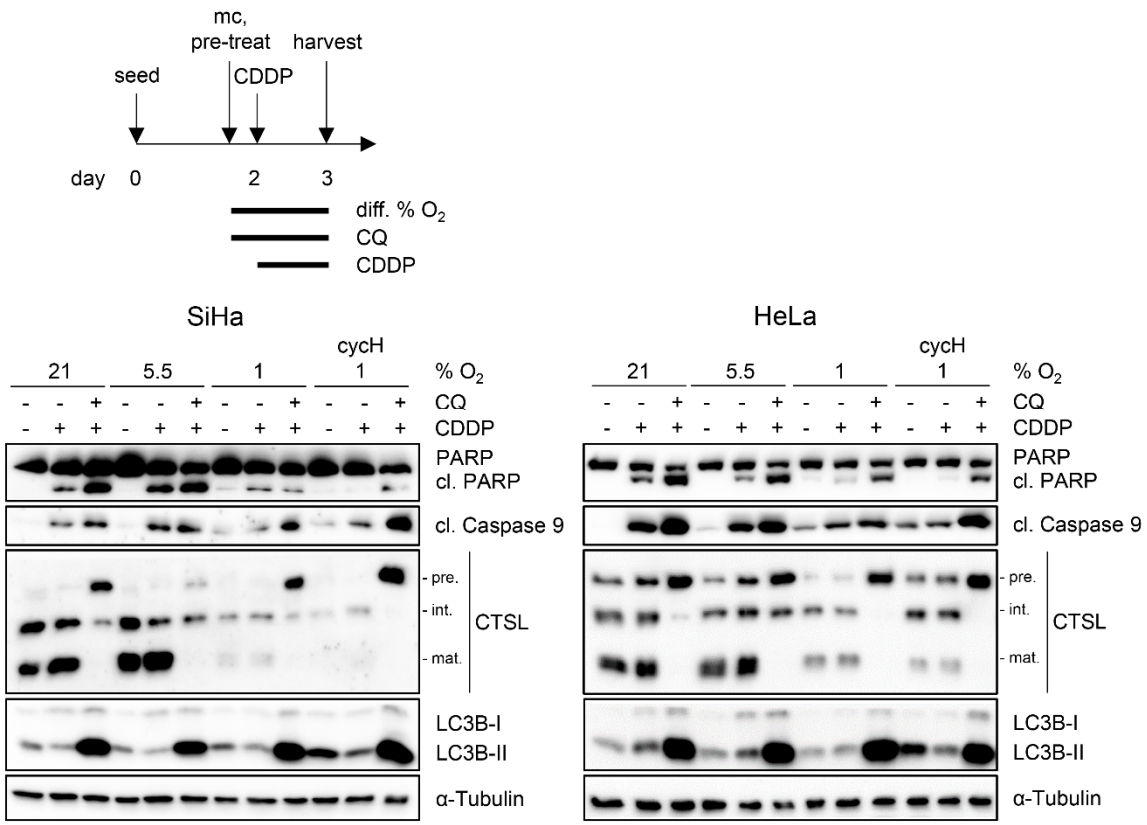

Figure 28. Chemical autophagy inhibition can sensitize cervical cancer cells to Cisplatin-induced apoptosis.

SiHa and HeLa cells cultivated under 21% O_2, 5.5% O_2, 1% O_2 or cycH were pre-treated for 4 h with 50 nM CQ or DMSO as solvent control (-) and subsequently treated with 30 µM (SiHa) or 15 µM (HeLa) CDDP for 24 h, as indicated. Immunoblot analyses show the protein levels of PARP, cl. PARP, cl. Caspase 9, CTSL and LC3B. Pre, precursor; int., intermediate; mat. mature cathepsin form; mc, medium change; diff, different. α-Tubulin, representative loading control.

In order to inhibit autophagy more specifically, I combined an RNAi-mediated knockdown of ATG5 expression with pro-apoptotic doses of Cisplatin in SiHa and HeLa cells. ATG5 plays an indispensable role in the autophagy initiation process and the extension of the phagophore membrane. Hence, ATG5 silencing is a common approach to genetically inhibit autophagy.[276,280]

Consistent with the findings from the combination of CQ and Cisplatin treatment, repression of ATG5 strongly enhanced the pro-apoptotic effects of Cisplatin in SiHa and HeLa cells under all tested oxygen concentrations, as indicated by increased levels of cl. PARP and cl. Caspase 9 compared to control siRNA-transfected cells (Figure 29A). As an exception, the increase in cleaved apoptosis markers upon ATG5 knockdown was not detected in HeLa cells under chronic hypoxia. This discrepancy might be due to the effects of the transfection procedure under chronic hypoxia, as evidenced by the

increased levels of cl. PARP and cl. Caspase 9 also in control siRNA-transfected cells (Figure 29A). Strikingly and irrespective of efficient ATG5 depletion, Cisplatin-treated cells under cycH still exhibited clearly reduced levels of cleaved apoptosis markers, compared to cells treated under normoxia or physoxia (Figure 29A). Accompanying TUNEL analyses confirmed the increased sensitivity of SiHa and HeLa cells to Cisplatin-induced apoptosis upon ATG5 knockdown compared to control siRNA-transfected cells under the tested oxygen conditions (Figure 29B).

Taken together, these results indicate cooperative pro-apoptotic effects of autophagy inhibition through CQ or ATG5 knockdown combined with Cisplatin treatment in cervical cancer cells. Importantly, autophagy inhibition can also sensitize cervical cancer cells under chronic hypoxia or cycH to Cisplatin treatment, suggesting a potential strategy for more efficient therapeutic targeting of these chemoresistant cell populations.

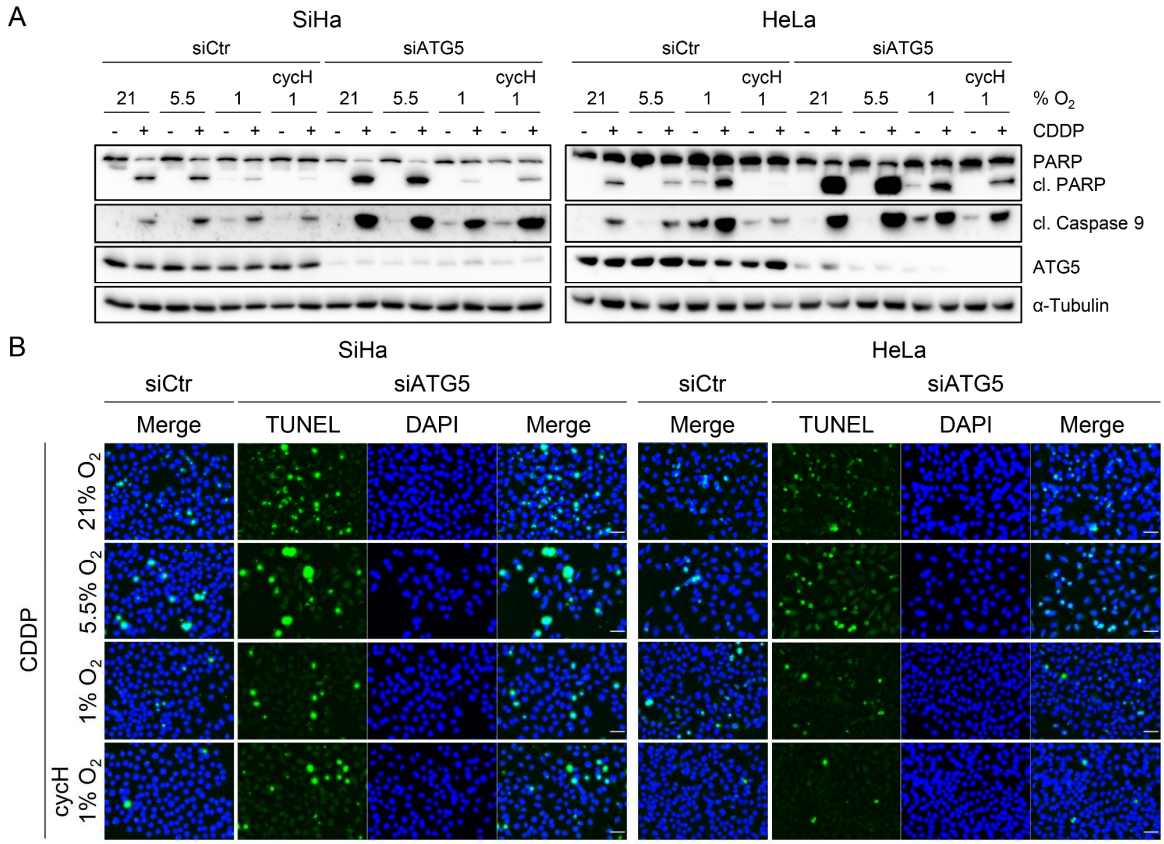

Figure 29. ATG5 knockdown enhances Cisplatin-induced apoptosis in cervical cancer cells.

(A) SiHa and HeLa cells were transfected with control siRNA (siCtr) or an ATG5-targeting siRNA (siATG5) and treated with 30 µM (SiHa) or 15 µM (HeLa) CDDP for 24 h under 21% O_2, 5.5% O_2, 1% O_2 or cycH. Immunoblot analyses of PARP, cl. PARP, cl. Caspase 9, and ATG5 are shown. α-Tubulin, representative loading control. (B) Corresponding TUNEL analyses of SiHa and HeLa cells transfected with siCtr or siATG5 and treated as described in subfigure A. Nuclei are counterstained with DAPI. Scale bar: 50 µm. Representative images of two biological replicates yielding consistent results are shown.

2.6 Comparative analyses of apoptosis signaling cascades in response to Cisplatin treatment under different oxygen conditions

2.6.1 Cisplatin-induced apoptosis is caspase-dependent

To identify factors that are responsible for the reduced apoptosis induction in cervical cancer cells under cycH in response to Cisplatin, I next investigated the role of caspases, the key regulators of apoptosis signaling.[95] Co-treatment with the pan-caspase inhibitor Z-VAD-FMK significantly reduced the levels of cl. PARP in Cisplatin-treated SiHa and HeLa cells under normoxia, physoxia, chronic hypoxia, and cycH (Figure 30). These findings indicate that caspase activity is essential for Cisplatin-induced apoptosis, even under conditions of oxygen deprivation.

Additionally, I analyzed the expression of the truncated BID (tBID) protein in SiHa and HeLa cells after Cisplatin treatment. tBID can be generated from BID by activated Caspases 8 and 10 in response to apoptotic stimuli, and it promotes the pro-apoptotic cascade by facilitating MOMP.[119] Interestingly, the levels of tBID showed a clear correlation with the levels of cl. PARP in Cisplatin-treated cervical cancer cells under all tested oxygen conditions, with the lowest tBID levels detectable under cycH. Moreover, I observed a similar reduction in pro-apoptotic tBID levels upon co-treatment with Z-VAD-FMK and Cisplatin (Figure 30).

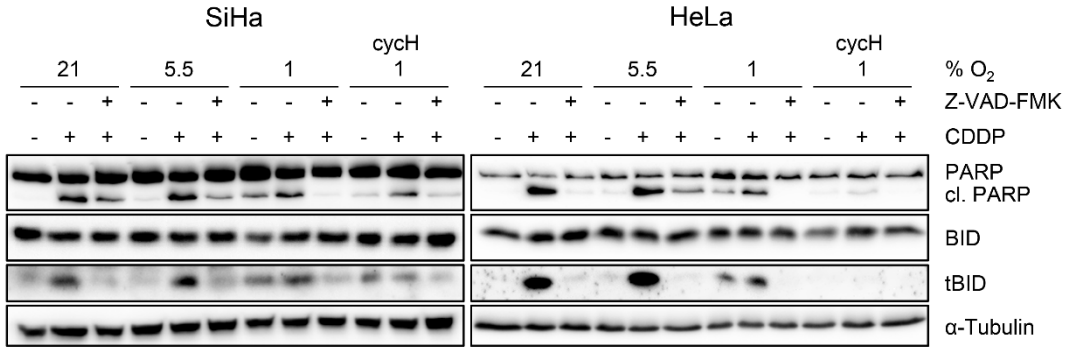

Figure 30. Cisplatin-induced apoptosis is caspase-dependent.

SiHa and HeLa cells cultivated under 21% O_2, 5.5% O_2, 1% O_2 or cycH were pre-treated for 4 h with 30 µM Z-VAD-FMK and subsequently exposed to 30 µM (SiHa) or 15 µM (HeLa) CDDP for 24 h. Protein levels of PARP, cl. PARP, BID and tBID were analyzed by immunoblots. α-Tubulin, representative loading control.

These results demonstrate that Cisplatin-induced apoptosis in HPV-positive cancer cells is highly dependent on caspase activity, irrespective of the present oxygen conditions. Furthermore, the pro-apoptotic effects of Cisplatin are associated with an increase in tBID levels, which are strongly reduced in Cisplatin-treated cells under cycH.

2.6.2 CycH reduces MOMP induction and cytosolic Cyt c release in Cisplatin-treated cervical cancer cells

Following BID activation, a key event in the apoptosis cascade is the induction of MOMP and the cytosolic release of pro-apoptotic mitochondrial proteins, such as Cyt c.[109,112] Therefore, I next investigated the effects of Cisplatin on the induction of MOMP in SiHa and HeLa cells under different oxygen conditions.

Strikingly, whereas Cisplatin treatment under normoxia, physoxia or chronic hypoxia led to a clear accumulation of Cyt c in the cytosol of SiHa and HeLa cells, this response was strongly impaired in Cisplatin-treated cells under cycH (Figure 31).

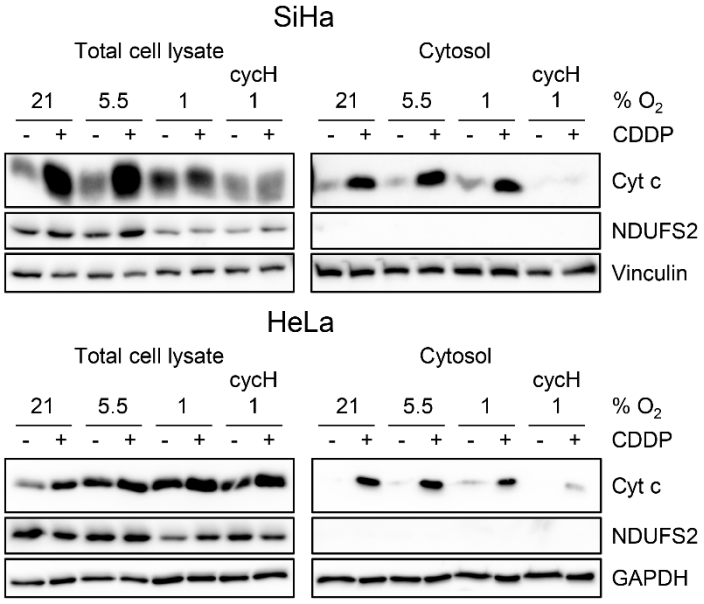

Figure 31. Cisplatin-induced MOMP is reduced under cycH.

Immunoblot analyses of Cyt c levels in total cell lysates (left panels) and cytosolic fractions (right panels) of SiHa and HeLa cells treated for 24 h with 30 µM (SiHa) or 15 µM (HeLa) CDDP under the indicated oxygen conditions. Analysis of the inner mitochondrial membrane protein NDUFS2 shows that the cytosolic fraction is efficiently depleted of mitochondria. Vinculin and GAPDH, representative loading controls.

Collectively, my results show that Cisplatin treatment of cervical cancer cells under cycH results in reduced activation of tBID, which correlates with diminished Cisplatin-induced MOMP and less efficient induction of apoptosis in comparison to cells treated under normoxia, physoxia or chronic hypoxia.

2.6.3 BID activation via Caspase 8 is critical for Cisplatin-induced apoptosis in cervical cancer cells under different oxygen conditions

To further investigate the role of BID in the response of HPV-positive cervical cancer cells to pro-apoptotic Cisplatin treatment under different oxygen conditions, I silenced BID expression via RNAi in SiHa and HeLa cells. Intriguingly, BID knockdown strongly diminished the levels of the apoptosis markers cl. PARP and cl. Caspase 9 in Cisplatin-treated cells under all tested oxygen conditions (Figure 32A). These results reveal that BID activation plays a pivotal role in the regulation of Cisplatin-induced apoptosis in HPV-positive cervical cancer cells.

Caspase 8 is a well-characterized upstream regulator of BID cleavage.[119] Therefore, I next tested whether Caspase 8 is responsible for tBID activation in Cisplatin-treated cervical cancer cells. Transient knockdown of Caspase 8 expression using RNAi also resulted in decreased levels of cl. PARP and cl. Caspase 9 after Cisplatin treatment in SiHa and HeLa cells under normoxia, physoxia, chronic hypoxia or cycH (Figure 32B). Additionally, the Cisplatin-induced increase of pro-apoptotic tBID protein was reduced in Caspase 8-depleted SiHa and HeLa cells compared to control siRNA-transfected cells under all tested oxygen conditions (Figure 32B).

Collectively, these results indicate a key role of BID and Caspase 8 during Cisplatin-induced apoptosis in cervical cancer cells.

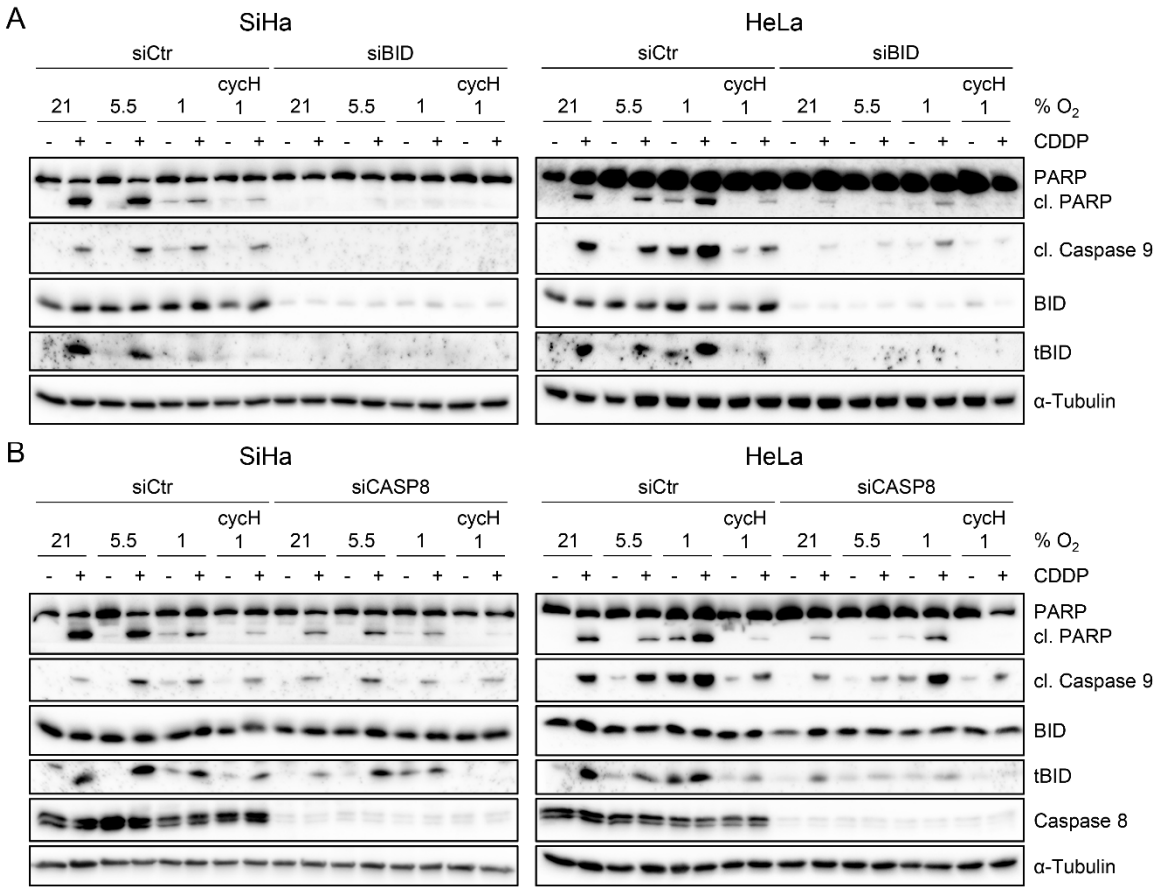

Figure 32. BID and Caspase 8 knockdown counteract Cisplatin-induced apoptosis in cervical cancer cells: Analysis of apoptosis markers.

SiHa and HeLa cells were transfected with control siRNA (siCtr) or either (A) a BID-specific siRNA (siBID) or (B) a Caspase 8-specific siRNA (siCASP8) and treated with 30 µM (SiHa) or 15 µM (HeLa) CDDP for 24 h under 21% O_2, 5.5% O_2, 1% O_2 or cycH. Immunoblot analyses of PARP, cl. PARP, cl. Caspase 9, BID, tBID, and Caspase 8 are shown. α-Tubulin, representative loading control.

The importance of BID and Caspase 8 in Cisplatin-induced apoptosis was further corroborated by accompanying TUNEL analyses. Silencing BID expression efficiently reduced the percentage of TUNEL-positive cells in Cisplatin-treated SiHa (Figure 33) and HeLa cells (Figure 34) under all tested oxygen conditions. Similarly, the number of TUNEL-positive cells after Cisplatin treatment was strongly reduced after Caspase 8 knockdown under normoxia, physoxia or chronic hypoxia, compared to control siRNA-transfected cells (Figure 33, Figure 34). However, no further reduction in TUNEL-positive cells under cycH, which were already very few, was detected.

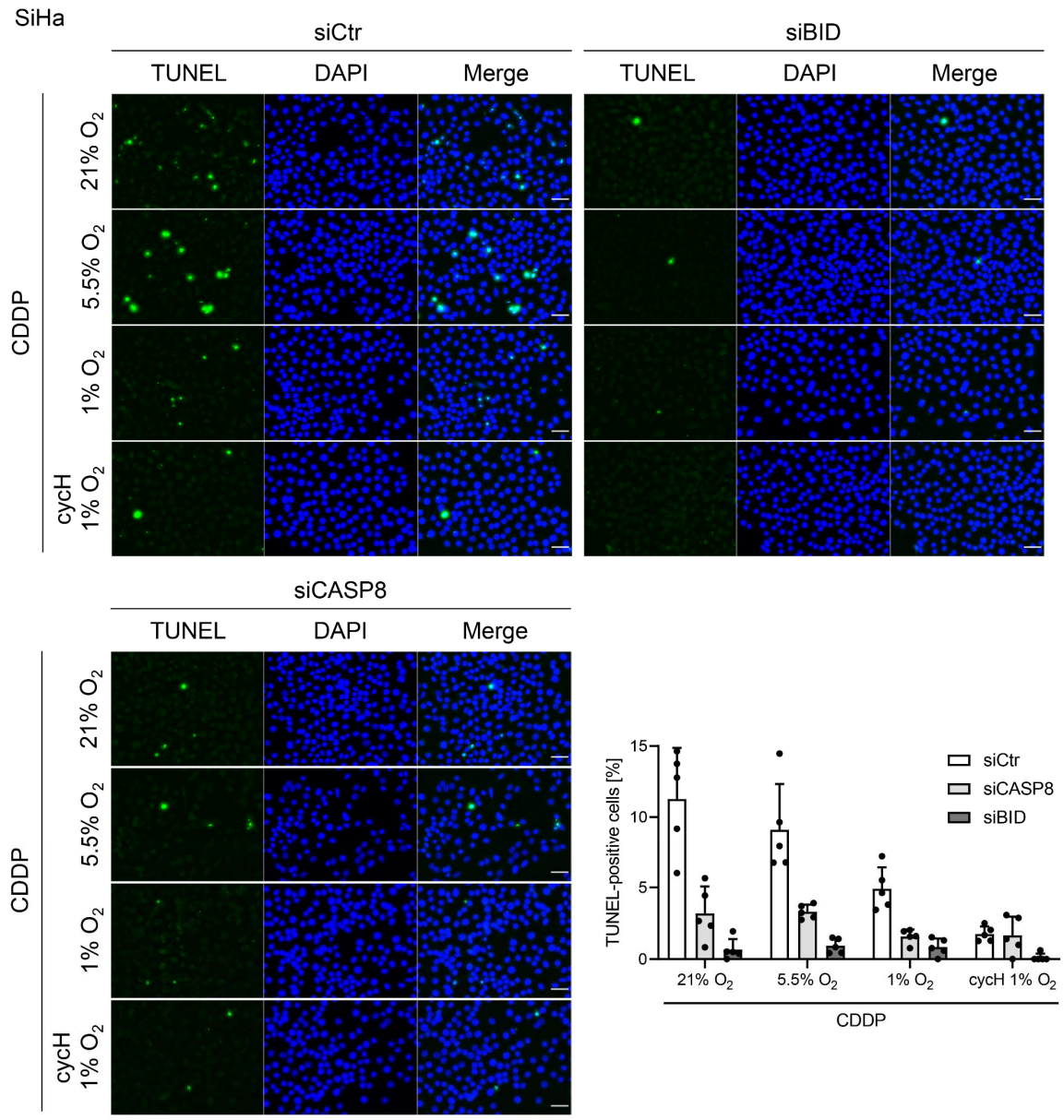

Figure 33. BID and Caspase 8 knockdown counteract Cisplatin-induced apoptosis in SiHa cervical cancer cells: TUNEL assays.

SiHa cells were transfected with control siRNA (siCtr), a BID-specific siRNA (siBID) or a Caspase 8-specific siRNA (siCASP8) and treated with 30 µM CDDP for 24 h under the indicated oxygen conditions. Nuclei are counterstained with DAPI. TUNEL-positive cells were quantified relative to the total number of DAPI stained cells from five different images per condition. Representative images of two biological replicates yielding consistent results are shown. Scale bar: 50 µm.

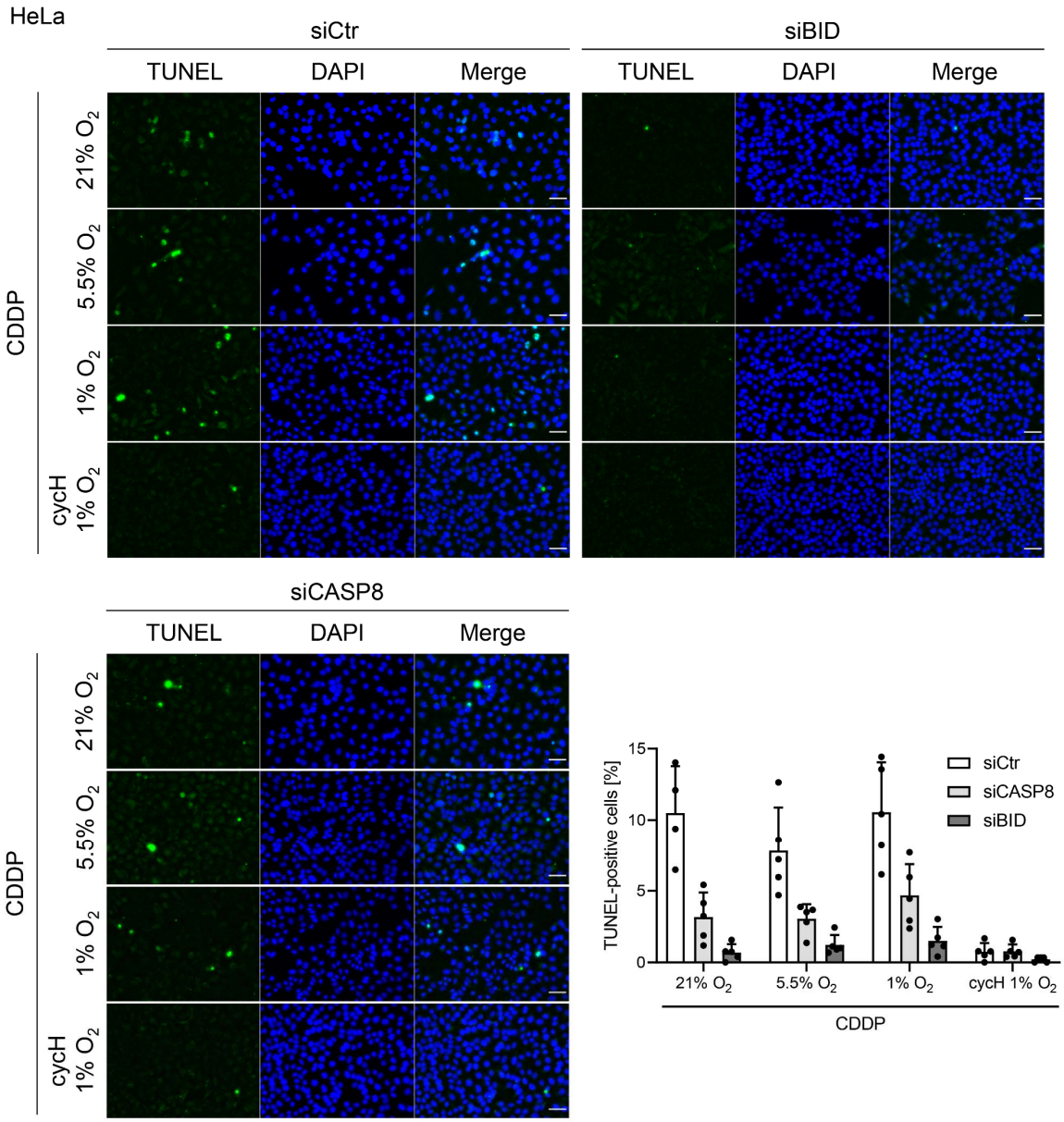

Figure 34. BID and Caspase 8 knockdown counteract Cisplatin-induced apoptosis in HeLa cervical cancer cells: TUNEL assays.

HeLa cells were transfected with control siRNA (siCtr), a BID-specific siRNA (siBID) or a Caspase 8-specific siRNA (siCASP8) and treated with 15 µM CDDP for 24 h under the indicated oxygen conditions. Nuclei are counterstained with DAPI. TUNEL-positive cells were quantified relative to the total number of DAPI stained cells from five different images per condition. Representative images of two biological replicates yielding consistent results are shown. Scale bar: 50 µm.

In conclusion, these results demonstrate the important role of Caspase 8 in the activation of tBID in Cisplatin-treated cervical cancer cells. The generation of tBID is a critical factor in the induction of apoptosis in response to Cisplatin treatment, and inhibiting BID efficiently protected cervical cancer cells against the pro-apoptotic effects of Cisplatin. Therefore, the reduced tBID levels in Cisplatin-treated cancer cells under cycH may contribute to their chemoresistant phenotype.

CHAPTER 3

DISCUSSION

3 Discussion

Although effective prophylactic vaccines against oncogenic high-risk HPV types are available, cervical cancer is predicted to remain a major global health concern for the next decades, particularly in low- and middle-income countries due to low immunization coverage.[281] Furthermore, the treatment of cervical cancers still constitutes a considerable therapeutic challenge and patients with advanced or recurrent cervical cancers often have a poor clinical prognosis.[28] Thus, understanding the molecular processes that govern the malignant phenotype of cervical cancer cells and their response to anticancer therapy is fundamental. The studies performed in this thesis provide first insights into the effects of cycH on the phenotype of HPV-positive cancer cells, uncovering significant alterations of virus/host cell interactions as well as of their overall proteome signature, lysosomal composition, autophagy regulation, senescence and apoptosis response, and susceptibility to chemotherapy.

3.1 Rationale for studying the effects of cycH in cervical cancer cells

Solid tumors, including cervical cancers, often comprise hypoxic subregions with oxygen concentrations below 1.5-2%.[171,173,282] These hypoxic regions are typically associated with increased resistance to chemo-, radio-, and immunotherapy, an elevated risk of tumor recurrence, and poor patient prognosis.[169,282,283] In the last decades, substantial progress has been made in understanding the effects of different forms of hypoxia on tumor cells with the aim to improve current therapeutic strategies to target hypoxic cancer cell populations more efficiently.[284]

Previously, our group provided evidence that chronic hypoxia (1% O_2) has a strong impact on the phenotype of HPV-positive cervical cancer cells, leading to a state of cellular dormancy.[224,225] This dormancy is characterized by a transient repression of the *E6/E7* oncogenes, that is in part mediated via hypoxia-induced PI3K/AKT signaling, and a reversible cell growth arrest, which can be reversed upon reoxygenation.[225,226] Furthermore, cells under chronic hypoxia can evade chemotherapy-induced senescence via hypoxia-linked impairment of mTORC1 activity and thus could provide a potent reservoir for tumor recurrence, e.g. following therapy-induced tumor shrinkage and improved access for residual tumor cells to oxygen.[225]

In this thesis, I aimed to investigate the phenotypic effects of a second major form of tumor hypoxia, cycling hypoxia (cycH), in HPV-positive cervical cancer cells, which were thus far unknown. Specifically, I focused on understanding the regulation of the virus/host

cell crosstalk, important cancer-related signaling pathways, and the response of cervical cancer cells to anticancer therapy under different oxygen conditions. During cycH, fluctuations in tissue perfusion cause recurring variations in oxygen supply for nearby tumor cells.[175] Intriguingly, as most cancer cells eventually undergo phases of hypoxia and reoxygenation, cycH is a prevalent form of hypoxia in solid tumors and is proposed to be the dominant form *in vivo*.[228,285] Notably, cycH and chronic hypoxia may cause distinct effects on molecular signaling pathways and cycH has been associated with an even more aggressive tumor behavior than chronic hypoxia.[175,230,232] Therefore, comprehensive investigations of the cellular phenotype and therapy resistance mechanisms, especially under cycH, are urgently required to develop novel strategies to therapeutically target hypoxic cell populations.

In the *in vitro* experimental setup, cycH was simulated by alternating between the reported median oxygen concentrations of healthy cervical tissue (ca. 5.5% O_2) and cervical cancers (ca. 1.2% O_2).[173] The effects of cycH on HPV-positive cancer cells were compared to normoxia (21% O_2, standard cell culture), physoxia (5.5% O_2) and chronic hypoxia (1% O_2). Furthermore, I cultivated the cells under physiological glucose levels (1 g/L) and generated an oxygen-glucose deprived environment over time, which is characteristic for hypoxic tumor regions.[286] It is important to note that *in vitro* cell culture studies have certain limitations. Firstly, cycH may not occur in consistently rhythmic patterns, but instead cycH is likely more variable in terms of duration and frequency. Secondly, the physiologic glucose supply during cycH also depends on blood perfusion and would thus alternate between hypoxic and reoxygenation phases. This is not covered in my experimental settings or other *in vitro* studies on cycH[236,239,242,247–249], in which medium glucose concentrations gradually decrease over time. My studies provide a suitable approach to investigate cycH in cervical cancer cells within an *in vitro* context, but it is important to validate and transfer my findings to *in vivo* settings to support their clinical relevance.

3.2 The virus/host cell crosstalk in HPV-positive cervical cancer cells under cycH

Interestingly, my experiments revealed significant phenotypic effects of cycH in HPV-positive cervical cancer cells that are distinct from the phenotypes under normoxia, physoxia, and chronic hypoxia. Firstly, I showed that the HPV *E6/E7* oncogene expression is largely maintained under cycH, which strongly contrasts the efficient *E6/E7* repression under chronic hypoxia. Moreover, the effects of E6/E7 on the regulation of the critical tumor suppressor proteins p53 and pRb, which are key cellular targets for the HPV-

induced transformation process, are preserved under cycH. This latter finding suggests that the HPV oncogenes contribute to the phenotype of cervical cancer cells under cycH. As a result, cervical cancer cells under cycH, in contrast to cells under chronic hypoxia, may benefit from the effects of E6 and E7 on the inhibition of apoptosis and the maintenance of cell proliferation.[21] However, I also showed that cervical cancer cells under cycH converge on the phenotype of cells under chronic hypoxia after prolonged exposure for up to 72 h, eventually resulting in the repression of viral oncoproteins and a decline in cell proliferation rates.

Regarding anticancer therapies, the sustained HPV E6/E7 oncoprotein expression under cycH is likely relevant to therapeutic approaches that specifically aim to target E6/E7 in HPV-positive cancers. For example, E6/E7 inhibitors could be less effective in cervical cancer cells exposed to chronic hypoxia, if their therapeutic targets are not expressed[225], whereas they could exhibit greater efficacy in cervical cancer cells under cycH, which maintain E6/E7 expression. Furthermore, the sustained expression of E6/E7 under cycH could favor the susceptibility of cervical cancer cells to immunotherapeutic strategies that target E6/E7-derived antigens presented on the cellular surface. In conclusion, the contrasting effects of chronic hypoxia and cycH on the viral E6/E7 oncoproteins show that the two forms of hypoxia differentially influence the virus/host cell crosstalk in cervical cancer cells, with distinct implications for the therapeutic success of specific antiviral strategies in HPV-positive cancers.

3.3 Oxygen-dependent phenotypic changes in cervical cancer cells

3.3.1 Physoxia induces the upregulation of hypoxia-associated factors

In addition to the oxygen-dependent effects on the virus/host cell crosstalk, I discovered several other unexpected alterations in HPV-positive cervical cancer cells in response to different oxygen conditions. These include, for instance, the upregulation of factors under physiological oxygen conditions, which are considered to be hypoxia-induced. For example, the HIF targets LOXL2[267] and SLC2A1[268] are significantly upregulated under physoxia compared to normoxia, hinting at an increased HIF transcriptional activity in cervical cancer cells under physoxia, which is not detected when performing experiments under standard cell culture conditions (normoxia). Indeed, HIF-related functions depend on the duration and degree of hypoxia and can be detected at physiologically relevant oxygen concentrations.[232,287] Importantly, elevated HIF signaling is a well-reported adaptation of tumor cells to upregulate pro-carcinogenic functions and thus could considerably influence tumorigenesis under physoxia.[288]

To gain further insights into physoxia-induced changes in HPV-positive cancer cells, I focused on NDRG1, a protein, which showed significant upregulation in cervical cancer cells under physoxia compared to normoxia. NDRG1 is widely considered to be a hypoxia-induced factor and possibly exerts oncogenic functions in cervical cancer cells.[200,217] In specific, elevated NDRG1 levels in cervical cancer have been associated with unfavorable prognosis, increased invasiveness, accelerated tumor growth, and increased resistance to chemoradiotherapy.[217,220] Therefore, NDRG1 has emerged as a promising therapeutic target in cancer research.[214] In my study, I showed that NDRG1 expression is already efficiently induced under physoxia in a HIF-1/HIF-2-dependent manner. In addition, the regulation of NDRG1 phosphorylation by SGK1 occurs similarly in HPV-positive cancer cells under physoxia and chronic hypoxia.

Collectively, these results implicate a need to re-evaluate so-called ‘hypoxia-induced’ genes carefully, since this designation often is based on comparing their regulation under hypoxia versus normoxia – yet they may be already considerably induced under physoxia.

3.3.2 Lysosomal alterations under cycH and chronic hypoxia

My studies also revealed that cervical cancer cells exposed to cycH are characterized by a unique proteome signature, which can be clearly distinguished from the proteome of cells cultivated under normoxia, physoxia or chronic hypoxia. As a major difference, I found that the levels of luminal lysosomal proteins are significantly downregulated under cycH, and to a lesser extent under chronic hypoxia, compared to the proteome of cervical cancer cells under physoxia. This finding is striking because lysosomes are important signaling hubs of the cell, affecting several critical cellular pathways, such as the regulation of cellular catabolism and homeostasis or the induction of different modes of cell death, including apoptosis.[134,147,148] The role of lysosomes in cancer progression and cell death is thus increasingly investigated, particularly regarding their potential as therapeutic targets in cancer cells.[145,147,148]

Several recent studies investigated the effects of tumor hypoxia on lysosomes. For instance, hypoxia-induced extracellular acidification leads to the redistribution of lysosomes from the perinuclear region to the cell periphery, which contributes to the inhibition of mTORC1 signaling.[289] Furthermore, hypoxia has been reported to inhibit lysosomal degradation of EGFR.[290]

Based on the results of my proteome analyses, which revealed a strong reduction in the levels of luminal lysosomal proteins, particularly under cycH, I investigated the regulation

and function of the cysteine cathepsins CTSB and CTSL in more detail. CTSB and CTSL are key enzymes for lysosomal catabolism, but also have been suggested to exert pro-apoptotic activity upon release from the lysosomes into the cytosol (see chapter 3.4.2.2 for more details).

Consistent with the reduction in mature CTSB and CTSL protein levels under chronic hypoxia and cycH, I observed a significant decrease in their total enzyme activities in cervical cancer cells under both hypoxia forms. It should, however, be noted that the proteolytic activity of cathepsins is not solely dependent on enzyme maturation but can also be influenced by factors such as pH and endogenous cathepsin inhibitors like stefins, cystatins, and kiniogens.[151] Interestingly, I also detected an increased secretion of cathepsin precursor forms into the extracellular space under cycH and chronic hypoxia. This raises the possibility that the maturation and activity of lysosomal enzymes under cycH and chronic hypoxia may be influenced, at least in part, by oxygen-dependent effects on lysosomal protein trafficking. In line with this, other studies have reported altered trafficking of lysosomes and lysosomal CTSD in breast cancer cells in response to hypoxia and/or extracellular acidification, resulting in increased secretion of lysosomal enzymes.[291,292]

Importantly, even though cathepsins are most active at a lysosomal pH of 4-5, several cathepsins can still exert proteolytic activity at higher pH levels.[151] This enables cathepsins to function outside of the endo-/lysosomal system, for instance when they are released into the extracellular space.[151,155] In cancer cells, extracellular cathepsins can contribute to ECM remodeling and the cleavage of cell adhesion molecules, promoting cancer cell migration and invasion.[151,155] Furthermore, extracellular cathepsins can activate pro-inflammatory cytokines and disrupt intracellular signaling pathways by cleaving cell surface receptors.[151,155]

Further, I found that CTSL protein levels decrease in a glucose-dependent manner in cervical cancer cells under cycH and chronic hypoxia. This possible connection between cathepsin activity and glucose availability is corroborated by similar findings in Ras-transformed fibroblasts.[293] Given the multifaceted and context-dependent functions of cathepsins within cancer cells, further insights in how their expression may intersect with hypoxia and glucose metabolism could be highly valuable.

Collectively, these findings underscore the need for further research on the functional role of intra- and extracellular cathepsins in cervical cancer cells, particularly under oxygen deprivation, which could be of substantial relevance for tumor cell adaptation, tumor growth, and therapy resistance mechanisms.

3.3.3 Effects of cycH on autophagy in cervical cancer cells

My results further indicated that autophagy, an important lysosomal catabolic process, is restrained in cervical cancer cells under cycH compared to normoxia or physoxia. This finding coincides with the observed reduction in mature lysosomal enzymes and their proteolytic function under cycH. HPV-positive cancer cells under cycH accumulated the autophagosomal marker protein LC3B-II and showed decreased autophagic flux compared to normoxia and physoxia. These observations contrast with studies that report an induction of autophagy under hypoxia in different cell systems, with both protective and detrimental effects.[235,294,295] For example, autophagy has been shown to play an essential role in the viability of MCF-7, HT29, and U373 tumor cells under cycH by clearing damage induced by reactive oxygen species.[235] However, it is important to consider that these studies were conducted in cells from different tumor entities, using different cycH setups, and may thus not be comparable without restrictions.

The regulation of autophagy in response to cellular stress, including hypoxia and nutrient starvation, is a finely balanced process. It is worth noting that, even though autophagy recycles proteins and damaged organelles to restore cellular energy levels, the autophagy process itself is energy-dependent.[296] Consequently, if the available energy resources are restricted, cancer cells may prioritize vital cellular functions over promoting autophagy.[297] This has been demonstrated in a recent study showing that glucose starvation blocks amino acid-induced autophagy in an AMPK-dependent mechanism.[297] Upon stress relief and glucose replenishment, cells can reinitiate autophagic flux and restore cellular homeostasis.[297] In light of these results, it could be hypothesized that cervical cancer cells under cycH adapt to the oxygen-glucose-deprived environment by inhibiting autophagic flux and thus preserve limited energy levels for other essential cellular processes. As autophagy can exert both tumor promoting and tumor suppressing functions depending on the cellular context, its contribution to the cellular phenotype of cervical cancer cells under cycH warrants further investigation.

3.4 Response of cervical cancer cells under cycH to cancer therapy

In previous studies, cycH has been associated with a more aggressive cellular phenotype, enhanced metastatic potential, and increased therapy resistance, particularly towards radiotherapy, in different cancer types.[175,230,232] So far, the effects of cycH on the therapy response of HPV-positive cervical cancer cells are unknown. In my thesis, I therefore investigated the response of cervical cancer cells under cycH to different anticancer treatments, including radio- and chemotherapy.

3.4.1 Radiotherapy

Radiotherapy is commonly applied to treat advanced cervical carcinomas.[28] During radiation therapy, ionizing radiation generates free radicals, which induce DNA double-strand breaks. Because the radical-induced DNA damage requires molecular oxygen to permanently 'fix' DNA lesions, hypoxic tumor cells are less radiosensitive than oxygenated tumor cells and represent a significant therapeutic challenge.[222,298,299]

In this study, I demonstrated that HeLa cervical cancer cells irradiated under chronic hypoxia or in the hypoxic phase of cycH are more resistant to γ-irradiation treatment compared to cells irradiated under normoxia, physoxia or in the reoxygenation phase of cycH. Supposedly, the oxygen concentrations present during the hypoxic and reoxygenation phases of cycH appear to influence the fixation of DNA damage and thus the response of cervical cancer cells to γ-irradiation. These findings differ to some extent from other studies that generally report a radioprotective effect of cycH, compared to normoxia as well as chronic hypoxia, without considering the two distinct H-R phases of cycH.[236,239,246,249] This increased radioresistance observed under cycH, also compared to chronic hypoxia, is suggested to be associated with the accumulation of HIF-1α and/or the reactive oxygen species formed under cycH.[236,239,241,243,246,249,256] Importantly, the cellular context and the applied parameters of cycH vary among existing studies and cannot be directly compared. Since the observed radioprotective effects of cycH on cervical cancer cells do not significantly differ from chronic hypoxia, further investigation into the underlying mechanisms was not pursued in more depth. However, the oxygenation status of cells should be carefully considered for the therapeutic success of radiotherapies in cervical cancer patients.

3.4.2 Chemotherapy

Chemotherapeutic strategies aim to inhibit cancer cell proliferation by inducing senescence, which is an irreversible growth arrest, and/or apoptosis, a programmed cell death.[79,260,262] The therapeutic outcome in cancer cells depends on the drug dose and the severity of DNA damage. While lower doses of chemotherapeutic agents can result in the induction of cellular senescence, higher doses can trigger apoptosis more efficiently.[72,262] To gain a comprehensive insight into the chemotherapy responses of HPV-positive cervical cancer cells, both pro-senescent and pro-apoptotic agents were tested under cycH and compared to their effects under other oxygen conditions.

3.4.2.1 Pro-senescent chemotherapy

Senescence is a permanent cell cycle arrest in response to various stressors, including telomere shortening, oxidative stress, and DNA damage.[263] Senescent cells cease cell division while remaining metabolically active and can induce a senescence-associated secretory phenotype (SASP) that activates an immune response and promotes the clearance of cancer cells.[263,300] However, therapy-induced senescence in cancer cells can also cause detrimental effects in certain contexts, as the pro-inflammatory SASP can favor tumor progression, angiogenesis, and chronic inflammation. Moreover, senescent cells appear more resistant to pro-apoptotic stimuli.[260,300]

The drug Etoposide is a reversible topoisomerase II inhibitor that is used for the treatment of different cancer types.[301,302] Etoposide interferes with DNA replication and causes DNA damage, which leads to the induction of cellular senescence or apoptosis, depending on the drug dose.[302] Previous studies of our group have demonstrated that HPV-positive cervical cancer cells under chronic hypoxia can escape the pro-senescent effects of Etoposide treatment due to the hypoxic impairment of mTORC1, which is required for an efficient induction of senescence.[182,225] Instead of undergoing senescence, cervical cancer cells under chronic hypoxia enter a state of dormancy and resume proliferation upon reoxygenation and drug release.[225]

In my experiments, I demonstrated that cervical cancer cells under cycH exhibit increased resistance to pro-senescent Etoposide treatment compared to cells under normoxia or physoxia. Notably, cells treated under cycH evade senescence induction to a similar extent as cells treated under chronic hypoxia. This is an interesting finding as I observed that mTORC1 signaling, which is a critical determinant for the conversion of transiently arrested cells to irreversibly arrested senescent cells[227], is differentially regulated under chronic hypoxia and cycH. Under chronic hypoxia, mTORC1 signaling is strongly impaired, favoring senescence evasion[225], whereas under cycH, active mTORC1 signaling is partially preserved in a cycH phase-dependent pattern. I found evidence of increased phosphorylation of the well-established markers for active mTORC1 signaling p70S6K, S6, and 4E-BP1 in the reoxygenation phases of cycH, which is rapidly reduced again in hypoxic phases of cycH. This dynamic regulation of mTORC1 activity in response to a fluctuating oxygen supply is corroborated by other studies.[252,303] However, the residual mTORC1 activity under cycH is apparently not sufficient to promote the efficient induction of senescence in response to Etoposide treatment. Instead, cervical cancer cells under cycH exhibited a similar capacity to evade pro-senescent chemotherapy as cells treated under chronic hypoxia, where mTORC1 activity is efficiently abrogated.

This finding was further underlined by analyzing a combined treatment with Etoposide and the mTOR inhibitors Rapamycin and KU-0063794 in cervical cancer cells under cycH. Inhibition of the remaining mTOR activity only slightly increased senescence evasion and the colony formation capacities of Etoposide-treated cells under cycH, indicating that mTOR activity levels under cycH are already sufficiently impaired to allow for senescence escape. In summary, cervical cancer cells under cycH can efficiently evade chemotherapy-induced senescence, which supports the notion that cycH is associated with increased therapy resistance.[247,248]

However, it should also be noted that the periodically active mTORC1 signaling observed under cycH could still affect the cellular phenotype, apart from the response to pro-senescent chemotherapy. For example, mTOR signaling is important for the regulation of cell growth and metabolism and the investigated mTORC1 targets p70S6K, S6, and 4E-BP1 all participate in the stimulation of mRNA translation.[250] Therefore, it is possible that cells under cycH may take advantage of partially restored mTORC1 activity during reoxygenation phases to facilitate intermittent protein synthesis and thereby enhance cell viability.

3.4.2.2 Pro-apoptotic chemotherapy

In addition to pro-senescent chemotherapy, a preferred therapeutic outcome is the induction of cell death.[79] Cisplatin is the main chemotherapeutic agent used in cervical cancer patients and possesses pronounced pro-apoptotic potential by inducing DNA damage through DNA inter- and intrastrand crosslinks.[66,73] In the present study, I thus investigated the response of cervical cancer cells to Cisplatin under different oxygen conditions. Strikingly, I found that HPV-positive cervical cancer cells under cycH exhibit increased resistance to pro-apoptotic Cisplatin treatment not only compared to cells under normoxia or physoxia, but also compared to cells under chronic hypoxia. These results are corroborated by findings in glioblastoma cells showing that chemoresistance under cycH can exceed the resistance observed under chronic hypoxia.[247,248] Furthermore, I observed that cervical cancer cells treated with Cisplatin under cycH eventually react with efficient senescence induction, while cells treated under normoxia, physoxia or chronic hypoxia do not enter senescence as they barely resist Cisplatin-induced apoptosis. The differences in senescence induction compared to Etoposide treatment could be explained by distinct modes of drug action. Cisplatin-induced damage persists even after treatment release, while Etoposide reversibly inhibits topoisomerase II.

Consequently, the question arose which factors may determine the particularly resistant phenotype of cervical cancer cells under cycH to pro-apoptotic Cisplatin treatment. Thus, I thoroughly evaluated potential hypotheses and functionally investigated candidate factors and pathways in more depth.

Most chemotherapeutic agents, including Cisplatin, preferentially target highly proliferating cells.[221] Therefore, the reduced cytotoxic effect of Cisplatin observed under both hypoxia forms could, at least in part, be attributed to the reduced proliferative capacity of these cells compared to normoxia or physoxia.[221] However, this cannot explain the observed differences in apoptosis induction in Cisplatin-treated cervical cancer cells under chronic hypoxia and cycH, since the cells exhibit higher proliferation rates under cycH than under chronic hypoxia, what should make cells under cycH more susceptible to the effects of Cisplatin. Consequently, differences in cell proliferation alone do not suffice to explain the particularly pronounced chemoresistant phenotype observed in cervical cancer cells under cycH.

Another important factor, which may influence the cellular phenotype of cervical cancer cells and their response to Cisplatin, is the expression of the HPV *E6/E7* oncogenes.[21] As found in my experiments, cervical cancer cells under cycH maintain viral *E6/E7* oncogene expression and their canonical transforming functions, which is a major difference to cells under chronic hypoxia. This could be relevant since genotoxic chemotherapeutic agents, such as Cisplatin, can repress the HPV oncogene expression.[264] Consequently, E6 can no longer mediate the degradation of p53, leading to an increase in p53 protein levels and the activation of its transcriptional target genes, such as *p21* and *bax,* which participate in the regulation of cell cycle arrest and apoptosis.[264,304] In the context of my study, Cisplatin treatment resulted in the reduction of E7 protein levels under normoxia and physoxia, in accordance with previous findings showing a downregulation of E6/E7 expression by a variety of chemotherapeutic agents.[264] However, this downregulation was also observed in my experiments under cycH. Under chronic hypoxia, E6/E7 expression is already suppressed in the absence of genotoxic treatment and cannot be further reduced by Cisplatin. Evidently, the pronounced differences in apoptosis induction by Cisplatin observed under the different tested oxygen conditions were not linked to differences in HPV oncoprotein expression, which was downregulated under all conditions.

An interesting finding of my proteome studies was the observation that the amounts of luminal lysosomal enzymes were reduced under chronic hypoxia and even more significantly under cycH. As mentioned above, apoptotic stimuli exerted by certain chemotherapeutic drugs can induce lysosomal membrane permeabilization, which leads

to the release of lysosomal enzymes, particularly of cathepsins, into the cytoplasm.[148,150] Cytoplasmic cathepsins can trigger and amplify cell death signaling pathways, for instance by cleaving pro-apoptotic BID or procaspases.[158] CTSB and CTSL both have been described to possess pro-apoptotic potential.[158–160] Therefore, I hypothesized that the reduction in mature cathepsin proteins and their proteolytic activity under cycH and chronic hypoxia could potentially contribute to the observed Cisplatin-resistant phenotype in comparison to cells under normoxia and physoxia. Indeed, I detected a strongly diminished or absent cytoplasmic release of mature cathepsins after Cisplatin treatment under cycH and chronic hypoxia compared to cells treated under normoxia or physoxia, which would be consistent with this hypothesis. However, inhibition of cathepsin activities, particularly of CTSB and CTSL, did not increase the resistance of cervical cancer cells to the pro-apoptotic effects of Cisplatin under any of the tested oxygen conditions. This indicates that these cathepsins do not play a decisive role for the susceptibility of cervical cancer cells to Cisplatin-induced apoptosis. This result differs from reports in other cancer cell models, indicating that the functional role of cathepsins in cell death may be cell- and context-dependent.[160] For instance, in Cisplatin-resistant A549 lung cancer cells, treatment with Cisplatin and CQ led to increased LMP and enhanced cell death mediated by cathepsins, which was partially independent of caspases.[305] Furthermore, a recent study has shown that Cathepsin L is involved in radiation-induced cell death in cervical cancer cells and SERPINB3, an intracellular cysteine protease inhibitor, protects against lysosomal damage and lysosome-mediated cell death.[306] Therefore, it cannot be excluded that the significant downregulation of luminal lysosomal enzymes under cycH, not only of CTSB and CTSL, could still have an impact on therapy response mechanisms in HPV-positive cervical cancer cells, beyond Cisplatin-induced apoptosis.

My results further showed that another lysosome-associated determinant of the Cisplatin response in cervical cancer cells under different oxygen conditions is the regulation of autophagy. Autophagy can influence (chemo)therapy responses and can have both pro- or anti-tumorigenic effects in cancer cells, depending on various factors such as tumor type, microenvironment, and disease stage.[166] Chemotherapeutic drugs such as Cisplatin can induce autophagic flux, which can affect drug efficacy and contribute to drug resistance.[307,308] The modulation of autophagy as adjuvant therapy is thus increasingly investigated as a chemosensitizing approach in tumor therapy in numerous clinical trials.[168,309] However, the dual role of autophagy in both tumor promoting and tumor suppressing functions represents a considerable challenge and limits its therapeutical exploitation.[309] Previous studies have shown that the antimalarial drug Chloroquine (CQ), an effective inhibitor of autophagy, can enhance the effectiveness of Cisplatin treatment in

different tumor types, *in vitro* and *in vivo,* including cervical cancer cells.[168,308,310] Since I detected decreased autophagic flux in cervical cancer cells under cycH compared to cells under normoxia and physoxia, the question arose whether this influences their response to Cisplatin treatment. Intriguingly, cervical cancer cells under all tested oxygen conditions showed enhanced induction of apoptosis after combination treatment of Cisplatin and CQ. The cooperative pro-apoptotic potential of autophagy inhibition and Cisplatin was further corroborated by combining Cisplatin treatment with the specific RNAi-mediated inhibition of ATG5, an important factor in the autophagic process.[162,280] Importantly, my findings demonstrate that even cells under chronic hypoxia and cycH, which are particularly chemoresistant, can be re-sensitized to the pro-apoptotic effects of Cisplatin by autophagy inhibition through prolonged CQ co-treatment or by genetic silencing of ATG5 expression. Hence, the reduction of autophagic flux in cervical cancer cells under cycH *per se* is likely not the critical determinant for their increased chemotherapy resistance to Cisplatin compared to other tested oxygen conditions. Strikingly, however, the application of Cisplatin in combination with autophagy inhibitors, such as CQ, could provide a basis to improve established therapeutic strategies, by counteracting the increased chemoresistance of cancer cells exposed to chronic hypoxia or cycH.

Evidently, the pronounced alterations in lysosomal composition under cycH did not appear to be a significant determinant for the apoptosis response of HPV-positive cervical cancer cells towards Cisplatin, at least under the experimental conditions employed in my studies. Therefore, I proceeded to investigate the apoptosis signaling cascade, specifically focusing on the role of BID in the response to Cisplatin under different oxygen conditions in more detail. Interestingly, my experiments revealed that the cleavage of BID upon Cisplatin treatment and the resulting amounts of tBID clearly correlate with the apoptosis induction in cervical cancer cells under different oxygen conditions. Specifically, I detected the lowest levels of tBID in cells treated with Cisplatin under cycH, which induce least apoptosis, compared to cells treated under normoxia, physoxia or chronic hypoxia. Consistent with the reduced amounts of tBID, Cisplatin-induced MOMP was also strongly reduced in cells under cycH as evidenced by a substantially decreased release of Cyt c into the cytosol. Furthermore, silencing of BID expression via RNAi strongly inhibited Cisplatin-induced apoptosis, particularly in cells treated under normoxia, physoxia or chronic hypoxia. These findings demonstrate that BID plays a crucial role in promoting pro-apoptotic signaling in HPV-positive cancer cells in response to Cisplatin. Notably, the activation of BID in Cisplatin-treated cervical cancer cells is dependent on caspases, as the pan-caspase inhibitor Z-VAD-FMK substantially diminished the generation of tBID and the induction of apoptosis. Moreover, specific inhibition of Caspase 8, which is a well-

characterized activator of BID[119], reduced tBID levels in Cisplatin-treated cervical cancer cells and enhanced their resistance to apoptosis under all tested oxygen conditions.

BID, as an upstream regulator of MOMP and a central link between the extrinsic and intrinsic apoptosis cascades, has an important role in chemotherapy-induced apoptosis in different cellular contexts, including cervical cancer cells.[119,133] In response to apoptotic stimuli, Caspase 8 and 10, but also Caspases 2 and 3, granzymes, calpains, and cathepsins can cleave and activate BID, which then recruits the pore forming proteins BAX and BAK to the outer mitochondrial membrane (Figure 35).[101,119,123,311] Thus, while Caspase 8, as shown in this study, is important, it may not be solely responsible for BID activation in Cisplatin-treated cervical cancer cells, as different factors can cooperatively cleave BID in response to chemotherapeutic agents. Interestingly, positive feedback loops involving executioner caspases can reinforce BID cleavage, enhance MOMP, and thus manifest the point of no return for apoptosis.[128,312,313] Therefore, BID silencing may also inhibit potential feedback loops, which amplify apoptosis signals and thus may comprehensively protect against Cisplatin-induced apoptosis.

Collectively, these latter findings revealed that BID plays a central role in Cisplatin-induced apoptosis in cervical cancer cells and its differential activation under different oxygen conditions critically determines the sensitivity of the cells to chemotherapy (Figure 35). Under cycH, Cisplatin-treated cells exhibit strongly reduced generation of tBID, which likely contributes to their chemoresistant phenotype in comparison to cells treated under normoxia, physoxia or chronic hypoxia. Mechanistically, the reduced cleavage of BID under cycH leads to attenuated MOMP and a decrease in the cytosolic release of Cyt c, which is a key determinant of the intrinsic apoptosis cascade and the subsequent activation of initiator and executioner caspases.

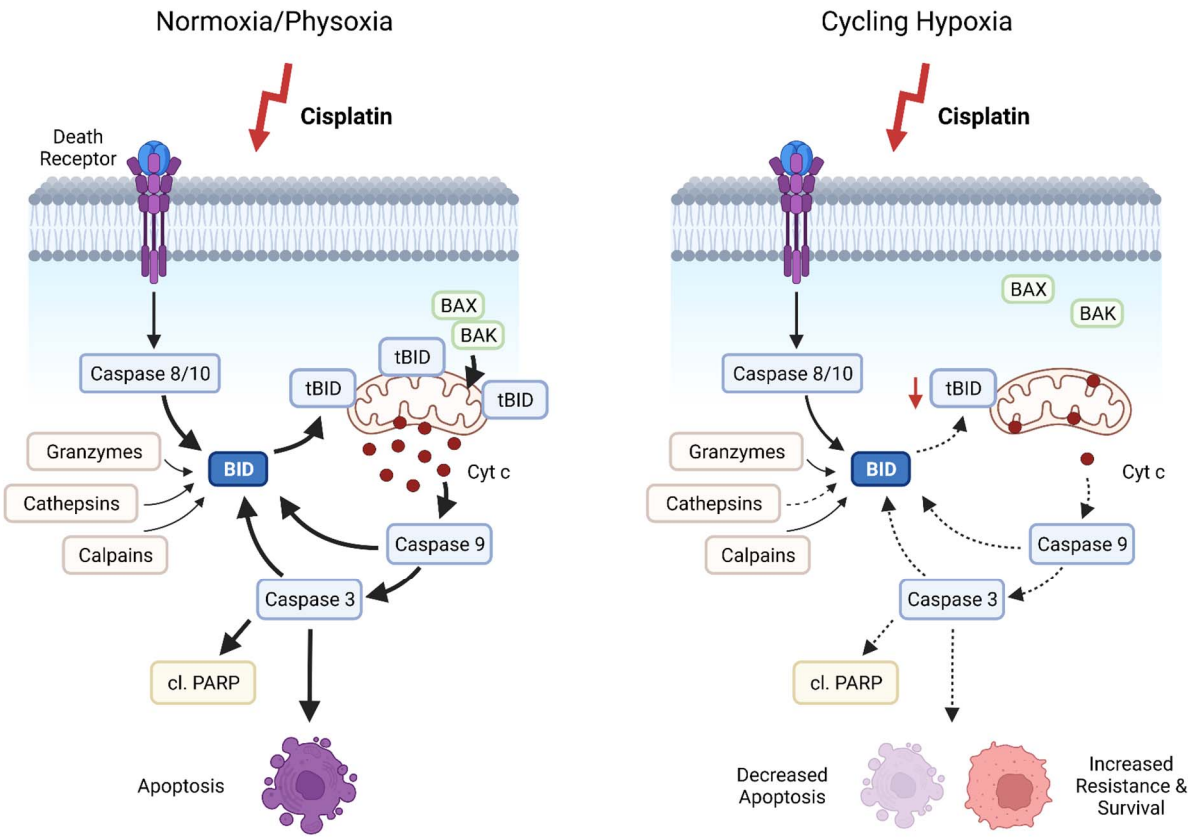

Figure 35. Proposed role of BID in Cisplatin-mediated apoptosis induction and resistance mechanisms in cervical cancer cells under different oxygen conditions.

Left: Under normoxia and physoxia, Cisplatin treatment induces apoptosis through both the intrinsic and the extrinsic pathways. In the extrinsic pathway, cell death receptor signaling activates Caspases 8 and 10, which can cleave BID to truncated BID (tBID). BID is the link between the extrinsic and intrinsic apoptosis pathway. tBID translocates to the outer mitochondrial membrane and recruits BAX and BAK to promote mitochondrial outer membrane permeabilization. The release of Cytochrome c (Cyt c) leads to the activation of initiator Caspase 9 and subsequent activation of executioner caspases, such as Caspase 3 or 7. Executioner caspases promote the induction of apoptosis by cleaving PARP, resulting in cleaved (cl.) PARP, and can reinforce BID activation. Other factors including granzymes, cathepsins, and calpains can also activate BID under certain circumstances and thus promote apoptosis. Right: Under cycling hypoxia (cycH), reduced amounts of tBID are generated in response to pro-apoptotic Cisplatin treatment. Consequently, less MOMP is induced, leading to a decreased release of Cyt c into the cytoplasm. As a result, the activation of caspases and the induction of apoptosis are diminished in Cisplatin-treated cells under cycH, resulting in increased cell survival.

Whereas my findings clearly point at a key role for BID for Cisplatin-induced apoptosis, they do not exclude the participation of other mechanisms in this response. Drug resistance often occurs multifaceted and can be influenced by various determinants, including drug delivery, sequestration, inactivation, and altered regulation of a variety of factors involved in apoptosis regulation.[73,83]

Further, as mentioned above, the phenotypic response to chemotherapy can depend on the degree of drug-induced DNA damage.[72,262] Lower doses of Cisplatin cause less severe DNA damage resulting in the induction of senescence, whereas higher doses efficiently trigger apoptosis.[72] I found that cervical cancer cells treated with Cisplatin under cycH show increased resistance to apoptosis, but eventually react with senescence induction. It thus will be interesting to investigate whether they may accumulate lower intracellular Cisplatin concentrations, leading to reduced DNA damage, or exhibit an elevated threshold for Cisplatin concentrations required for efficient induction of apoptosis. In principle, therapy-induced senescence could be beneficial for cancer treatment by irreversibly blocking the proliferation of tumor cells. However, therapy-induced senescence can also lead to undesired effects due to the pro-inflammatory SASP of senescent cells, which can result in increased resistance towards pro-apoptotic stimuli, including chemotherapeutic agents.[262,300] Hence, the senescent cervical cancer cells emerging from Cisplatin treatment under cycH may require targeted removal, e.g. by senolysis, which is the selective induction of cell death in senescent cells.[262]

3.5 Conclusion and perspectives

Overall, my results provide novel insights into the oxygen-dependent modulation of the phenotype of HPV-positive cervical cancer cells, with a focus on cycH. My main findings reveal that cycH results in pronounced phenotypic effects, differing not only from normoxia or physoxia but also from chronic hypoxia. Critically affected cellular pathways include the response of cervical cancer cells to radiotherapy, pro-senescent and pro-apoptotic chemotherapy. Collectively, my findings indicate that cells exposed to cycH are characterized by increased resistance to the pro-apoptotic effects of Cisplatin and thereby could represent a particularly problematic cell population for cervical cancer therapy. Mechanistically, the increased resistance under cycH is linked to an impaired activation of pro-apoptotic BID signaling in response to Cisplatin treatment.

The results of my thesis should also provide a basis for further investigations. For example, it will be interesting to further explore functional consequences of the reduced activity of luminal lysosomal enzymes under cycH, particularly of cathepsins, since the deregulation of cathepsin synthesis and function has far-reaching consequences and is associated with a variety of diseases (e.g. neurodegenerative or metabolic diseases[314,315]), cancer progression and drug resistance.[156] Additionally, lysosomal dysfunctions can critically influence important cellular processes, including energy metabolism, degradation of endocytosed cargo, and antigen presentation.[147]

Furthermore, it will be interesting to characterize the regulatory mechanisms, which act upstream of BID, in more detail, particularly addressing the question why cervical cancer cells under cycH do not efficiently generate tBID in response to Cisplatin treatment and thus are protected from apoptosis. Understanding the mechanisms of chemoresistance is pivotal for the development and refinement of therapeutic strategies for cervical cancer patients to target challenging and aggressive cancer cell subpopulations. Combination therapies that enhance BID cleavage and activation could represent a promising approach for efficient targeting of oxygen-deprived HPV-positive cervical cancer cells. For instance, a recent study demonstrated that the ectopic expression of tBID from adenoviral vectors could significantly increase chemotherapy-induced apoptosis in ovarian cancer cells[316], suggesting a potential strategy to improve Cisplatin sensitivity of cervical cancer cells under cycH or chronic hypoxia. Additionally, it is warranted to investigate the response of cervical cancer cells under cycH to other chemotherapeutic agents, immunotherapy, and different combinatorial therapies (e.g. with autophagy inhibitors) to further increase our understanding of key determinants governing their therapeutic response.

CHAPTER 4

MATERIAL AND METHODS

4 Material and Methods

4.1 Reagents

Molecular biology grade reagents for buffers and media were purchased from AppliChem (Darmstadt, Germany), Applied Biosystems (Waltham, MA, USA), BD Biosciences (Franklin Lakes, NJ, USA), Bio-Rad (Hercules, CA, USA), Carl Roth GmbH (Karlsruhe, Germany), Enzo Life Sciences (Farmingdale, NY, USA), Invitrogen (Waltham, MA, USA), New England Biolabs (Ipswich, MA, USA), Merck (Darmstadt, Germany), Promega (Madison, WI, USA), Roche Diagnostics (Basel, Switzerland), Sigma-Aldrich (St. Louis, MO, USA, now Merck) and Thermo Fisher Scientific (Waltham, MA, USA). Manufacturers of non-standard reagents are specified in the text. All buffers and solutions were prepared with ddH_2O if not stated otherwise.

4.2 Cellular biology techniques

4.2.1 Cell culture

HPV-positive HeLa, SiHa and CaSki cervical carcinoma cells were maintained in Dulbecco's minimal essential medium (DMEM, 1 g/L glucose (5 mM), Gibco, Thermo Fisher Scientific). HPV-negative HCT116 colorectal cancer cells were cultivated in McCoy's 5A medium, and A549 lung cancer cells in RPMI 1640 medium (both Gibco, Thermo Fisher Scientific). The standard media were supplemented with 10% fetal calf serum (FCS, PAN-Biotech, Aidenbach, Germany), 100 U/mL penicillin, 100 µg/mL streptomycin and 2 mM L-glutamine (all Sigma-Aldrich). All cell lines were routinely tested for mycoplasma contamination and were authenticated within the last 3 years by single nucleotide polymorphism profiling (Multiplexion GmbH, Heidelberg, Germany).

Cell stock cultures were cultivated at 37 °C and 5% CO_2 at 21% O_2 ("normoxia") in a humidified incubator. For routine passage, cells were split every 3-4 days when reaching 80-90% confluency, using 0.25% Trypsin-EDTA solution (Thermo Fisher Scientific) for detaching. Prior to cell seeding for experiments, viable cells were counted using the trypan blue method and the Countess™ Automated Cell Counter (Invitrogen). For most experiments, 6 x 10^5 cells were seeded in 3 mL DMEM in 6 cm dishes.

During experiments, cells were cultivated under different oxygen conditions, as stated. Cultivations under physoxia (5.5% O_2) and chronic hypoxia (1% O_2) were performed at 37 °C and 5% CO_2 in a humidified incubator. Cycling hypoxia (cycH) incubations with hypoxia-reoxygenation cycles of 1 h at 1% O_2 and 1 h at 5.5% O_2 were performed at 37 °C and

5% CO_2 in the Invivo$_2$ 400 physiological oxygen workstation (Ruskinn Technology Ltd. Bridgend, United Kingdom). The H-R cycles were conducted with an automated cycle programming inside the oxygen workstation. For experiments under chronic hypoxic and cycH conditions, pre-conditioned hypoxic medium was used. Where indicated, DMEM supplemented with 4.5 g/L glucose (25 mM) (Gibco, Thermo Fisher Scientific) was used to mimic unphysiologically high glucose conditions.

4.2.2 Cryopreservation and thawing of cells

For long-term storage, cells were trypsinized, pelleted at 800 g for 3 min and resuspended in cryo-medium containing 30% FCS and 10% dimethyl sulfoxide (DMSO). Cell aliquots in cryotubes were transferred into an isopropanol-filled freezing container (Nalgene, Thermo Fisher Scientific) for gradual, slow freezing over multiple days at -80 °C and finally stored in liquid nitrogen.

For thawing, cells were rapidly warmed to 37 °C, resuspended in fresh culture medium and seeded in a cell culture flask. Fresh medium was replenished the following day to remove residual DMSO.

4.2.3 Treatment of cells with chemical compounds

Treatment with inhibitors or small molecule compounds was performed 1-2 days after cell seeding, as stated. Before treatment, cell culture medium was exchanged with normoxic or hypoxic preconditioned DMEM, if not stated otherwise. The compounds were added directly into the cell culture medium. Respective volume of solvent was added to control cells.

Following chemicals were used for treatment: AKT inhibitor VIII (Sigma-Aldrich); Bafilomycin A1 (Enzo Life Sciences); CA-074-Me (Selleckchem, Houston, TX, USA); Chloroquine (Jena Biosciences, Germany); Cisplatin (Sigma-Aldrich); E64 (Cayman Chemical, Ann Arbor, MI, USA); Etoposide (Enzo Life Sciences); GSK2334470 (MedChemExpress); KU-0063794 (Sigma-Aldrich); Rapamycin (AdipoGen, San Diego, CA, USA); SGK1 Inhibitor (Cayman Chemical); Z-VAD(OMe)-FMK (TargetMol Chemicals Inc, Boston, MA, USA). Cisplatin was dissolved in 0.9% NaCl/H_2O, E64 was dissolved in H_2O and the other drugs were dissolved in DMSO.

4.2.4 Transfection of synthetic siRNAs

Gene expression was silenced via RNA interference using chemically synthesized small interfering RNAs (siRNAs) (Silencer® Select, Life Technologies, Thermo Fisher Scientific). For reverse transfection of 10 nM siRNAs, 2.5 µL of the 10 µM siRNA stock solution were pre-incubated with Opti-MEM medium (Gibco, Thermo Fisher Scientific) in a final volume of 250 µL. In parallel, 5 µL Lipofectamine™ RNAiMAX transfection reagent (Invitrogen) were mixed with Opti-MEM medium in a final volume of 250 µL and incubated for 5 min at room temperature (RT). The RNAiMAX mix was added to the siRNA dilutions and incubated for 20 min at RT. 500 µL siRNA transfection mix were added per 6 cm dish. Meanwhile, cell stocks were trypsinized, and resuspended in DMEM containing 10% FCS but lacking penicillin, streptomycin and L-glutamine. Subsequently, 8 x 10^5 cells were seeded on top of the siRNA mix in a final volume of 2.5 mL and distributed gently. 24 h after transfection, medium was exchanged to standard cell culture medium and cells were treated as indicated.

siRNA target sequences and used siRNA pools are listed in Table 1. For silencing of HPV E6/E7 expression, a pool of three different siRNAs targeting all HPV *E6/E7* transcript classes was used to diminish off-target effects.[55] The non-targeting control siRNA (siCtr) contains at least four mismatches to all known human genes.

Table 1. Synthetic siRNAs.

Target transcript	siRNA	siRNA target sequence (5' – 3')	pool
-	siCtr	CAGUCGCGUUUGCGACUGG	
ATG5	siATG5	GGAUGCAAUUGAAGCUCAU	
BID	siBID	CUUGCUCCGUGAUGUCUUU	
Caspase 8	siCASP8	GAUACUGUCUGAUCAUCAA	
HIF-1α	siHIF-1α-1	CUAACUGGACACAGUGUGU	siHIF-1α
	siHIF-1α-2	CUGAUGACCAGCAACUUGA	
HIF-2α	siHIF-2α-1	GCGACAGCUGGAGUAUGAA	siHIF-2α
	siHIF-2α-2	CAGCAUCUUUGAUAGCAGU	
HPV16 E6/E7	si16E6/E7-1	CCGGACAGAGCCCAUUACA	si16E6/E7
	si16E6/E7-2	CACCUACAUUGCAUGAAUA	
	si16E6/E7-3	CAACUGAUCUCUACUGUUA	
HPV18 E6/E7	si18E6/E7-1	CCACAACGUCACACAAUGU	si18E6/E7
	si18E6/E7-2	CAGAGAAACACAAGUAUAA	
	si18E6/E7-3	UCCAGCAGCUGUUUCUGAA	

4.2.5 Proliferation assay

For the analysis of cell proliferation, 2 x 10^5 cells (HeLa) or 3 x 10^5 cells (SiHa) cells were seeded in 6 cm dishes. Cells were cultivated under 21% O_2, 5.5% O_2, 1% O_2 or cycH (1 h 1% O_2, 1 h 5.5% O_2) and viable cell numbers were determined after 24 h, 48 h and 72 h in duplicates using a CellDrop Automated Cell Counter (DeNovix Inc., Wilmington, DE, USA).

4.2.6 Cell cycle analysis

In parallel to proliferation assays, cell cycle analyses were performed using flow cytometry. Cells grown under indicated oxygen conditions were washed with phosphate-buffered saline (PBS; 137 mM NaCl; 2.7 mM KCl; 4.3 mM Na_2HPO_4; 1.4 mM KH_2PO_4 (pH 7.4)) and trypsinized at indicated time points. Cells were centrifuged for 5 min at 1000 g, resuspended in 300 µL cold PBS before 900 µL ice-cold 100% EtOH were added while constant vortexing. Fixed cells were kept at -20 °C until further processing. Subsequently, cells were pelleted, resuspended in 925 µL cold PBS and stained with 25 µL of 1 mg/mL propidium iodide solution to reach a final concentration of 25 µg/mL. To degrade RNA, 50 µL of 10 mg/mL RNase were added to a final concentration of 500 µg/mL. After staining for 30 min at RT in the dark, cells were filtered through gaze in FACS tubes. Cell cycle distribution was analyzed by flow cytometry at the BD LSR Fortessa (BD Biosciences) using 600 long pass (LP) filters and 610/20 band pass (BP) filters and the BD FACS Diva Software version v8.0.1. Cell cycle phases G0/G1, S and G2/M were distinguished by manual gating. Analyses and image generation were performed with FlowJo version 10.8.1 (BD Life Sciences).

4.2.7 Acridine orange staining

Acridine orange (AO) staining was performed to detect acidic vesicular organelles in living cells cultivated under different oxygen conditions. AO hemi(zinc chloride) (Sigma Aldrich/Merck) was dissolved in PBS to a stock concentration of 1 mg/mL. For analysis of AO-stained cells by fluorescence microscopy, cells were grown on glass coverslips, 1 µg/mL AO was added to the cell culture medium and incubated for 20 min at 37 °C. Subsequently, cells were washed for 2-3 times with PBS and immediately analyzed at a Zeiss Cell Observer Microscope using a 40x objective. For flow cytometry analysis, cells were trypsinized, resuspended in 1 mL AO medium (DMEM without phenol red, supplemented with 10% FCS and 1.5 µg/mL AO) and stained for 15 min at RT in the dark. Then, cells were filtered in FACS tubes and analyzed directly at the BD LSR Fortessa (BD Biosciences). For excitation, the blue laser (488 nm) was used. For detection of green fluorescence, 505 LP, 530/30 BP

filters and for detection of red fluorescence 635 LP, 685/35 BP filters were used. Analyses and image generation were performed with FlowJo version 10.8.1 (BD Life Sciences).

4.2.8 TUNEL assay

Late-stage apoptotic cells can be detected by terminal deoxynucleotidyl transferase-mediated UTP end labeling (TUNEL) assays. The terminal deoxynucleotidyl transferase enzyme attaches fluorescently labeled nucleotides to 3'-hydroxyl termini that are exposed after DNA double strand breaks.[317]

Cells were grown on glass coverslips and treated as described. Cells were fixed in 4% paraformaldehyde (PFA) in PBS for 30 min at RT, washed with PBS and stored in 80% EtOH at -20 °C until further processing. Subsequently, cells were washed with PBS, permeabilized in 0.1% Triton X-100, 0.1% sodium citrate in PBS for 2 min at 4 °C and washed twice with PBS. TUNEL assays were performed using the "In Situ Cell Death Detection Kit" (Roche) according to the manufacturer's instructions. Briefly, cells were stained with 25 µL TUNEL solution (mix of enzyme solution:label solution = 1:10) for 60-90 min at 37 °C in a humidified chamber in the dark. Then, cells were washed with PBS (2x 10 min) and nuclei were stained with 1 µg/mL DAPI (4',6-diamidino-2-phenylindole, Roche) for 5 min at RT in the dark. After repeated washing with PBS (2x 10 min), coverslips were dipped in H_2O and 100% EtOH before being air-dried. Coverslips were mounted with Vectashield (Vector Laboratories Inc., USA) onto microscope slides.

Cells were imaged with a Zeiss Cell Observer Microscope using the LED module Colibri.2 and the 20x / 0.4 LD PlnN Ph2 DICII objective. Image analysis was performed with Fiji/ImageJ software (NIH, Bethesda, MD, USA).[318] The percentages of TUNEL-positive cells in relation to total cell counts (determined by DAPI staining) were quantified using an Fiji/ImageJ macro (gently provided by Damir Krunic, Light Microscopy Core Facility, DKFZ Heidelberg) from at least five images per condition.

4.2.9 Immunofluorescence

For immunofluorescence stainings, cells were seeded on glass coverslips, cultivated under different oxygen conditions, and treated as described. Cells were fixed with 4% PFA in PBS for 15 min at RT and washed twice in PBS. Subsequently, cells were first permeabilized in 100% ice-cold methanol for 10 min at -20 °C, washed in PBS and then incubated in 0.1% Triton X-100, 0.1% sodium citrate in PBS for 2 min at 4 °C. Cells were blocked with

3% bovine serum albumin (BSA) in PBS for 30 min and incubated with primary antibodies diluted in blocking buffer for 1 h at RT in a humidified chamber. After repeated washing in PBS, cells were incubated with the secondary antibodies diluted in blocking buffer and DAPI (1 µg/mL) for 30 min at RT in a humidified chamber. Cells were washed with PBS and mounted with Vectashield onto microscope slides as described.

Primary antibodies were rabbit anti-LC3B (1:500, NB100-2220, Novus Biologicals LLC, Centennial, CO, USA), mouse anti-LAMP1 (1:200, sc-20011, Santa Cruz, Dallas, TX, USA), mouse anti-eIF3B (1:500, sc-374156, Santa Cruz). Secondary antibodies were goat anti-mouse FITC-conjugate (1:400; Jackson ImmunoResearch, West Grove, PA, USA), donkey anti-mouse Cy3-conjugate and goat anti-rabbit Cy3-conjugate (both 1:400; Pierce Biotechnology, Thermo Fisher Scientific). Cells were imaged with a Zeiss Cell Observer Microscope using 20x or 40x objectives or a Zeiss LSM 710 ConfoCor 3 confocal microscope (Zeiss, Germany) using 40x or 63x, 1.40 oil objectives.

Quantification of fluorescent signal per cell was performed using Fiji/ImageJ (NIH) [318], where indicated. For this purpose, the area of the fluorescent signal was normalized to the total cell number (determined by DAPI staining) in 3-5 randomized fields of view, containing at least 50 cells per image.

4.2.10 Senescence assay

To analyze senescence induction in response to different stress stimuli such as pro-senescent chemotherapy, senescent cells can be detected by their distinctive enlarged and flattened morphology and the activity of senescence-associated β-Galactosidase (SA-β-Gal). The enzymatic activity of SA-β-Gal can be observed at pH 6.0 using the chromogenic substrate X-Gal (5-bromo-4-chloro-3-indolyl β D-Galactopyranoside).[319] Upon hydroxylation, X-Gal forms an insoluble blue product that is visible by bright field microscopy.

To investigate the effects of Etoposide treatment on senescence induction under different oxygen conditions, cells were incubated under 21% O_2, 5.5% O_2, 1% O_2 or cycH, in presence or absence of the mTORC inhibitors Rapamycin or KU-0063794, as indicated. After 24 h, Etoposide was added for 48 h under the respective oxygen conditions. Subsequently, cells were trypsinized, counted and plated at defined cell numbers into new 6 cm dishes. Cells were cultivated in drug-free medium under normoxia for 5-6 days for senescence assays (SAs) or for 10-15 days for colony formation assays (CFAs, see chapter 4.2.11). Medium was exchanged every 3-4 days.

For staining of senescent cells, the cells were washed with PBS, fixed in 1 mL senescence assay fixation buffer (2% formaldehyde, 0.2% glutaraldehyde in PBS) for 3 min at RT and washed again with PBS. Subsequently, 1.5 mL senescence assay buffer (40 mM citric acid, 150 mM NaCl, 2 mM $MgCl_2$, adjusted to pH 6.0 with Na_2HPO_4 and freshly supplemented with 5 mM $K_3[Fe(CN)_6]$, 5 mM $K_4[Fe(CN)_6]$ and 1 mg/mL X-Gal in DMF) were added per 6 cm dish, and cells were incubated in a wet chamber for 16-24 h at 37 °C. When the chromogenic reaction was completed, SA buffer was replaced by PBS and images of representative cells were taken with a brightfield microscope (EVOS XL Core Cell Imaging System, Life Technologies).

4.2.11 Colony formation assay

A colony formation assay (CFA) is an established *in vitro* method to determine the effects of ionizing radiation or chemotherapeutic drugs on the reproductive viability of cells.[320]

To investigate the survival and proliferative capacity of HPV-positive cervical cancer cells upon drug treatment under different oxygen conditions, cells were split as described in chapter 4.2.10. 10-15 days after splitting, colonies were fixed and stained. For that, the cells were washed with PBS and simultaneously fixed and stained with 350 µL of a formaldehyde-crystal violet solution (12 mM crystal violet, 29 mM NaCl, 3.7% formaldehyde, 22% EtOH) for 5 min at RT. CFAs were washed with H_2O and dried at 37 °C before images were taken using the Epson Perfection 4990 Photo Scanner (Epson, Suwa, Japan).

4.2.12 Irradiation of cells

γ-irradiation of cells was performed using a Gammacell® 40 Exactor Low Dose Rate Research Irradiator (Best Theratronics, Ottawa, Canada) with a Caesium-137 source at a constant rate of 0.933 Gy/min. Cells cultivated under 21% O_2, 5.5% O_2, 1% O_2 or cycH were irradiated under their respective oxygen conditions in airtight boxes (LocknLock, Seoul, South Korea). Controls were sham-irradiated. Subsequently, cells were trypsinized, counted with the CellDrop Automated Cell Counter (DeNovix Inc.) and plated at defined cell numbers of 1000-10000 cells per 6 cm plate for clonogenic survival assays. Cells were cultivated under normoxia for 10-14 days and colonies were fixed with a formaldehyde-crystal violet solution as described above.

4.3 Protein-based techniques

4.3.1 Protein extraction from cells and preparation for immunoblot analyses

4.3.1.1 Total cell lysate

To extract total protein for immunoblot analyses, cells were washed with ice-cold PBS and lysed in 150 µL ice-cold CSK-1 lysis buffer (10 mM PIPES pH 6.8, 300 mM NaCl, 1 mM EDTA, 300 mM sucrose, 1 mM $MgCl_2$, 0.5% Triton X-100) that was freshly supplemented with 100 µL PhosSTOP phosphatase inhibitor cocktail (Roche Diagnostics), 25 µL Pefabloc serine protease inhibitor (Merck) and 10 µL P8340 protease inhibitor cocktail (Sigma-Aldrich) per 900 µL CSK-1 buffer. Cells lysates were incubated for 30 min on ice and subsequently centrifuged at 16000 g for 5 min at 4 °C to remove cellular debris. Subsequently, protein concentrations were determined using the Bio-Rad Protein Assay (Bio-Rad, USA). For this purpose, 1-5 µL of the cell lysates were mixed with 1 mL of the 1:5 diluted protein assay dye reagent concentrate in a cuvette (BRAND® semi-micro disposable cuvettes, Sigma-Aldrich) and incubated for 5 min at RT. Absorption at 595 nm was measured with a photometer (BioPhotometer D30, Eppendorf, Germany) and protein concentrations were calculated using a BSA standard curve. Protein extracts were diluted to a desired concentration in 4x protein loading buffer (8% SDS, 250 mM Tris-HCl, 20% β-mercaptoethanol, 40% glycerol, 0.008% bromphenol blue), boiled at 95 °C for 5 min and stored at -80 °C until further analysis.

4.3.1.2 Secreted proteins

To investigate secreted proteins, cells were cultured in DMEM containing 5% FCS, 100 U/mL penicillin, 100 µg/mL streptomycin and 2 mM L-glutamine under different oxygen conditions for 24 h. The supernatants were cleared by centrifugation at 1000 g for 5 min and transferred to a new reaction tube. Then, the supernatants were diluted with 4x protein loading buffer and boiled at 95 °C for 5 min. The proteins in the supernatant were analyzed proportional to the protein concentration of the corresponding cell lysate.

4.3.1.3 Subcellular fractionation

For the analysis of NDRG1 subcellular localization, cells were grown in 15 cm tissue culture dishes and cultivated for 24 h under 5.5% O_2 and 1% O_2. Cells were harvested by scraping in PBS and subcellular fractionation was performed using the "Minute™ Plasma Membrane Protein Isolation and Cell Fractionation Kit" (Invent Biotechnologies, Plymouth, MN, USA)

according to the manufacturer's instructions. Briefly, cell pellets were resuspended in 200 µL of the provided Buffer A, incubated on ice for 5-10 min and vortexed. Afterwards, the cell suspension was transferred to filter cartridges and centrifuged at 16000 g for 30 s to obtain the cell lysate containing intact nuclei, organelles, and ruptured cell membranes. Nuclei were pelleted by centrifugation at 700 g for 1 min. The supernatant was centrifuged at 16000 g, 4 °C for 30 min to separate the cytosolic fraction and the total membrane fraction, containing organelles and plasma membranes (pellet). Subsequently, the pellet containing the total membrane fraction was resuspended in 200 µL of the provided Buffer B and centrifuged at 7800 g, 4 °C for 5 min to separate the organelle membrane proteins (pellet). The resulting supernatant was mixed carefully with 1.6 mL cold PBS before plasma membrane proteins were pelleted at 16000 g, 4 °C for 30 min. All pelleted fractions were resuspended in CSK-1 lysis buffer and processed as described in chapter 4.3.1.1.

For the analysis of cytosolic fractions upon Cisplatin treatment, cells were grown in 15 cm tissue culture dishes and treated as indicated. Cells were washed twice with ice-cold PBS, scraped in 500 µL PBS and centrifuged at 800 g for 5 min. Afterwards, cells were resuspended in homogenization buffer (10 mM HEPES (pH 7.4), 250 mM sucrose, 1 mM $MgCl_2$, 1 mM $CaCl_2$, 1.5 mM magnesium acetate), freshly supplemented with 1 mM DTT, 1x PhosSTOP phosphatase inhibitor cocktail, 25 µL/mL Pefabloc and 10 µL/mL P8340 protease inhibitor cocktail and incubated on ice for 30 min. Using a KIMBLE Dounce tissue grinder with a large clearance pestle (Sigma-Aldrich), cells were homogenized in 20 strokes, and centrifuged at 800 g for 5 min to pellet intact nuclei. The post-nuclear supernatant containing organelles and cytoplasmic proteins was centrifuged at 16000 g, 4 °C for 30 min to separate cytosolic and organelle fractions. Pelleted organelles were washed with PBS, centrifuged again at 16000 g, 4 °C for 30 min and finally resuspended in CSK-1 lysis buffer. Protein concentrations for all cellular fractions were determined with Bradford assay and prepared for immunoblot analysis as described above.

4.3.2 SDS-PAGE

To analyze protein levels after different experimental procedures, proteins were separated by sodium dodecyl sulfate-polyacrylamide gel electrophoresis (SDS-PAGE) according to their molecular weight. 12.5% polyacrylamide gels were cast between two glass plates sealed with 1% agarose according to Table 2.

Table 2. Recipe for SDS polyacrylamide gels.

Components for stacking gel	For 2 gels (5%)	Components for resolving gel	For 2 gels (12.5%)
H_20	3.5 mL	H_20	4.5 mL
30% Acrylamide/bisacrylamide	830 µL	30% Acrylamide/bisacrylamide	4.2 mL
0.47 M Tris-HCl (pH 6.7)	620 µL	3 M Tris-HCl (pH 8.9)	1.2 mL
10% SDS	50 µL	10% SDS	100 µL
10% APS	100 µL	10% APS	10 µL
TEMED	5 µL	TEMED	50 µL

The gels were installed into a XCell SureLock™ Mini-Cell Electrophoresis System (Life Technologies), filled with Tris-glycine SDS running buffer (2.5 mM Tris, 19.2 mM glycin, 0.1% SDS). Equal amounts of protein extract (10-60 µg per lane) were loaded on the gel and PageRuler™ Prestained Protein Ladder (Thermo Scientific) was loaded as a size standard for the molecular weight. Gels were run at 90-120 V for approximately 2 h.

4.3.3 Western blotting and immunodetection of proteins

After SDS-PAGE, the separated proteins were transferred from the gel to a methanol-activated Immobilon-P PVDF membrane (Merck Millipore, Burlington, MA USA) by semi-dry blotting. The PVDF membrane and Whatman filter papers were soaked with Towbin transfer buffer (2.5 mM Tris, 19.2 mM glycine, 20% methanol, pH 8.3). For blotting, a stack of four Whatman papers at the bottom (anode), PVDF membrane, protein gel and four Whatman papers at the top (cathode) was assembled into a Trans-Blot® SD Semi-Dry Electrophoretic Transfer Cell (Bio-Rad). Electroblotting was performed at 20 V for 1 h.

Subsequently, membranes were incubated in blocking buffer (0.2% Tween-20, 5% skim milk powder, 1% BSA in PBS) for 1 h at RT to saturate unspecific binding sites. The membranes were then probed with primary antibodies diluted in blocking solution (according to Table 3) at 4 °C overnight. The next day, membranes were washed thrice with PBS-T (0.2% Tween-20 in PBS) for 10 min and incubated with the respective horseradish peroxidase (HRP)-conjugated secondary antibody (Table 4) diluted in blocking buffer for 1 h at RT. After three washes with PBS-T, proteins were detected using the principle of enhanced chemiluminescence (ECL). The ECL reagents WesternBright Sirius (Advansta, San Jose, CA, USA) or Amersham ECL Prime (Cytiva, Marlborough, MA, USA) were applied to the membrane according to the manufacturer's instructions and signals were detected with the Fusion SL Gel Detection System (Vilber Lourmat, Eberhardzell, Germany). All immunoblots were performed from three independent replicates with consistent results.

Table 3. Primary antibodies used in this thesis.

Primary Antibodies				
Specificity	**Source**	**Dilution**	**Molecular Weight**	**Supplier**
4E-BP1 Phospho (S65)	rabbit	1:1000	15-20 kDa	Cell Signaling Technology #9451 (Boston, MA, USA)
AKT Phospho (S473)	rabbit	1:1000	60 kDa	Cell Signaling Technology #4058
β-Actin	mouse	1:50000	40 kDa	Santa Cruz sc-47778
ATG5	mouse	1:500	~60 kDa	Santa Cruz sc-133158
BID	rabbit	1:1000	22, 15 kDa	Cell Signaling Technology #2002
Cathepsin B	goat	1:1000	25-30 kDa	R&D Systems AF953 (Minneapolis, MN, USA)
Cathepsin L	goat	1:1000	35 kDa	R&D Systems AF952
Caspase 8	mouse	1:2000	55, 36, 23 kDa	BD Pharmingen #551242
Caspase 9, cleaved (Asp330)	rabbit	1:1000	37 kDa	Cell Signaling Technology #7237
Cytochrome c	mouse	1:1000	15 kDa	Santa Cruz sc-13156
E-Cadherin	rabbit	1:1000	135 kDa	Cell Signaling Technology #3195
GAPDH	rabbit	1:4000	37 kDa	Santa Cruz sc-25778
HIF-1α	mouse	1:500	120 kDa	BD Pharmingen #610959
HIF-2α/EPAS1	mouse	1:500	115 kDa	Santa Cruz sc-46691
HPV16E6	mouse	1:3000	14 kDa	ACV #849 (Arbor Vita Corporation, Fremont, CA, USA)
HPV16E7 (NM2)	mouse	1:1000	16 kDa	M. Müller, DKFZ, Heidelberg
HPV18E6	mouse	1:2000	18 kDa	ACV #399
HPV18E7	chicken	1:1000	12 kDa	H. Zentgraf, DKFZ, Heidelberg
Lamin A/C	mouse	undiluted	70 kDa	H. Zentgraf, DKFZ, Heidelberg
LAMP1	mouse	1:500	120 kDa	Santa Cruz sc-20011
LC3B	rabbit	1:2000	15, 17 kDa	Novus Biologicals NB100-2220
NDRG1	rabbit	1:2000	46, 48 kDa	Cell Signaling Technology #9485
NDRG1 Phospho (T346)	rabbit	1:2000	46, 48 kDa	Cell Signaling Technology #5482
NDUFS2	mouse	1:1000	49 kDa	Santa Cruz sc-390596
p21	mouse	1:1000	21 kDa	Santa Cruz sc-6246
p53 (DO1)	mouse	1:1000	53 kDa	Santa Cruz sc-126
PARP	mouse	1:1000	116, 89 kDa	Cell Signaling Technology #9546
pRb	mouse	1:1000	112 kDa	Cell Signaling #9309
pRb Phospho (S807/811)	rabbit	1:1000	112 kDa	Cell Signaling Technology #9308
S6 Phospho (S235/236)	rabbit	1:1000	32 kDa	Cell Signaling Technology #2211
S6Kinase p70 Phospho (T389)	rabbit	1:1000	70/85 kDa	Cell Signaling Technology #9234
α-Tubulin	mouse	1:5000	55 kDa	Calbiochem CP06
Vinculin	mouse	1:4000	117 kDa	Santa Cruz sc-73614

Table 4. Secondary antibodies used in this thesis.

Secondary Antibodies (HRP-coupled)			
Specificity	**Species**	**Dilution**	**Supplier**
anti-chicken IgY	goat	1:5000	Santa Cruz sc-2428
anti-mouse IgG	goat	1:10000	W4021, Promega (Fitchburg, WI, USA)
anti-rabbit IgG	goat	1:10000	W4011, Promega
anti-goat IgG	donkey	1:5000	Santa Cruz sc-2020

4.3.4 Cathepsin activity assays

To measure cellular CTSB and CTSL activity levels under different oxygen conditions, cells were lysed with ice-cold 0.5% Triton X-100 in PBS and centrifuged at 12000 g for 5 min. Protein concentration was determined by Bradford assay and 200 µg cell lysates were diluted in cathepsin assay buffer (88 mM KH_2PO_4, 12 mM Na_2HPO_4, 1 mM EDTA (pH 6.0)) in a final volume of 200 µL. The samples were preincubated for 5 min at 40 °C, transferred to a black 96-well plate in duplicates, and mixed with 10 µM of either the CTSB substrate Z-Arg-Arg-7-amido-4-methylcoumarin hydrochloride (C5429, Sigma Aldrich) or the CTSL substrate Z-Phe-Arg-7-amido-4-methylcoumarin hydrochloride (sc-3136, Santa Cruz Biotechnology). The enzyme activity reactions were further incubated for 75 min at 40 °C. Cleavage of cathepsin substrates was measured by fluorescence of free 7-amino-4-methylcoumarin with excitation at 355 nm and emission at 450 nm using the Mithras² LB 943 multimode microplate reader (Berthold Technologies, Bad Wildbad, Germany). As negative control, CTSB and CTSL activities were measured in cell lysates treated with Halt™ Protease Inhibitor Mix (Thermo Fisher Scientific).

4.3.5 Tandem mass tag (TMT) mass spectrometry (MS) analyses

To analyze global changes in the protein levels of HPV-positive SiHa cells under different oxygen conditions, mass spectrometry (MS)-based quantitative proteome analysis was performed in cooperation with Dr. Bianca J. Kuhn in the lab of Prof. Dr. Jeroen Krijgsveld (DKFZ, Heidelberg). Proteins were labelled with Thermo Fischer Scientific's tandem mass tags (TMTs), which are isobaric tags with the same overall mass but varying distributions of light and heavy isotopes. The light and heavy isotopes within the tags generate unique reporter ions that allow simultaneous measurement of up to 10 samples (TMT10plex) using liquid chromatography combined with mass spectrometry (LC)-MS/MS. Relative quantification of protein abundances was performed by comparing the detected intensities of the unique reporter ions between treatment conditions.

For the proteome analysis, exponentially growing SiHa cells were cultivated at 21% O_2, 5.5% O_2, 1% O_2 or cycH (1 h 1% O_2, 1 h 5.5% O_2) for 24 h. Cells incubated under cycH were harvested at the end of both the hypoxic and the reoxygenation phase. Proteomes of four independent biological replicates were analyzed. To harvest, cells were scraped in 500 µL ice-cold PBS, pelleted by centrifugation and stored at -80 °C.

Further sample processing and MS analysis was kindly performed by Bianca J. Kuhn using the following protocol:[226,321]

Cell pellets were resuspended in 100 mM triethylammonium bicarbonate (TEAB, pH 8) containing 0.1% (w/v) RapiGest-SF (Waters, Milford, MA). Cell lysis and chromatin shearing was conducted using a Bioruptor Pico sonicator device (Diagenode, Denville, NJ, USA) in a final volume of max. 300 µL, for 15-20 cycles of 30''/30'' (ON/OFF) pulses at 4°C. Protein concentrations were determined using the Pierce™ BCA protein assay according to the manufacturer's instructions (Thermo Fisher Scientific). 50 µg protein per sample were adjusted with 100 mM TEAB to a final volume of 100 µL and disulfide bonds were reduced by 5 mM DTT for 30 min at 60 °C. Subsequently, proteins were alkylated with 15 mM 2-chloroacetamide for 30 min at RT, followed by proteolytic digestion with trypsin (sequencing grade modified, Promega) in a trypsin-to-protein ratio of 1:50 (w/w) overnight at 37 °C, while shaking. Afterwards, samples were treated with 1% trifluoroacetic acid (pH < 2), incubated at 37 °C for 30-45 min to stop the digestion reaction and break down RapiGest-SF, and centrifuged at 20000 g for 10 min. Supernatants were transferred to new reaction tubes and dried in a speed vacuum concentrator.

Next, isobaric labeling of the peptides was performed using the 10-plex TMT reagents according to the manufacturer's protocol (Thermo Fisher Scientific). For this purpose, 10 µg of each sample were dissolved in 100 mM TEAB buffer to obtain a concentration of 1 µg/µL, vortexed, and incubated for 10 min at RT. TMT10-plex reagents (0.8 mg) were dissolved in 41 µL acetonitrile (ACN, LC-MS grade). 4.1 µL of one defined TMT reagent (TMT-126, TMT-127N, TMT-127C, TMT-128N, TMT-128C, TMT-129N, TMT-129C, TMT-130N, TMT-130C, and TMT-131) was combined with 10 µg of a peptide sample and incubated for 1 h at RT. Afterwards, the labeling reaction was quenched for 15 min using 8 µL of 5% hydroxylamine. Labeling efficacy was controlled for each sample by MS before the labeled samples were pooled in equal amounts and vacuum dried.

For fractionation by high pH reverse phase liquid chromatography, the dried sample mix was dissolved in 20 mM ammonium formate (pH 10), and loaded on a 1200 Infinity HPLC system (Agilent, Santa Clara, CA, USA) with a Gemini C18 column (3 µm, 110 Å, 100 × 1.0 mm; Phenomenex, Torrance, CA, USA) using a linear 60 min gradient from 0% to 35% (v/v) ACN

in 20 mM ammonium formate (pH 10) at a flow rate of 0.1 mL/min. The elution of peptides was traced with a variable wavelength UV detector set to 254 nm. After collecting sixty 1 min-fractions, the fractions were pooled into twelve fractions, dried and reconstituted in 0.1% formic acid (FA). Afterwards, the pooled fractions were injected by an Easy-nLC 1200 nano-UPLC (Thermo Fisher Scientific) onto a trap column (Pepmap, 100 µm x 2 cm, C18, 5 µm 100Å pores) and separated on an analytical column (PepMap RSLC, 75 µm × 50 cm, nanoViper, C18, 2 µM, 100Å). For the peptide separation, a multistep gradient (Solvent A: 0.1% FA in H_2O, Solvent B: 0.1% FA, 80% ACN in H_2O) was applied with a gradient from 3-8% B over 4 min, 8-10% B over 2 min, 10-32% B over 68 min, 32–50% B over 12 min and 50-100% B over 1 min, followed by holding at 100% B for 7 min. The flow rate was set to 300 nL/min.

Afterwards, using electrospray ionization, the eluted peptides were electro-sprayed by applying 2 kV on a 10 µm Picotip coated emitter (New Objective, Littleton, MA, USA) into an Orbitrap Fusion™ Tribrid™ (Thermo Fisher Scientific) mass spectrometer. The Orbitrap Fusion™ Tribrid™ mass spectrometer operated in data-dependent mode of acquisition using the vendor-supplied default settings for synchronous precursor selection MS3 fragmentation.

The obtained mass spectra were analyzed using MaxQuant Version 1.6.0.17 and protein identification was performed using the Andromeda search engine. Using the protein sequence databases UniProtKB/Swiss-Prot *Homo sapiens* (obtained 06.11.2020), UniProtKB/Swiss-Prot UP000106459 *Human papillomavirus type 16* (obtained 15.05.2021), in combination with the contaminants.fasta, which is enabled by default in the MaxQuant software, peptide search was performed. Following search settings were used: digestion reagent was set to trypsin/P, allowing up for two missed cleavages. Carbamidomethylation of cysteine was set as a fixed modification, oxidation of methionine and acetylation of the peptide N-term were set as variable modifications. The type of quantification was set to ‘reporter ion MS3’ and correction factors for individual 10-plex TMT-kit batch were specified for each channel. Precursor and product ion tolerances were set at 4.5 ppm and 20 ppm, respectively. Label minimum ratio count was set to 2. The FDR filter for peptides and protein hits was set to 1%, calculated by using the reverse decoy database. The remaining settings of MaxQuant were set as default.

For further analysis, the MaxQuant output files were processed in R version 4.0.4 (https://www.R-project.org; R Core Team 2021) operated in Rstudio version 1.1.453 (http://www.rstudio.com; Rstudio Team 2020). Raw peptide intensities were $\log_2$-transformed to ensure normal distribution and median normalized. Proteins of the following categories were filtered out prior to differential expression analysis: only identified by site, potential

contaminants, and reverse. Sample clustering was evaluated using t-distributed Stochastic Neighbor Embedding (t-SNE). A batch effect, caused by the two TMT batches used, was corrected. Differential expression of proteins was tested with “linear Models for Microarray Data“ (limma)-moderated test statistics[322] in R, with an adjusted p-value below 0.05. Significant events (FDR < 0.05) were identified after adjusting for multiple testing using Benjamini & Hochberg correction.

The MS proteomics data have been deposited to the ProteomeXchange Consortium[323] via the PRIDE[324] partner repository with the dataset identifier PXD044908.

Volcano plots and heatmaps showing differential expression between different oxygen conditions were generated using GraphPad Prism 9.5.1 (GraphPad Software Inc., CA, USA). Gene set enrichment analyses were performed using the gene set enrichment analysis software GSEA Desktop v4.1.[325] Average log2 fold change values (n = 4) of all detected proteins were subjected to a preranked GSEA analysis against the current molecular signature database (MSigDB, v. 7.4). Following parameters were used: number of permutations, 1000; enrichment statistic, weighted; gene set size filters, min = 15, max = 500; normalization mode, meandiv; seed for permutation, timestamp. Top ranked significantly enriched gene sets were screened for further investigation.

4.4 RNA-based techniques

4.4.1 RNA extraction from cells

To analyze mRNA expression after different experimental conditions, RNA was isolated and purified using the column based PureLink™ RNA Mini Kit (Invitrogen) according to the manufacturer’s protocol. Briefly, to harvest RNA, cells were washed once with PBS and lysed in 600 µL RNA lysis buffer (Invitrogen, freshly supplemented with 100 µL β-mercaptoethanol per 10 mL lysis buffer). The cell lysate was resuspended and either short-term stored at -20 °C or directly subjected to RNA isolation. For purification of total RNA, the lysate was mixed with 600 µL 70% EtOH and loaded onto a provided column. DNA contaminations were removed using the PureLink DNase set (Invitrogen). The purified RNA was eluted from the column in 60-80 µL RNAse-free H_2O and RNA concentration was measured with the NanoDrop ND-1000 spectrophotometer (Peqlab, Erlangen, Germany) at 260 nm. Purified RNA was stored at -80 °C until further use.

4.4.2 Reverse transcription

Purified RNA was transcribed into cDNA using the ProtoScript® II First Strand cDNA Synthesis Kit (NEB) according to the manufacturer's protocol.

In brief, 500 ng purified RNA were adjusted to 3 µL with RNAse-free H_2O and mixed with 0.5 µL of oligo dT and random primers, respectively. The RNA-primer mix was denatured for 5 min at 70 °C and kept on ice. Subsequently, 5 µL of the 2x M-MulV Reaction mix, containing dNTPs and an optimized buffer, and 1 µL of the 10x M-MuLV Reverse Transcriptase enzyme mix were added. The samples were incubated in a thermal cycler (MJ Research PTC-200 thermal cycler, Global Medical Instrumentation, Ramsey, MN, USA) for 5 min at 25 °C, followed by 60 min at 42 °C to allow cDNA transcription, and 5 min at 80 °C to deactivate the enzyme activity. The cDNA product was filled up with 40 µL RNase-free H_2O and stored at -20 °C.

4.4.3 Quantitative real-time PCR (qRT-PCR)

For qRT-PCR analysis, 2 µL cDNA were mixed with 10 µL SYBR™ Green PCR Master Mix (Applied Biosystems), 0.4 µL of forward and reverse primer, respectively (for a final concentration of 100 nM each), and 7.2 µL nuclease-free H_20 in a 96-well plate (MicroAmp™ Optical 96-Well Reaction Plate, Life Technologies). Duplicate measurements were performed and an H_2O control without cDNA template was included for each primer pair to control for contaminations. The qRT-PCR was run on a 7300 Real Time PCR System (Applied Biosystems) according to the following program (Table 5):

Table 5. qRT-PCR program.

Step	Temperature	Time	
Initiation	50 °C	2 min	
Polymerase activation	95 °C	10 min	
Denaturation	95 °C	15 s	} 40 cycles
Annealing and elongation	60 °C	1 min	
Dissociation curves	95 °C	15 s	
	60 °C	1 min	
	95 °C	15 s	
	60 °C	15 s	

Relative quantification of target gene expression was performed using the comparative Ct ($2^{-\Delta\Delta Ct}$) method.[326] Ct values were normalized to *TMBIM6* as internal reference.[327] Statistical analyses of fold change values were performed after logarithmic transformation.

Used primer sequences are listed in Table 6. Initially, all primer pairs were tested for adequate efficiency and screened for unspecific amplification artefacts.

Table 6. Primer sequences used for qRT-PCR.

Target RNA	Forward (for) primer (5'-3')	Reverse (rev) primer (5'-3')	amplicon length
CTSB	AGTGGAGAATGGCACACCCTA	AAGAAGCCATTGTCACCCCA	72 bp
CTSL	AAACACAGCTTCACAATGGCC	TTTGAAAGCCATTCATCACCTG	82 bp
HK2	GCCCACCTACGTGTGTGCTA	CACCCCACTTCCCATTCCGA	119 bp
HPV16 E6/E7	CAATGTTTCAGGACCCACAGG	CTCACGTCGCAGTAACTGTTG	125 bp
HPV18 E6/E7	ATGCATGGACCTAAGGCAAC	AGGTCGTCTGCTGAGCTTTC	247 bp
LOXL2	ATGTCACCTGCGAGAATGGG	TGCTCTGGCTTGTACGCTTT	106 bp
NDRG1	TCTCCTCAAGATGGCGGACT	TGCCATCCAGAGAAGTGACG	173 bp
P4HA1	GGCTCTCTGGCTATGAAAATCC	TCCGTGCAAAGTCAAAATGGG	150 bp
PLOD2	TGGACTTTTGCCGTCAGGAT	CCACAGCTTTCCATGACGAGT	149 bp
SLC2A1	CTTCACTGTCGTGTCGCTGT	TGAAGAGTTCAGCCACGATG	230 bp
TMBIM6	GTGGTCATGTGTGGCTTCGT	GGAAAGGCTGGATGGTCACT	200 bp

4.5 Software

Table 7. Software used in this thesis.

Software	Version	Supplier
BioRender.com	2023	BioRender, Canada
Fusion SL Gel Detection System	15.18	Vilber Lourmat, Germany
Fiji is just ImageJ	1.53q	NIH, USA; Multiple contributors
FlowJo	10.8.1	BD Life Sciences
Graph Pad Prism	9.5.1	GraphPad Software
GSEA	4.1.0	The Broad Institute, Inc., Massachusetts Institute of Technology and Regents of the University of California, USA
Microsoft Office 365 ProPlus	2020	Microsoft, USA
NanoDrop ND-1000	1.5	PEQLAB Biotechnologie GmbH, DE

4.6 Statistical analyses

Experiments were performed at least in three biological replicates, if not indicated otherwise. Mean values and standard deviations were calculated using Graph Pad Prism 9.5.1 software. Statistical analyses of fold change values were carried out after logarithmic transformation. Statistical significance comparing the means of more than two groups was determined by one-way ANOVA (analysis of variance), using Graph Pad Prism 9.5.1 software. P-values of ≤ 0.05 (*), ≤ 0.01 (**), or ≤ 0.001 (***) were considered statistically significant. MS data was analyzed as described in chapter 4.3.5.

APPENDIX

Appendix

List of figures

Figure 1-6 and Figure 35 were created with BioRender.com. Figure 3 was adapted from “Apoptosis Extrinsic and Intrinsic Pathways”, and Figure 4 was adapted from “Intracellular Transport”, by BioRender.com (2023).

List of tables

List of abbreviations

4E-BP1	Eukaryotic translation initiation factor 4E binding protein 1
AIF	Apoptosis inducing factor
AMPK	Adenosine monophosphate-activated protein kinase
ANOVA	Analysis of variance
AO	Acridine orange
APAF1	Apoptotic protease activating factor 1
APS	Ammonium persulfate
Ars	Sodium arsenite
ATG	Autophagy-related gene
ATR	Ataxia telangiectasia and Rad3-related
ATP	Adenosine triphosphate
AVO	Acidic vesicular organelle
BafA1	Bafilomycin A1
BCL-2	B-cell lymphoma 2
BID	BH3 interacting domain death agonist
BP	Band pass filter
BSA	Bovine serum albumin
CBP	CREB-binding protein
CDDP	Cisplatin
cDNA	Complementary DNA
CFA	Colony formation assay
CIN	Cervical intraepithelial neoplasia
cl.	cleaved
CO_2	Carbon dioxide
CQ	Chloroquine
CT	Chemotherapy
CTSB	Cathepsin B
CTSL	Cathepsin L
cycH	Cycling hypoxia
Cyt c	Cytochrome c
DISC	Death-inducing signaling complex
DMEM	Dulbecco’s Modified Eagle’s Medium
DMSO	Dimethyl sulfoxide
DNA	Deoxyribonucleic acid
DR	Death receptor

DREAM	Dimerization partner, Rb-like, E2F and multi-vulval class B
E6AP	E6-associated protein
EBSS	Earle's Balanced Salt Solution
ECL	Enhanced chemiluminescence
ECM	Extracellular matrix
EDTA	Ethylenediaminetetraacetic acid
EGFR	Epidermal growth factor receptor
eIF3B	Eukaryotic translation initiation factor 3 subunit B
EMT	Epithelial-mesenchymal transition
ER	Endoplasmic reticulum
ERK	Extracellular signal-regulated kinase
EtOH	Ethanol
FasL	Fas ligand
FasR	Fas receptor
FC	Fold change
FCS	Fetal calf serum
FDR	False discovery rate
FIH1	Factor-inhibiting HIF-1
for	forward
GSEA	Gene Set Enrichment Analysis
GSH	Glutathione
GSK	Glycogen synthase kinase
H	Hypoxic phase of cycH
HIF	Hypoxia-inducible factor
HIV	Human immunodeficiency virus
HPV	Human papillomavirus
H-R cycle	Hypoxia-reoxygenation cycle
HRE	Hypoxia-responsive element
HRP	Horseradish peroxidase
HSPG	Heparan sulphate proteoglycan
IAP	Inhibitor of apoptosis protein
kb	Kilo base
LAMP1/2	Lysosome-associated membrane glycoprotein 1/2
LC	Liquid chromatography
LC3	Microtubule-associated light chain 3
LCR	Long coding region

LDCD	Lysosome-dependent cell death
LMP	Lysosomal membrane permeabilization
log2	Binary logarithm
LP	Long pass filter
M6P	Mannose-6-phosphate
MAPK	Mitogen-activated protein kinase
mc	Medium change
MEK	Mitogen-activated protein kinase kinase
MeOH	Methanol
MHC	Major histocompatibility complex
MOMP	Mitochondrial outer membrane permeabilization
MPR	M6P receptor
mRNA	Messenger RNA
MS	Mass spectrometry
mTOR	Mechanistic target of rapamycin
mTORC1/2	mTOR complex 1/2
NDRG	N-myc downregulated gene
NDUFS2	NADH:Ubiquinone oxidoreductase core subunit S2
NES	Normalized enrichment score
NF-κB	Nuclear factor kappa-light-chain-enhancer of activated B cells
O_2	Oxygen
ORF	Open reading frame
PARP	Poly (adenosine diphosphate-ribose) polymerase
PBS	Phosphate-buffered saline
PBS-T	PBS with Tween 20
PD-1	Programmed cell death protein 1
PD-L1	Programmed death ligand 1
PDZ	PSD-95/DLG/ZO-1 domain
PFA	Paraformaldehyde
PHD	Prolyl hydroxylase
PI	Protease inhibitor
PI3K	Phosphoinositide 3-kinase
PI3P	Phosphatidylinositol 3-phosphate
pRb	Retinoblastoma protein
qRT-PCR	Quantitative real-time polymerase chain reaction
R	Reoxygenation phase of cycH

rev	reverse
RNA	Ribonucleic acid
RNAi	RNA interference
ROS	Reactive oxygen species
RT	Room temperature
SA	Senescence assay
SA-β-Gal	Senescence-associated β-Galactosidase
SASP	Senescence-associated secretory phenotype
SDS-PAGE	Sodium dodecyl sulfate-polyacrylamide gel electrophoresis
SG	Stress granule
SGK1	Serum/glucocorticoid regulated kinase 1
siRNA	Small interfering RNA
Smac	second mitochondria derived activator of caspases
t-SNE	t-distributed Stochastic Neighbor Embedding
tBID	truncated BID
TEMED	Tetramethylethylenediamine
TERT	Telomerase reverse transcriptase
TGF-β	Transforming growth factor beta
TMT	Tandem mass tag
TNF	Tumor necrosis factor
TNFR1/2	TNF receptor 1/2
TRAIL	TNF-related apoptosis-inducing ligand
TUNEL	Terminal deoxynucleotidyltransferase-mediated dUTP-biotin nick end labeling
Tx	Transfection
UCE	Uncovering enzyme
ULK1	Unc-51-like kinase 1
URR	Upstream regulatory region
V-ATPase	Vacuolar H^+ ATPase
VHP	Von Hippel-Lindau protein
VLP	Virus-like particles
WHO	World Health Organization

Units

Symbol	Unit
%	percent
°C	degree Celsius
d	day
Da	Dalton
g	gravitational acceleration
g	gram
Gy	Gray
h	hour
Hg	Mercury
L	liter
M	molar
m	meter
min	minute
mol	mole
rpm	revolutions per minute
s	second
V	volt

Prefixes

Symbol	Prefix	Factor
n	nano	10^{-9}
µ	micro	10^{-6}
m	milli	10^{-3}
k	kilo	10^{3}

References

1 Bray F, Laversanne M, Weiderpass E, Soerjomataram I. The ever-increasing importance of cancer as a leading cause of premature death worldwide. *Cancer*. 2021;127(16):3029-3030. doi:10.1002/cncr.33587.

2 Sung H, Ferlay J, Siegel RL, et al. Global Cancer Statistics 2020: GLOBOCAN Estimates of Incidence and Mortality Worldwide for 36 Cancers in 185 Countries. *CA Cancer J Clin*. 2021;71(3):209-249. doi:10.3322/caac.21660.

3 Wu S, Zhu W, Thompson P, Hannun YA. Evaluating intrinsic and non-intrinsic cancer risk factors. *Nat Commun*. 2018;9(1):3490. doi:10.1038/s41467-018-05467-z.

4 de Martel C, Georges D, Bray F, Ferlay J, Clifford GM. Global burden of cancer attributable to infections in 2018: a worldwide incidence analysis. *Lancet Glob Health*. 2020;8(2):e180-e190. doi:10.1016/S2214-109X(19)30488-7.

5 zur Hausen H. Papillomaviruses and cancer: from basic studies to clinical application. *Nat Rev Cancer*. 2002;2(5):342-350. doi:10.1038/nrc798.

6 Doorbar J, Egawa N, Griffin H, Kranjec C, Murakami I. Human papillomavirus molecular biology and disease association. *Rev Med Virol*. 2015;25 Suppl 1(Suppl Suppl 1):2-23. doi:10.1002/rmv.1822.

7 Rodríguez AC, Schiffman M, Herrero R, et al. Rapid clearance of human papillomavirus and implications for clinical focus on persistent infections. *J Natl Cancer Inst*. 2008;100(7):513-517. doi:10.1093/jnci/djn044.

8 Schiffman M, Doorbar J, Wentzensen N, et al. Carcinogenic human papillomavirus infection. *Nat Rev Dis Primers*. 2016;2:16086. doi:10.1038/nrdp.2016.86.

9 Bernard H-U, Burk RD, Chen Z, van Doorslaer K, zur Hausen H, de Villiers E-M. Classification of papillomaviruses (PVs) based on 189 PV types and proposal of taxonomic amendments. *Virology*. 2010;401(1):70-79. doi:10.1016/j.virol.2010.02.002.

10 Bzhalava D, Eklund C, Dillner J. International standardization and classification of human papillomavirus types. *Virology*. 2015;476:341-344. doi:10.1016/j.virol.2014.12.028.

11 de Villiers E-M, Fauquet C, Broker TR, Bernard H-U, zur Hausen H. Classification of papillomaviruses. *Virology*. 2004;324(1):17-27. doi:10.1016/j.virol.2004.03.033.

12 Serrano B, Brotons M, Bosch FX, Bruni L. Epidemiology and burden of HPV-related disease. *Best Pract Res Clin Obstet Gynaecol*. 2018;47:14-26. doi:10.1016/j.bpobgyn.2017.08.006.

13 Johansson C, Schwartz S. Regulation of human papillomavirus gene expression by splicing and polyadenylation. *Nat Rev Microbiol*. 2013;11(4):239-251. doi:10.1038/nrmicro2984.

14 Doorbar J. The E4 protein; structure, function and patterns of expression. *Virology*. 2013;445(1-2):80-98. doi:10.1016/j.virol.2013.07.008.

15 Basukala O, Banks L. The Not-So-Good, the Bad and the Ugly: HPV E5, E6 and E7 Oncoproteins in the Orchestration of Carcinogenesis. *Viruses*. 2021;13(10). doi:10.3390/v13101892.

16 Pim D, Collins M, Banks L. Human papillomavirus type 16 E5 gene stimulates the transforming activity of the epidermal growth factor receptor. *Oncogene*. 1992;7(1):27-32.

17 Ashrafi GH, Haghshenas MR, Marchetti B, O'Brien PM, Campo MS. E5 protein of human papillomavirus type 16 selectively downregulates surface HLA class I. *Int J Cancer*. 2005;113(2):276-283. doi:10.1002/ijc.20558.

18 DiMaio D, Petti LM. The E5 proteins. *Virology*. 2013;445(1-2):99-114. doi:10.1016/j.virol.2013.05.006.

19 Kabsch K, Alonso A. The human papillomavirus type 16 E5 protein impairs TRAIL- and FasL-mediated apoptosis in HaCaT cells by different mechanisms. *J Virol*. 2002;76(23):12162-12172. doi:10.1128/JVI.76.23.12162-12172.2002.

20 Oh J-M, Kim S-H, Cho E-A, Song Y-S, Kim W-H, Juhnn Y-S. Human papillomavirus type 16 E5 protein inhibits hydrogen-peroxide-induced apoptosis by stimulating ubiquitin-proteasome-mediated degradation of Bax in human cervical cancer cells. *Carcinogenesis*. 2010;31(3):402-410. doi:10.1093/carcin/bgp318.

21 Hoppe-Seyler K, Bossler F, Braun JA, Herrmann AL, Hoppe-Seyler F. The HPV E6/E7 Oncogenes: Key Factors for Viral Carcinogenesis and Therapeutic Targets. *Trends Microbiol*. 2018;26(2):158-168. doi:10.1016/j.tim.2017.07.007.

22 Roden RBS, Stern PL. Opportunities and challenges for human papillomavirus vaccination in cancer. *Nat Rev Cancer*. 2018;18(4):240-254. doi:10.1038/nrc.2018.13.

23 Moody CA, Laimins LA. Human papillomavirus oncoproteins: pathways to transformation. *Nat Rev Cancer*. 2010;10(8):550-560. doi:10.1038/nrc2886.

24 Graham SV. The human papillomavirus replication cycle, and its links to cancer progression: a comprehensive review. *Clin Sci (Lond)*. 2017;131(17):2201-2221. doi:10.1042/CS20160786.

25 Doorbar J, Quint W, Banks L, et al. The biology and life-cycle of human papillomaviruses. *Vaccine*. 2012;30 Suppl 5:F55-70. doi:10.1016/j.vaccine.2012.06.083.

26 Dürst M, Gissmann L, Ikenberg H, zur Hausen H. A papillomavirus DNA from a cervical carcinoma and its prevalence in cancer biopsy samples from different geographic regions. *Proc Natl Acad Sci U S A*. 1983;80(12):3812-3815. doi:10.1073/pnas.80.12.3812.

27 Guan P, Howell-Jones R, Li N, et al. Human papillomavirus types in 115,789 HPV-positive women: a meta-analysis from cervical infection to cancer. *Int. J. Cancer*. 2012;131(10):2349-2359. doi:10.1002/ijc.27485.

28 Burmeister CA, Khan SF, Schäfer G, et al. Cervical cancer therapies: Current challenges and future perspectives. *Tumour Virus Res*. 2022;13:200238. doi:10.1016/j.tvr.2022.200238.

29 Kyrgiou M, Mitra A, Moscicki A-B. Does the vaginal microbiota play a role in the development of cervical cancer? *Transl Res*. 2017;179:168-182. doi:10.1016/j.trsl.2016.07.004.

30 Denny L, Adewole I, Anorlu R, et al. Human papillomavirus prevalence and type distribution in invasive cervical cancer in sub-Saharan Africa. *Int J Cancer*. 2014;134(6):1389-1398. doi:10.1002/ijc.28425.

31 Schiffman M, Wentzensen N. Human papillomavirus infection and the multistage carcinogenesis of cervical cancer. *Cancer Epidemiol Biomarkers Prev*. 2013;22(4):553-560. doi:10.1158/1055-9965.EPI-12-1406.

32 Burd EM. Human papillomavirus and cervical cancer. *Clin Microbiol Rev*. 2003;16(1):1-17. doi:10.1128/CMR.16.1.1-17.2003.

33 Martin CM, O'Leary JJ. Histology of cervical intraepithelial neoplasia and the role of biomarkers. *Best Pract Res Clin Obstet Gynaecol*. 2011;25(5):605-615. doi:10.1016/j.bpobgyn.2011.04.005.

34 Cullen AP, Reid R, Campion M, Lörincz AT. Analysis of the physical state of different human papillomavirus DNAs in intraepithelial and invasive cervical neoplasm. *J Virol*. 1991;65(2):606-612. doi:10.1128/JVI.65.2.606-612.1991.

35 Pett M, Coleman N. Integration of high-risk human papillomavirus: a key event in cervical carcinogenesis? *J Pathol*. 2007;212(4):356-367. doi:10.1002/path.2192.

36 McBride AA, Warburton A. The role of integration in oncogenic progression of HPV-associated cancers. *PLoS Pathog*. 2017;13(4):e1006211. doi:10.1371/journal.ppat.1006211.

37 Dooley KE, Warburton A, McBride AA. Tandemly Integrated HPV16 Can Form a Brd4-Dependent Super-Enhancer-Like Element That Drives Transcription of Viral Oncogenes. *mBio*. 2016;7(5). doi:10.1128/mBio.01446-16.

38 Pirami L, Giachè V, Becciolini A. Analysis of HPV16, 18, 31, and 35 DNA in pre-invasive and invasive lesions of the uterine cervix. *J Clin Pathol*. 1997;50(7):600-604. doi:10.1136/jcp.50.7.600.

39 Butz K, Hoppe-Seyler F. Transcriptional control of human papillomavirus (HPV) oncogene expression: composition of the HPV type 18 upstream regulatory region. *J Virol*. 1993;67(11):6476-6486. doi:10.1128/JVI.67.11.6476-6486.1993.

40 Tang S, Tao M, McCoy JP, Zheng Z-M. The E7 oncoprotein is translated from spliced E6*I transcripts in high-risk human papillomavirus type 16- or type 18-positive cervical cancer cell lines via translation reinitiation. *J Virol*. 2006;80(9):4249-4263. doi:10.1128/JVI.80.9.4249-4263.2006.

41 Olmedo-Nieva L, Muñoz-Bello JO, Contreras-Paredes A, Lizano M. The Role of E6 Spliced Isoforms (E6*) in Human Papillomavirus-Induced Carcinogenesis. *Viruses*. 2018;10(1). doi:10.3390/v10010045.

42 Butz K, Denk C, Ullmann A, Scheffner M, Hoppe-Seyler F. Induction of apoptosis in human papillomaviruspositive cancer cells by peptide aptamers targeting the viral E6 oncoprotein. *Proc Natl Acad Sci U S A*. 2000;97(12):6693-6697. doi:10.1073/pnas.110538897.

43 Butz K, Ristriani T, Hengstermann A, Denk C, Scheffner M, Hoppe-Seyler F. siRNA targeting of the viral E6 oncogene efficiently kills human papillomavirus-positive cancer cells. *Oncogene*. 2003;22(38):5938-5945. doi:10.1038/sj.onc.1206894.

44 Goodwin EC, DiMaio D. Repression of human papillomavirus oncogenes in HeLa cervical carcinoma cells causes the orderly reactivation of dormant tumor suppressor pathways. *Proc Natl Acad Sci U S A*. 2000;97(23):12513-12518. doi:10.1073/pnas.97.23.12513.

45 Hall AHS, Alexander KA. RNA interference of human papillomavirus type 18 E6 and E7 induces senescence in HeLa cells. *J Virol*. 2003;77(10):6066-6069. doi:10.1128/jvi.77.10.6066-6069.2003.

46 Hawley-Nelson P, Vousden KH, Hubbert NL, Lowy DR, Schiller JT. HPV16 E6 and E7 proteins cooperate to immortalize human foreskin keratinocytes. *EMBO J*. 1989;8(12):3905-3910. doi:10.1002/j.1460-2075.1989.tb08570.x.

47 Mesri EA, Feitelson MA, Munger K. Human viral oncogenesis: a cancer hallmarks analysis. *Cell Host Microbe*. 2014;15(3):266-282. doi:10.1016/j.chom.2014.02.011.

48 Hanahan D. Hallmarks of Cancer: New Dimensions. *Cancer Discov*. 2022;12(1):31-46. doi:10.1158/2159-8290.CD-21-1059.

49 Scheffner M, Huibregtse JM, Vierstra RD, Howley PM. The HPV-16 E6 and E6-AP complex functions as a ubiquitin-protein ligase in the ubiquitination of p53. *Cell*. 1993;75(3):495-505. doi:10.1016/0092-8674(93)90384-3.

50 Scheffner M, Werness BA, Huibregtse JM, Levine AJ, Howley PM. The E6 oncoprotein encoded by human papillomavirus types 16 and 18 promotes the degradation of p53. *Cell*. 1990;63(6):1129-1136. doi:10.1016/0092-8674(90)90409-8.

51 Ganti K, Broniarczyk J, Manoubi W, et al. The Human Papillomavirus E6 PDZ Binding Motif: From Life Cycle to Malignancy. *Viruses*. 2015;7(7):3530-3551. doi:10.3390/v7072785.

52 Klingelhutz AJ, Foster SA, McDougall JK. Telomerase activation by the E6 gene product of human papillomavirus type 16. *Nature*. 1996;380(6569):79-82. doi:10.1038/380079a0.

53 Roman A, Munger K. The papillomavirus E7 proteins. *Virology*. 2013;445(1-2):138-168. doi:10.1016/j.virol.2013.04.013.

54 Fischer M, Uxa S, Stanko C, Magin TM, Engeland K. Human papilloma virus E7 oncoprotein abrogates the p53-p21-DREAM pathway. *Sci Rep*. 2017;7(1):2603. doi:10.1038/s41598-017-02831-9.

55 Honegger A, Schilling D, Bastian S, et al. Dependence of intracellular and exosomal microRNAs on viral E6/E7 oncogene expression in HPV-positive tumor cells. *PLoS Pathog*. 2015;11(3):e1004712. doi:10.1371/journal.ppat.1004712.

56 Duensing S, Münger K. Mechanisms of genomic instability in human cancer: insights from studies with human papillomavirus oncoproteins. *Int. J. Cancer*. 2004;109(2):157-162. doi:10.1002/ijc.11691.

57 McLaughlin-Drubin ME, Crum CP, Münger K. Human papillomavirus E7 oncoprotein induces KDM6A and KDM6B histone demethylase expression and causes epigenetic reprogramming. *Proc Natl Acad Sci U S A*. 2011;108(5):2130-2135. doi:10.1073/pnas.1009933108.

58 Klingelhutz AJ, Roman A. Cellular transformation by human papillomaviruses: lessons learned by comparing high- and low-risk viruses. *Virology*. 2012;424(2):77-98. doi:10.1016/j.virol.2011.12.018.

59 World Health Organization. Human papillomavirus vaccines: WHO position paper, December 2022. https://www.who.int/publications/i/item/who-wer9750-645-672. Accessed June 13, 2023.

60 Stanley M, Pinto LA, Trimble C. Human papillomavirus vaccines--immune responses. *Vaccine*. 2012;30 Suppl 5:F83-7. doi:10.1016/j.vaccine.2012.04.106.

61 Mo Y, Ma J, Zhang H, et al. Prophylactic and Therapeutic HPV Vaccines: Current Scenario and Perspectives. *Front Cell Infect Microbiol*. 2022;12:909223. doi:10.3389/fcimb.2022.909223.

62 Bruni L, Diaz M, Barrionuevo-Rosas L, et al. Global estimates of human papillomavirus vaccination coverage by region and income level: a pooled analysis. *Lancet Glob Health*. 2016;4(7):e453-63. doi:10.1016/S2214-109X(16)30099-7.

63 Schiller JT, Müller M. Next generation prophylactic human papillomavirus vaccines. *Lancet Oncol*. 2015;16(5):e217-25. doi:10.1016/S1470-2045(14)71179-9.

64 Kunda NK, Peabody J, Zhai L, et al. Evaluation of the thermal stability and the protective efficacy of spray-dried HPV vaccine, Gardasil® 9. *Hum Vaccin Immunother*. 2019;15(7-8):1995-2002. doi:10.1080/21645515.2019.1593727.

65 Yang F, Mariz FC, Zhao X, Spagnoli G, Ottonello S, Müller M. Broad Neutralization Responses Against Oncogenic Human Papillomaviruses Induced by a Minor Capsid L2 Polytope Genetically Incorporated Into Bacterial Ferritin Nanoparticles. *Front Immunol*. 2020;11:606569. doi:10.3389/fimmu.2020.606569.

66 Rose PG, Bundy BN, Watkins EB, et al. Concurrent cisplatin-based radiotherapy and chemotherapy for locally advanced cervical cancer. *N Engl J Med*. 1999;340(15):1144-1153. doi:10.1056/NEJM199904153401502.

67 Lorusso D, Petrelli F, Coinu A, Raspagliesi F, Barni S. A systematic review comparing cisplatin and carboplatin plus paclitaxel-based chemotherapy for recurrent or metastatic cervical cancer. *Gynecol Oncol*. 2014;133(1):117-123. doi:10.1016/j.ygyno.2014.01.042.

68 Mauricio D, Zeybek B, Tymon-Rosario J, Harold J, Santin AD. Immunotherapy in Cervical Cancer. *Curr Oncol Rep*. 2021;23(6):61. doi:10.1007/s11912-021-01052-8.

69 Yang A, Farmer E, Wu TC, Hung C-F. Perspectives for therapeutic HPV vaccine development. *J Biomed Sci*. 2016;23(1):75. doi:10.1186/s12929-016-0293-9.

70 Dasari S, Tchounwou PB. Cisplatin in cancer therapy: molecular mechanisms of action. *Eur J Pharmacol*. 2014;740:364-378. doi:10.1016/j.ejphar.2014.07.025.

71 Eastman A. The formation, isolation and characterization of DNA adducts produced by anticancer platinum complexes. *Pharmacol Ther*. 1987;34(2):155-166. doi:10.1016/0163-7258(87)90009-x.

72 Wang X, Wong SC, Pan J, et al. Evidence of cisplatin-induced senescent-like growth arrest in nasopharyngeal carcinoma cells. *Cancer Res*. 1998;58(22):5019-5022.

73 Siddik ZH. Cisplatin: mode of cytotoxic action and molecular basis of resistance. *Oncogene*. 2003;22(47):7265-7279. doi:10.1038/sj.onc.1206933.

74 Shieh SY, Ahn J, Tamai K, Taya Y, Prives C. The human homologs of checkpoint kinases Chk1 and Cds1 (Chk2) phosphorylate p53 at multiple DNA damage-inducible sites. *Genes Dev*. 2000;14(3):289-300.

75 Zhao H, Piwnica-Worms H. ATR-mediated checkpoint pathways regulate phosphorylation and activation of human Chk1. *Mol Cell Biol*. 2001;21(13):4129-4139. doi:10.1128/MCB.21.13.4129-4139.2001.

76 Damia G, Filiberti L, Vikhanskaya F, et al. Cisplatinum and taxol induce different patterns of p53 phosphorylation. *Neoplasia*. 2001;3(1):10-16. doi:10.1038/sj.neo.7900122.

77 Chipuk JE, Kuwana T, Bouchier-Hayes L, et al. Direct activation of Bax by p53 mediates mitochondrial membrane permeabilization and apoptosis. *Science*. 2004;303(5660):1010-1014. doi:10.1126/science.1092734.

78 Müller M, Wilder S, Bannasch D, et al. p53 activates the CD95 (APO-1/Fas) gene in response to DNA damage by anticancer drugs. *J Exp Med*. 1998;188(11):2033-2045. doi:10.1084/jem.188.11.2033.

79 Kaufmann SH, Earnshaw WC. Induction of apoptosis by cancer chemotherapy. *Exp Cell Res*. 2000;256(1):42-49. doi:10.1006/excr.2000.4838.

80 Wang X, Martindale JL, Holbrook NJ. Requirement for ERK activation in cisplatin-induced apoptosis. *J Biol Chem*. 2000;275(50):39435-39443. doi:10.1074/jbc.M004583200.

81 Miller RP, Tadagavadi RK, Ramesh G, Reeves WB. Mechanisms of Cisplatin nephrotoxicity. *Toxins (Basel)*. 2010;2(11):2490-2518. doi:10.3390/toxins2112490.

82 Gore ME, Fryatt I, Wiltshaw E, Dawson T, Robinson BA, Calvert AH. Cisplatin/carboplatin cross-resistance in ovarian cancer. *Br J Cancer*. 1989;60(5):767-769. doi:10.1038/bjc.1989.356.

83 Galluzzi L, Senovilla L, Vitale I, et al. Molecular mechanisms of cisplatin resistance. *Oncogene*. 2012;31(15):1869-1883. doi:10.1038/onc.2011.384.

84 Safaei R, Katano K, Larson BJ, et al. Intracellular localization and trafficking of fluorescein-labeled cisplatin in human ovarian carcinoma cells. *Clin Cancer Res*. 2005;11(2 Pt 1):756-767.

85 Safaei R, Larson BJ, Cheng TC, et al. Abnormal lysosomal trafficking and enhanced exosomal export of cisplatin in drug-resistant human ovarian carcinoma cells. *Mol Cancer Ther*. 2005;4(10):1595-1604. doi:10.1158/1535-7163.MCT-05-0102.

86 Zhu H, Luo H, Zhang W, Shen Z, Hu X, Zhu X. Molecular mechanisms of cisplatin resistance in cervical cancer. *Drug Des Devel Ther*. 2016;10:1885-1895. doi:10.2147/DDDT.S106412.

87 Frensemeier K, Holzer A, Hoppe-Seyler K, Hoppe-Seyler F. Dickkopf-1 expression is repressed by oncogenic human papillomaviruses (HPVs) and regulates the Cisplatin sensitivity of HPV-positive cancer cells in a JNK-dependent manner. *Int. J. Cancer*. 2022;151(12):2215-2228. doi:10.1002/ijc.34250.

88 Tang D, Kang R, Berghe TV, Vandenabeele P, Kroemer G. The molecular machinery of regulated cell death. *Cell Res*. 2019;29(5):347-364. doi:10.1038/s41422-019-0164-5.

89 Bertheloot D, Latz E, Franklin BS. Necroptosis, pyroptosis and apoptosis: an intricate game of cell death. *Cell Mol Immunol*. 2021;18(5):1106-1121. doi:10.1038/s41423-020-00630-3.

90 Galluzzi L, Vitale I, Aaronson SA, et al. Molecular mechanisms of cell death: recommendations of the Nomenclature Committee on Cell Death 2018. *Cell Death Differ*. 2018;25(3):486-541. doi:10.1038/s41418-017-0012-4.

91 Kerr JF, Wyllie AH, Currie AR. Apoptosis: a basic biological phenomenon with wide-ranging implications in tissue kinetics. *Br J Cancer*. 1972;26(4):239-257. doi:10.1038/bjc.1972.33.

92 Elmore S. Apoptosis: a review of programmed cell death. *Toxicol Pathol*. 2007;35(4):495-516. doi:10.1080/01926230701320337.

93 Carneiro BA, El-Deiry WS. Targeting apoptosis in cancer therapy. *Nat Rev Clin Oncol*. 2020;17(7):395-417. doi:10.1038/s41571-020-0341-y.

94 Wong RSY. Apoptosis in cancer: from pathogenesis to treatment. *J Exp Clin Cancer Res*. 2011;30(1):87. doi:10.1186/1756-9966-30-87.

95 Shi Y. Mechanisms of caspase activation and inhibition during apoptosis. *Mol Cell*. 2002;9(3):459-470. doi:10.1016/s1097-2765(02)00482-3.

96 Gon S, Gatanaga T, Sendo F. Involvement of two types of TNF receptor in TNF-alpha induced neutrophil apoptosis. *Microbiol Immunol*. 1996;40(6):463-465. doi:10.1111/j.1348-0421.1996.tb01095.x.

97 MacFarlane M, Ahmad M, Srinivasula SM, Fernandes-Alnemri T, Cohen GM, Alnemri ES. Identification and molecular cloning of two novel receptors for the cytotoxic ligand TRAIL. *J Biol Chem*. 1997;272(41):25417-25420. doi:10.1074/jbc.272.41.25417.

98 Schneider P, Bodmer JL, Holler N, et al. Characterization of Fas (Apo-1, CD95)-Fas ligand interaction. *J Biol Chem*. 1997;272(30):18827-18833. doi:10.1074/jbc.272.30.18827.

99 Schneider P, Thome M, Burns K, et al. TRAIL receptors 1 (DR4) and 2 (DR5) signal FADD-dependent apoptosis and activate NF-kappaB. *Immunity*. 1997;7(6):831-836. doi:10.1016/s1074-7613(00)80401-x.

100 Micheau O, Tschopp J. Induction of TNF receptor I-mediated apoptosis via two sequential signaling complexes. *Cell*. 2003;114(2):181-190. doi:10.1016/s0092-8674(03)00521-x.

101 Li H, Zhu H, Xu CJ, Yuan J. Cleavage of BID by caspase 8 mediates the mitochondrial damage in the Fas pathway of apoptosis. *Cell*. 1998;94(4):491-501. doi:10.1016/s0092-8674(00)81590-1.

102 Wang J, Chun HJ, Wong W, Spencer DM, Lenardo MJ. Caspase-10 is an initiator caspase in death receptor signaling. *Proc Natl Acad Sci U S A*. 2001;98(24):13884-13888. doi:10.1073/pnas.241358198.

103 Liu X, Kim CN, Yang J, Jemmerson R, Wang X. Induction of apoptotic program in cell-free extracts: requirement for dATP and cytochrome c. *Cell*. 1996;86(1):147-157. doi:10.1016/s0092-8674(00)80085-9.

104 Kim H, Tu H-C, Ren D, et al. Stepwise activation of BAX and BAK by tBID, BIM, and PUMA initiates mitochondrial apoptosis. *Mol Cell*. 2009;36(3):487-499. doi:10.1016/j.molcel.2009.09.030.

105 Youle RJ, Strasser A. The BCL-2 protein family: opposing activities that mediate cell death. *Nat Rev Mol Cell Biol*. 2008;9(1):47-59. doi:10.1038/nrm2308.

106 Del Bello B, Valentini MA, Zunino F, Comporti M, Maellaro E. Cleavage of Bcl-2 in oxidant- and cisplatin-induced apoptosis of human melanoma cells. *Oncogene*. 2001;20(33):4591-4595. doi:10.1038/sj.onc.1204618.

107 Kuwana T, Mackey MR, Perkins G, et al. Bid, Bax, and lipids cooperate to form supramolecular openings in the outer mitochondrial membrane. *Cell*. 2002;111(3):331-342. doi:10.1016/s0092-8674(02)01036-x.

108 Kroemer G, Galluzzi L, Brenner C. Mitochondrial membrane permeabilization in cell death. *Physiol Rev*. 2007;87(1):99-163. doi:10.1152/physrev.00013.2006.

109 Garrido C, Galluzzi L, Brunet M, Puig PE, Didelot C, Kroemer G. Mechanisms of cytochrome c release from mitochondria. *Cell Death Differ*. 2006;13(9):1423-1433. doi:10.1038/sj.cdd.4401950.

110 Li P, Nijhawan D, Budihardjo I, et al. Cytochrome c and dATP-dependent formation of Apaf-1/caspase-9 complex initiates an apoptotic protease cascade. *Cell*. 1997;91(4):479-489. doi:10.1016/s0092-8674(00)80434-1.

111 Slee EA, Harte MT, Kluck RM, et al. Ordering the cytochrome c-initiated caspase cascade: hierarchical activation of caspases-2, -3, -6, -7, -8, and -10 in a caspase-9-dependent manner. *J Cell Biol*. 1999;144(2):281-292. doi:10.1083/jcb.144.2.281.

112 Jiang X, Wang X. Cytochrome C-mediated apoptosis. *Annual review of biochemistry*. 2004;73:87-106. doi:10.1146/annurev.biochem.73.011303.073706.

113 Srinivasula SM, Hegde R, Saleh A, et al. A conserved XIAP-interaction motif in caspase-9 and Smac/DIABLO regulates caspase activity and apoptosis. *Nature*. 2001;410(6824):112-116. doi:10.1038/35065125.

114 Suzuki Y, Imai Y, Nakayama H, Takahashi K, Takio K, Takahashi R. A serine protease, HtrA2, is released from the mitochondria and interacts with XIAP, inducing cell death. *Mol Cell*. 2001;8(3):613-621. doi:10.1016/s1097-2765(01)00341-0.

115 Walsh JG, Cullen SP, Sheridan C, Lüthi AU, Gerner C, Martin SJ. Executioner caspase-3 and caspase-7 are functionally distinct proteases. *Proc Natl Acad Sci U S A*. 2008;105(35):12815-12819. doi:10.1073/pnas.0707715105.

116 Chaitanya GV, Steven AJ, Babu PP. PARP-1 cleavage fragments: signatures of cell-death proteases in neurodegeneration. *Cell Commun Signal*. 2010;8:31. doi:10.1186/1478-811X-8-31.

117 Kaufmann SH, Desnoyers S, Ottaviano Y, Davidson NE, Poirier GG. Specific proteolytic cleavage of poly(ADP-ribose) polymerase: an early marker of chemotherapy-induced apoptosis. *Cancer Res*. 1993;53(17):3976-3985.

118 Luo X, Budihardjo I, Zou H, Slaughter C, Wang X. Bid, a Bcl2 interacting protein, mediates cytochrome c release from mitochondria in response to activation of cell surface death receptors. *Cell*. 1998;94(4):481-490. doi:10.1016/s0092-8674(00)81589-5.

119 Kantari C, Walczak H. Caspase-8 and bid: caught in the act between death receptors and mitochondria. *Biochim Biophys Acta*. 2011;1813(4):558-563. doi:10.1016/j.bbamcr.2011.01.026.

120 Sax JK, Fei P, Murphy ME, Bernhard E, Korsmeyer SJ, El-Deiry WS. BID regulation by p53 contributes to chemosensitivity. *Nat Cell Biol*. 2002;4(11):842-849. doi:10.1038/ncb866.

121 Gross A, Yin XM, Wang K, et al. Caspase cleaved BID targets mitochondria and is required for cytochrome c release, while BCL-XL prevents this release but not tumor necrosis factor-R1/Fas death. *J Biol Chem*. 1999;274(2):1156-1163. doi:10.1074/jbc.274.2.1156.

122 Wei MC, Lindsten T, Mootha VK, et al. tBID, a membrane-targeted death ligand, oligomerizes BAK to release cytochrome c. *Genes Dev*. 2000;14(16):2060-2071.

123 Eskes R, Desagher S, Antonsson B, Martinou JC. Bid induces the oligomerization and insertion of Bax into the outer mitochondrial membrane. *Mol Cell Biol*. 2000;20(3):929-935. doi:10.1128/MCB.20.3.929-935.2000.

124 Flores-Romero H, Hohorst L, John M, et al. BCL-2-family protein tBID can act as a BAX-like effector of apoptosis. *EMBO J*. 2022;41(2):e108690. doi:10.15252/embj.2021108690.

125 Cirman T, Oresić K, Mazovec GD, et al. Selective disruption of lysosomes in HeLa cells triggers apoptosis mediated by cleavage of Bid by multiple papain-like lysosomal cathepsins. *J Biol Chem*. 2004;279(5):3578-3587. doi:10.1074/jbc.M308347200.

126 Blomgran R, Zheng L, Stendahl O. Cathepsin-cleaved Bid promotes apoptosis in human neutrophils via oxidative stress-induced lysosomal membrane permeabilization. *J Leukoc Biol*. 2007;81(5):1213-1223. doi:10.1189/jlb.0506359.

127 Wagner KW, Engels IH, Deveraux QL. Caspase-2 can function upstream of bid cleavage in the TRAIL apoptosis pathway. *J Biol Chem*. 2004;279(33):35047-35052. doi:10.1074/jbc.M400708200.

128 Slee EA, Keogh SA, Martin SJ. Cleavage of BID during cytotoxic drug and UV radiation-induced apoptosis occurs downstream of the point of Bcl-2 action and is catalysed by caspase-3: a potential feedback loop for amplification of apoptosis-associated mitochondrial cytochrome c release. *Cell Death Differ*. 2000;7(6):556-565. doi:10.1038/sj.cdd.4400689.

129 Sutton VR, Davis JE, Cancilla M, et al. Initiation of apoptosis by granzyme B requires direct cleavage of bid, but not direct granzyme B-mediated caspase activation. *J Exp Med*. 2000;192(10):1403-1414. doi:10.1084/jem.192.10.1403.

130 Mandic A, Viktorsson K, Strandberg L, et al. Calpain-mediated Bid cleavage and calpain-independent Bak modulation: two separate pathways in cisplatin-induced apoptosis. *Mol Cell Biol*. 2002;22(9):3003-3013. doi:10.1128/MCB.22.9.3003-3013.2002.

131 Barry M, Heibein JA, Pinkoski MJ, et al. Granzyme B short-circuits the need for caspase 8 activity during granule-mediated cytotoxic T-lymphocyte killing by directly cleaving Bid. *Mol Cell Biol*. 2000;20(11):3781-3794. doi:10.1128/MCB.20.11.3781-3794.2000.

132 Valentijn AJ, Gilmore AP. Translocation of full-length Bid to mitochondria during anoikis. *J Biol Chem*. 2004;279(31):32848-32857. doi:10.1074/jbc.M313375200.

133 Köhler B, Anguissola S, Concannon CG, Rehm M, Kögel D, Prehn JHM. Bid participates in genotoxic drug-induced apoptosis of HeLa cells and is essential for death receptor ligands' apoptotic and synergistic effects. *PLoS One*. 2008;3(7):e2844. doi:10.1371/journal.pone.0002844.

134 Ballabio A, Bonifacino JS. Lysosomes as dynamic regulators of cell and organismal homeostasis. *Nat Rev Mol Cell Biol*. 2020;21(2):101-118. doi:10.1038/s41580-019-0185-4.

135 Mindell JA. Lysosomal acidification mechanisms. *Annu Rev Physiol*. 2012;74:69-86. doi:10.1146/annurev-physiol-012110-142317.

136 Ohkuma S, Moriyama Y, Takano T. Identification and characterization of a proton pump on lysosomes by fluorescein-isothiocyanate-dextran fluorescence. *Proc Natl Acad Sci U S A*. 1982;79(9):2758-2762. doi:10.1073/pnas.79.9.2758.

137 Sancak Y, Bar-Peled L, Zoncu R, Markhard AL, Nada S, Sabatini DM. Ragulator-Rag complex targets mTORC1 to the lysosomal surface and is necessary for its activation by amino acids. *Cell*. 2010;141(2):290-303. doi:10.1016/j.cell.2010.02.024.

138 Braulke T, Bonifacino JS. Sorting of lysosomal proteins. *Biochim Biophys Acta*. 2009;1793(4):605-614. doi:10.1016/j.bbamcr.2008.10.016.

139 Lazzarino DA, Gabel CA. Mannose processing is an important determinant in the assembly of phosphorylated high mannose-type oligosaccharides. *J Biol Chem*. 1989;264(9):5015-5023.

140 Rohrer J, Kornfeld R. Lysosomal hydrolase mannose 6-phosphate uncovering enzyme resides in the trans-Golgi network. *Mol Biol Cell*. 2001;12(6):1623-1631. doi:10.1091/mbc.12.6.1623.

141 Varki A, Kornfeld S. Identification of a rat liver alpha-N-acetylglucosaminyl phosphodiesterase capable of removing "blocking" alpha-N-acetylglucosamine residues from phosphorylated high mannose oligosaccharides of lysosomal enzymes. *J Biol Chem*. 1980;255(18):8398-8401.

142 Dahms NM, Lobel P, Kornfeld S. Mannose 6-phosphate receptors and lysosomal enzyme targeting. *J Biol Chem*. 1989;264(21):12115-12118.

143 Pohlmann R, Boeker MW, Figura K von. The two mannose 6-phosphate receptors transport distinct complements of lysosomal proteins. *J Biol Chem*. 1995;270(45):27311-27318. doi:10.1074/jbc.270.45.27311.

144 Ishidoh K, Kominami E. Processing and activation of lysosomal proteinases. *Biol Chem*. 2002;383(12):1827-1831. doi:10.1515/BC.2002.206.

145 Machado ER, Annunziata I, van de Vlekkert D, Grosveld GC, d'Azzo A. Lysosomes and Cancer Progression: A Malignant Liaison. *Front Cell Dev Biol*. 2021;9:642494. doi:10.3389/fcell.2021.642494.

146 Platt FM, d'Azzo A, Davidson BL, Neufeld EF, Tifft CJ. Lysosomal storage diseases. *Nat Rev Dis Primers*. 2018;4(1):27. doi:10.1038/s41572-018-0025-4.

147 Tang T, Yang Z-Y, Di Wang, et al. The role of lysosomes in cancer development and progression. *Cell Biosci*. 2020;10(1):131. doi:10.1186/s13578-020-00489-x.

148 Wang F, Gómez-Sintes R, Boya P. Lysosomal membrane permeabilization and cell death. *Traffic*. 2018;19(12):918-931. doi:10.1111/tra.12613.

149 Geisslinger F, Müller M, Vollmar AM, Bartel K. Targeting Lysosomes in Cancer as Promising Strategy to Overcome Chemoresistance-A Mini Review. *Front Oncol*. 2020;10:1156. doi:10.3389/fonc.2020.01156.

150 Boya P, Kroemer G. Lysosomal membrane permeabilization in cell death. *Oncogene*. 2008;27(50):6434-6451. doi:10.1038/onc.2008.310.

151 Yadati T, Houben T, Bitorina A, Shiri-Sverdlov R. The Ins and Outs of Cathepsins: Physiological Function and Role in Disease Management. *Cells*. 2020;9(7). doi:10.3390/cells9071679.

152 Turk V, Stoka V, Vasiljeva O, et al. Cysteine cathepsins: from structure, function and regulation to new frontiers. *Biochim Biophys Acta*. 2012;1824(1):68-88. doi:10.1016/j.bbapap.2011.10.002.

153 Pratt MR, Sekedat MD, Chiang KP, Muir TW. Direct measurement of cathepsin B activity in the cytosol of apoptotic cells by an activity-based probe. *Chem Biol*. 2009;16(9):1001-1012. doi:10.1016/j.chembiol.2009.07.011.

154 Almeida PC, Nantes IL, Chagas JR, et al. Cathepsin B activity regulation. Heparin-like glycosaminogylcans protect human cathepsin B from alkaline pH-induced inactivation. *J Biol Chem*. 2001;276(2):944-951. doi:10.1074/jbc.M003820200.

155 Vidak E, Javoršek U, Vizovišek M, Turk B. Cysteine Cathepsins and their Extracellular Roles: Shaping the Microenvironment. *Cells*. 2019;8(3). doi:10.3390/cells8030264.

156 Rudzińska M, Parodi A, Soond SM, et al. The Role of Cysteine Cathepsins in Cancer Progression and Drug Resistance. *Int J Mol Sci*. 2019;20(14). doi:10.3390/ijms20143602.

157 Papadopoulos C, Kravic B, Meyer H. Repair or Lysophagy: Dealing with Damaged Lysosomes. *J Mol Biol*. 2020;432(1):231-239. doi:10.1016/j.jmb.2019.08.010.

158 Repnik U, Stoka V, Turk V, Turk B. Lysosomes and lysosomal cathepsins in cell death. *Biochim Biophys Acta*. 2012;1824(1):22-33. doi:10.1016/j.bbapap.2011.08.016.

159 Droga-Mazovec G, Bojic L, Petelin A, et al. Cysteine cathepsins trigger caspase-dependent cell death through cleavage of bid and antiapoptotic Bcl-2 homologues. *J Biol Chem*. 2008;283(27):19140-19150. doi:10.1074/jbc.M802513200.

160 Chwieralski CE, Welte T, Bühling F. Cathepsin-regulated apoptosis. *Apoptosis*. 2006;11(2):143-149. doi:10.1007/s10495-006-3486-y.

161 Bröker LE, Huisman C, Span SW, Rodriguez JA, Kruyt FAE, Giaccone G. Cathepsin B mediates caspase-independent cell death induced by microtubule stabilizing agents in non-small cell lung cancer cells. *Cancer Res*. 2004;64(1):27-30. doi:10.1158/0008-5472.can-03-3060.

162 Aman Y, Schmauck-Medina T, Hansen M, et al. Autophagy in healthy aging and disease. *Nat Aging*. 2021;1(8):634-650. doi:10.1038/s43587-021-00098-4.

163 Yang Z, Klionsky DJ. An overview of the molecular mechanism of autophagy. *Curr Top Microbiol Immunol*. 2009;335:1-32. doi:10.1007/978-3-642-00302-8_1.

164 Kim J, Kundu M, Viollet B, Guan K-L. AMPK and mTOR regulate autophagy through direct phosphorylation of Ulk1. *Nat Cell Biol*. 2011;13(2):132-141. doi:10.1038/ncb2152.

165 Glick D, Barth S, Macleod KF. Autophagy: cellular and molecular mechanisms. *J Pathol*. 2010;221(1):3-12. doi:10.1002/path.2697.

166 Mulcahy Levy JM, Thorburn A. Autophagy in cancer: moving from understanding mechanism to improving therapy responses in patients. *Cell Death Differ*. 2020;27(3):843-857. doi:10.1038/s41418-019-0474-7.

167 Mathew R, Karantza-Wadsworth V, White E. Role of autophagy in cancer. *Nat Rev Cancer*. 2007;7(12):961-967. doi:10.1038/nrc2254.

168 Gąsiorkiewicz BM, Koczurkiewicz-Adamczyk P, Piska K, Pękala E. Autophagy modulating agents as chemosensitizers for cisplatin therapy in cancer. *Invest New Drugs*. 2021;39(2):538-563. doi:10.1007/s10637-020-01032-y.

169 Vaupel P, Mayer A. Hypoxia in cancer: significance and impact on clinical outcome. *Cancer Metastasis Rev*. 2007;26(2):225-239. doi:10.1007/s10555-007-9055-1.

170 Vaupel P, Harrison L. Tumor hypoxia: causative factors, compensatory mechanisms, and cellular response. *Oncologist*. 2004;9 Suppl 5:4-9. doi:10.1634/theoncologist.9-90005-4.

171 Höckel M, Vaupel P. Tumor hypoxia: definitions and current clinical, biologic, and molecular aspects. *J Natl Cancer Inst*. 2001;93(4):266-276. doi:10.1093/jnci/93.4.266.

172 Vaupel P, Höckel M, Mayer A. Detection and characterization of tumor hypoxia using pO2 histography. *Antioxid Redox Signal*. 2007;9(8):1221-1235. doi:10.1089/ars.2007.1628.

173 McKeown SR. Defining normoxia, physoxia and hypoxia in tumours-implications for treatment response. *Br J Radiol*. 2014;87(1035):20130676. doi:10.1259/bjr.20130676.

174 Brown JM. Evidence for acutely hypoxic cells in mouse tumours, and a possible mechanism of reoxygenation. *Br J Radiol*. 1979;52(620):650-656. doi:10.1259/0007-1285-52-620-650.

175 Michiels C, Tellier C, Feron O. Cycling hypoxia: A key feature of the tumor microenvironment. *Biochim Biophys Acta*. 2016;1866(1):76-86. doi:10.1016/j.bbcan.2016.06.004.

176 Matsumoto S, Yasui H, Mitchell JB, Krishna MC. Imaging cycling tumor hypoxia. *Cancer Res*. 2010;70(24):10019-10023. doi:10.1158/0008-5472.CAN-10-2821.

177 Eales KL, Hollinshead KER, Tennant DA. Hypoxia and metabolic adaptation of cancer cells. *Oncogenesis*. 2016;5(1):e190. doi:10.1038/oncsis.2015.50.

178 Krock BL, Skuli N, Simon MC. Hypoxia-induced angiogenesis: good and evil. *Genes & cancer*. 2011;2(12):1117-1133. doi:10.1177/1947601911423654.

179 Rankin EB, Giaccia AJ. Hypoxic control of metastasis. *Science*. 2016;352(6282):175-180. doi:10.1126/science.aaf4405.

180 Bristow RG, Hill RP. Hypoxia and metabolism. Hypoxia, DNA repair and genetic instability. *Nat Rev Cancer*. 2008;8(3):180-192. doi:10.1038/nrc2344.

181 Erler JT, Cawthorne CJ, Williams KJ, et al. Hypoxia-mediated down-regulation of Bid and Bax in tumors occurs via hypoxia-inducible factor 1-dependent and -independent mechanisms and contributes to drug resistance. *Mol Cell Biol*. 2004;24(7):2875-2889. doi:10.1128/MCB.24.7.2875-2889.2004.

182 Leontieva OV, Natarajan V, Demidenko ZN, Burdelya LG, Gudkov AV, Blagosklonny MV. Hypoxia suppresses conversion from proliferative arrest to cellular senescence. *Proc Natl Acad Sci U S A*. 2012;109(33):13314-13318. doi:10.1073/pnas.1205690109.

183 Noman MZ, Hasmim M, Messai Y, et al. Hypoxia: a key player in antitumor immune response. A Review in the Theme: Cellular Responses to Hypoxia. *Am J Physiol Cell Physiol*. 2015;309(9):C569-79. doi:10.1152/ajpcell.00207.2015.

184 Kaelin WG, Ratcliffe PJ. Oxygen sensing by metazoans: the central role of the HIF hydroxylase pathway. *Mol Cell*. 2008;30(4):393-402. doi:10.1016/j.molcel.2008.04.009.

185 Majmundar AJ, Wong WJ, Simon MC. Hypoxia-inducible factors and the response to hypoxic stress. *Mol Cell*. 2010;40(2):294-309. doi:10.1016/j.molcel.2010.09.022.

186 Ivan M, Kondo K, Yang H, et al. HIFalpha targeted for VHL-mediated destruction by proline hydroxylation: implications for O2 sensing. *Science*. 2001;292(5516):464-468. doi:10.1126/science.1059817.

187 Mahon PC, Hirota K, Semenza GL. FIH-1: a novel protein that interacts with HIF-1alpha and VHL to mediate repression of HIF-1 transcriptional activity. *Genes Dev*. 2001;15(20):2675-2686. doi:10.1101/gad.924501.

188 Lando D, Peet DJ, Gorman JJ, Whelan DA, Whitelaw ML, Bruick RK. FIH-1 is an asparaginyl hydroxylase enzyme that regulates the transcriptional activity of hypoxia-inducible factor. *Genes Dev*. 2002;16(12):1466-1471. doi:10.1101/gad.991402.

189 Semenza GL, Jiang BH, Leung SW, et al. Hypoxia response elements in the aldolase A, enolase 1, and lactate dehydrogenase A gene promoters contain essential binding sites for hypoxia-inducible factor 1. *J Biol Chem*. 1996;271(51):32529-32537. doi:10.1074/jbc.271.51.32529.

190 Benita Y, Kikuchi H, Smith AD, Zhang MQ, Chung DC, Xavier RJ. An integrative genomics approach identifies Hypoxia Inducible Factor-1 (HIF-1)-target genes that form the core response to hypoxia. *Nucleic Acids Res*. 2009;37(14):4587-4602. doi:10.1093/nar/gkp425.

191 Downes NL, Laham-Karam N, Kaikkonen MU, Ylä-Herttuala S. Differential but Complementary HIF1α and HIF2α Transcriptional Regulation. *Mol Ther*. 2018;26(7):1735-1745. doi:10.1016/j.ymthe.2018.05.004.

192 Uchida T, Rossignol F, Matthay MA, et al. Prolonged hypoxia differentially regulates hypoxia-inducible factor (HIF)-1alpha and HIF-2alpha expression in lung epithelial cells: implication of natural antisense HIF-1alpha. *J Biol Chem*. 2004;279(15):14871-14878. doi:10.1074/jbc.M400461200.

193 Hu C-J, Sataur A, Wang L, Chen H, Simon MC. The N-terminal transactivation domain confers target gene specificity of hypoxia-inducible factors HIF-1alpha and HIF-2alpha. *Mol Biol Cell*. 2007;18(11):4528-4542. doi:10.1091/mbc.E06-05-0419.

194 Hu C-J, Wang L-Y, Chodosh LA, Keith B, Simon MC. Differential roles of hypoxia-inducible factor 1alpha (HIF-1alpha) and HIF-2alpha in hypoxic gene regulation. *Mol Cell Biol*. 2003;23(24):9361-9374. doi:10.1128/MCB.23.24.9361-9374.2003.

195 Ellen TP, Ke Q, Zhang P, Costa M. NDRG1, a growth and cancer related gene: regulation of gene expression and function in normal and disease states. *Carcinogenesis*. 2008;29(1):2-8. doi:10.1093/carcin/bgm200.

196 Shaw E, McCue LA, Lawrence CE, Dordick JS. Identification of a novel class in the alpha/beta hydrolase fold superfamily: the N-myc differentiation-related proteins. *Proteins*. 2002;47(2):163-168. doi:10.1002/prot.10083.

197 Lachat P, Shaw P, Gebhard S, van Belzen N, Chaubert P, Bosman FT. Expression of NDRG1, a differentiation-related gene, in human tissues. *Histochem Cell Biol*. 2002;118(5):399-408. doi:10.1007/s00418-002-0460-9.

198 Shimono A, Okuda T, Kondoh H. N-myc-dependent repression of ndr1, a gene identified by direct subtraction of whole mouse embryo cDNAs between wild type and N-myc mutant. *Mech Dev*. 1999;83(1-2):39-52. doi:10.1016/s0925-4773(99)00025-8.

199 Cangul H, Salnikow K, Yee H, Zagzag D, Commes T, Costa M. Enhanced overexpression of an HIF-1/hypoxia-related protein in cancer cells. *Environ Health Perspect*. 2002;110 Suppl 5(Suppl 5):783-788. doi:10.1289/ehp.02110s5783.

200 Cangul H. Hypoxia upregulates the expression of the NDRG1 gene leading to its overexpression in various human cancers. *BMC Genet*. 2004;5:27. doi:10.1186/1471-2156-5-27.

201 Salnikow K, Kluz T, Costa M, et al. The regulation of hypoxic genes by calcium involves c-Jun/AP-1, which cooperates with hypoxia-inducible factor 1 in response to hypoxia. *Mol Cell Biol*. 2002;22(6):1734-1741. doi:10.1128/MCB.22.6.1734-1741.2002.

202 Zhang P, Tchou-Wong K-M, Costa M. Egr-1 mediates hypoxia-inducible transcription of the NDRG1 gene through an overlapping Egr-1/Sp1 binding site in the promoter. *Cancer Res*. 2007;67(19):9125-9133. doi:10.1158/0008-5472.CAN-07-1525.

203 Stein S, Thomas EK, Herzog B, et al. NDRG1 is necessary for p53-dependent apoptosis. *J Biol Chem*. 2004;279(47):48930-48940. doi:10.1074/jbc.M400386200.

204 Bandyopadhyay S, Pai SK, Hirota S, et al. PTEN up-regulates the tumor metastasis suppressor gene Drg-1 in prostate and breast cancer. *Cancer Res*. 2004;64(21):7655-7660. doi:10.1158/0008-5472.CAN-04-1623.

205 Zhou D, Salnikow K, Costa M. Cap43, a novel gene specifically induced by Ni2+ compounds. *Cancer Res*. 1998;58(10):2182-2189.

206 Le NTV, Des Richardson R. Iron chelators with high antiproliferative activity up-regulate the expression of a growth inhibitory and metastasis suppressor gene: a link between iron metabolism and proliferation. *Blood*. 2004;104(9):2967-2975. doi:10.1182/blood-2004-05-1866.

207 Murray JT, Campbell DG, Morrice N, et al. Exploitation of KESTREL to identify NDRG family members as physiological substrates for SGK1 and GSK3. *Biochem J*. 2004;384(Pt 3):477-488. doi:10.1042/BJ20041057.

208 Murakami Y, Hosoi F, Izumi H, et al. Identification of sites subjected to serine/threonine phosphorylation by SGK1 affecting N-myc downstream-regulated gene 1 (NDRG1)/Cap43-dependent suppression of angiogenic CXC chemokine expression in human pancreatic cancer cells. *Biochem Biophys Res Commun*. 2010;396(2):376-381. doi:10.1016/j.bbrc.2010.04.100.

209 Agarwala KL, Kokame K, Kato H, Miyata T. Phosphorylation of RTP, an ER stress-responsive cytoplasmic protein. *Biochem Biophys Res Commun*. 2000;272(3):641-647. doi:10.1006/bbrc.2000.2833.

210 Sugiki T, Murakami M, Taketomi Y, Kikuchi-Yanoshita R, Kudo I. N-myc downregulated gene 1 is a phosphorylated protein in mast cells. *Biol Pharm Bull*. 2004;27(5):624-627. doi:10.1248/bpb.27.624.

211 McCaig C, Potter L, Abramczyk O, Murray JT. Phosphorylation of NDRG1 is temporally and spatially controlled during the cell cycle. *Biochem Biophys Res Commun*. 2011;411(2):227-234. doi:10.1016/j.bbrc.2011.06.092.

212 Shi X-H, Larkin JC, Chen B, Sadovsky Y. The expression and localization of N-myc downstream-regulated gene 1 in human trophoblasts. *PLoS One*. 2013;8(9):e75473. doi:10.1371/journal.pone.0075473.

213 Park KC, Menezes SV, Kalinowski DS, et al. Identification of differential phosphorylation and sub-cellular localization of the metastasis suppressor, NDRG1. *Biochim Biophys Acta Mol Basis Dis*. 2018;1864(8):2644-2663. doi:10.1016/j.bbadis.2018.04.011.

214 Park KC, Paluncic J, Kovacevic Z, Des Richardson R. Pharmacological targeting and the diverse functions of the metastasis suppressor, NDRG1, in cancer. *Free Radic Biol Med*. 2020;157:154-175. doi:10.1016/j.freeradbiomed.2019.05.020.

215 Sun J, Zhang D, Bae D-H, et al. Metastasis suppressor, NDRG1, mediates its activity through signaling pathways and molecular motors. *Carcinogenesis*. 2013;34(9):1943-1954. doi:10.1093/carcin/bgt163.

216 Cheng J, Xie H-Y, Xu X, et al. NDRG1 as a biomarker for metastasis, recurrence and of poor prognosis in hepatocellular carcinoma. *Cancer Lett*. 2011;310(1):35-45. doi:10.1016/j.canlet.2011.06.001.

217 Nishio S, Ushijima K, Tsuda N, et al. Cap43/NDRG1/Drg-1 is a molecular target for angiogenesis and a prognostic indicator in cervical adenocarcinoma. *Cancer Lett*. 2008;264(1):36-43. doi:10.1016/j.canlet.2008.01.020.

218 Zhao G, Chen J, Deng Y, et al. Identification of NDRG1-regulated genes associated with invasive potential in cervical and ovarian cancer cells. *Biochem Biophys Res Commun*. 2011;408(1):154-159. doi:10.1016/j.bbrc.2011.03.140.

219 Song JY, Lee JK, Lee NW, Jung HH, Kim SH, Lee KW. Microarray analysis of normal cervix, carcinoma in situ, and invasive cervical cancer: identification of candidate genes in pathogenesis of invasion in cervical cancer. *Int J Gynecol Cancer*. 2008;18(5):1051-1059. doi:10.1111/j.1525-1438.2007.01164.x.

220 Buttarelli M, Babini G, Raspaglio G, et al. A combined ANXA2-NDRG1-STAT1 gene signature predicts response to chemoradiotherapy in cervical cancer. *J Exp Clin Cancer Res*. 2019;38(1):279. doi:10.1186/s13046-019-1268-y.

221 Cosse J-P, Michiels C. Tumour hypoxia affects the responsiveness of cancer cells to chemotherapy and promotes cancer progression. *Anticancer Agents Med Chem*. 2008;8(7):790-797. doi:10.2174/187152008785914798.

222 Hill RP, Bristow RG, Fyles A, Koritzinsky M, Milosevic M, Wouters BG. Hypoxia and Predicting Radiation Response. *Semin Radiat Oncol*. 2015;25(4):260-272. doi:10.1016/j.semradonc.2015.05.004.

223 Wilson WR, Hay MP. Targeting hypoxia in cancer therapy. *Nat Rev Cancer*. 2011;11(6):393-410. doi:10.1038/nrc3064.

224 Hoppe-Seyler K, Mändl J, Adrian S, Kuhn BJ, Hoppe-Seyler F. Virus/Host Cell Crosstalk in Hypoxic HPV-Positive Cancer Cells. *Viruses*. 2017;9(7). doi:10.3390/v9070174.

225 Hoppe-Seyler K, Bossler F, Lohrey C, et al. Induction of dormancy in hypoxic human papillomavirus-positive cancer cells. *Proc Natl Acad Sci U S A*. 2017;114(6):E990-E998. doi:10.1073/pnas.1615758114.

226 Bossler F, Kuhn BJ, Günther T, et al. Repression of Human Papillomavirus Oncogene Expression under Hypoxia Is Mediated by PI3K/mTORC2/AKT Signaling. *mBio*. 2019;10(1). doi:10.1128/mBio.02323-18.

227 Blagosklonny MV. Geroconversion: irreversible step to cellular senescence. *Cell Cycle*. 2014;13(23):3628-3635. doi:10.4161/15384101.2014.985507.

228 Bennewith KL, Raleigh JA, Durand RE. Orally administered pimonidazole to label hypoxic tumor cells. *Cancer Res*. 2002;62(23):6827-6830.

229 Cárdenas-Navia LI, Mace D, Richardson RA, Wilson DF, Shan S, Dewhirst MW. The pervasive presence of fluctuating oxygenation in tumors. *Cancer Res*. 2008;68(14):5812-5819. doi:10.1158/0008-5472.CAN-07-6387.

230 Bader SB, Dewhirst MW, Hammond EM. Cyclic Hypoxia: An Update on Its Characteristics, Methods to Measure It and Biological Implications in Cancer. *Cancers (Basel)*. 2020;13(1). doi:10.3390/cancers13010023.

231 Ellingsen C, Ovrebø KM, Galappathi K, Mathiesen B, Rofstad EK. pO_2 fluctuation pattern and cycling hypoxia in human cervical carcinoma and melanoma xenografts. *Int J Radiat Oncol Biol Phys*. 2012;83(4):1317-1323. doi:10.1016/j.ijrobp.2011.09.037.

232 Saxena K, Jolly MK. Acute vs. Chronic vs. Cyclic Hypoxia: Their Differential Dynamics, Molecular Mechanisms, and Effects on Tumor Progression. *Biomolecules*. 2019;9(8). doi:10.3390/biom9080339.

233 Boidot R, Branders S, Helleputte T, Rubio LI, Dupont P, Feron O. A generic cycling hypoxia-derived prognostic gene signature: application to breast cancer profiling. *Oncotarget*. 2014;5(16):6947-6963. doi:10.18632/oncotarget.2285.

234 Koritzinsky M, Wouters BG. The roles of reactive oxygen species and autophagy in mediating the tolerance of tumor cells to cycling hypoxia. *Semin Radiat Oncol*. 2013;23(4):252-261. doi:10.1016/j.semradonc.2013.05.006.

235 Rouschop KMA, Ramaekers CHMA, Schaaf MBE, et al. Autophagy is required during cycling hypoxia to lower production of reactive oxygen species. *Radiother Oncol*. 2009;92(3):411-416. doi:10.1016/j.radonc.2009.06.029.

236 Hsieh CH, Lee CH, Liang JA, Yu CY, Shyu WC. Cycling hypoxia increases U87 glioma cell radioresistance via ROS induced higher and long-term HIF-1 signal transduction activity. *Oncol Rep*. 2010;24(6). doi:10.3892/or_00001027.

237 Dewhirst MW. Relationships between cycling hypoxia, HIF-1, angiogenesis and oxidative stress. *Radiat Res*. 2009;172(6):653-665. doi:10.1667/RR1926.1.

238 Tellier C, Desmet D, Petit L, et al. Cycling hypoxia induces a specific amplified inflammatory phenotype in endothelial cells and enhances tumor-promoting inflammation in vivo. *Neoplasia*. 2015;17(1):66-78. doi:10.1016/j.neo.2014.11.003.

239 Martinive P, Defresne F, Bouzin C, et al. Preconditioning of the tumor vasculature and tumor cells by intermittent hypoxia: implications for anticancer therapies. *Cancer Res*. 2006;66(24):11736-11744. doi:10.1158/0008-5472.CAN-06-2056.

240 Toffoli S, Roegiers A, Feron O, et al. Intermittent hypoxia is an angiogenic inducer for endothelial cells: role of HIF-1. *Angiogenesis*. 2009;12(1):47-67. doi:10.1007/s10456-009-9131-y.

241 Martinive P, Defresne F, Quaghebeur E, et al. Impact of cyclic hypoxia on HIF-1alpha regulation in endothelial cells--new insights for anti-tumor treatments. *FEBS J*. 2009;276(2):509-518. doi:10.1111/j.1742-4658.2008.06798.x.

242 Toffoli S, Feron O, Raes M, Michiels C. Intermittent hypoxia changes HIF-1alpha phosphorylation pattern in endothelial cells: unravelling of a new PKA-dependent regulation of HIF-1alpha. *Biochim Biophys Acta*. 2007;1773(10):1558-1571. doi:10.1016/j.bbamcr.2007.06.002.

243 Dewhirst MW, Cao Y, Moeller B. Cycling hypoxia and free radicals regulate angiogenesis and radiotherapy response. *Nat Rev Cancer*. 2008;8(6):425-437. doi:10.1038/nrc2397.

244 Miao Z-F, Zhao T-T, Wang Z-N, et al. Influence of different hypoxia models on metastatic potential of SGC-7901 gastric cancer cells. *Tumour Biol*. 2014;35(7):6801-6808. doi:10.1007/s13277-014-1928-7.

245 Liu L, Liu W, Wang L, Zhu T, Zhong J, Xie N. Hypoxia-inducible factor 1 mediates intermittent hypoxia-induced migration of human breast cancer MDA-MB-231 cells. *Oncol Lett*. 2017;14(6):7715-7722. doi:10.3892/ol.2017.7223.

246 Liu Y, Song X, Wang X, et al. Effect of chronic intermittent hypoxia on biological behavior and hypoxia-associated gene expression in lung cancer cells. *J Cell Biochem*. 2010;111(3):554-563. doi:10.1002/jcb.22739.

247 Chou C-W, Wang C-C, Wu C-P, et al. Tumor cycling hypoxia induces chemoresistance in glioblastoma multiforme by upregulating the expression and function of ABCB1. *Neuro Oncol*. 2012;14(10):1227-1238. doi:10.1093/neuonc/nos195.

248 Chen W-L, Wang C-C, Lin Y-J, Wu C-P, Hsieh C-H. Cycling hypoxia induces chemoresistance through the activation of reactive oxygen species-mediated B-cell lymphoma extra-long pathway in glioblastoma multiforme. *J Transl Med*. 2015;13:389. doi:10.1186/s12967-015-0758-8.

249 Hsieh C-H, Wu C-P, Lee H-T, Liang J-A, Yu C-Y, Lin Y-J. NADPH oxidase subunit 4 mediates cycling hypoxia-promoted radiation resistance in glioblastoma multiforme. *Free Radic Biol Med*. 2012;53(4):649-658. doi:10.1016/j.freeradbiomed.2012.06.009.

250 Saxton RA, Sabatini DM. mTOR Signaling in Growth, Metabolism, and Disease. *Cell*. 2017;168(6):960-976. doi:10.1016/j.cell.2017.02.004.

251 Lee P, Chandel NS, Simon MC. Cellular adaptation to hypoxia through hypoxia inducible factors and beyond. *Nat Rev Mol Cell Biol*. 2020;21(5):268-283. doi:10.1038/s41580-020-0227-y.

252 Arsham AM, Howell JJ, Simon MC. A novel hypoxia-inducible factor-independent hypoxic response regulating mammalian target of rapamycin and its targets. *J Biol Chem*. 2003;278(32):29655-29660. doi:10.1074/jbc.M212770200.

253 Protter DSW, Parker R. Principles and Properties of Stress Granules. *Trends Cell Biol*. 2016;26(9):668-679. doi:10.1016/j.tcb.2016.05.004.

254 Kedersha N, Anderson P. Mammalian stress granules and processing bodies. *Methods Enzymol*. 2007;431:61-81. doi:10.1016/S0076-6879(07)31005-7.

255 Hofmann S, Kedersha N, Anderson P, Ivanov P. Molecular mechanisms of stress granule assembly and disassembly. *Biochim Biophys Acta Mol Cell Res*. 2021;1868(1):118876. doi:10.1016/j.bbamcr.2020.118876.

256 Moeller BJ, Cao Y, Li CY, Dewhirst MW. Radiation activates HIF-1 to regulate vascular radiosensitivity in tumors: role of reoxygenation, free radicals, and stress granules. *Cancer Cell*. 2004;5(5):429-441. doi:10.1016/s1535-6108(04)00115-1.

257 Wippich F, Bodenmiller B, Trajkovska MG, Wanka S, Aebersold R, Pelkmans L. Dual specificity kinase DYRK3 couples stress granule condensation/dissolution to mTORC1 signaling. *Cell*. 2013;152(4):791-805. doi:10.1016/j.cell.2013.01.033.

258 Timalsina S, Arimoto-Matsuzaki K, Kitamura M, et al. Chemical compounds that suppress hypoxia-induced stress granule formation enhance cancer drug sensitivity of human cervical cancer HeLa cells. *J Biochem*. 2018;164(5):381-391. doi:10.1093/jb/mvy062.

259 Horsman MR, Mortensen LS, Petersen JB, Busk M, Overgaard J. Imaging hypoxia to improve radiotherapy outcome. *Nat Rev Clin Oncol*. 2012;9(12):674-687. doi:10.1038/nrclinonc.2012.171.

260 Ewald JA, Desotelle JA, Wilding G, Jarrard DF. Therapy-induced senescence in cancer. *J Natl Cancer Inst*. 2010;102(20):1536-1546. doi:10.1093/jnci/djq364.

261 Childs BG, Baker DJ, Kirkland JL, Campisi J, van Deursen JM. Senescence and apoptosis: dueling or complementary cell fates? *EMBO Rep*. 2014;15(11):1139-1153. doi:10.15252/embr.201439245.

262 Wang B, Kohli J, Demaria M. Senescent Cells in Cancer Therapy: Friends or Foes? *Trends Cancer*. 2020;6(10):838-857. doi:10.1016/j.trecan.2020.05.004.

263 Campisi J. Aging, cellular senescence, and cancer. *Annu Rev Physiol*. 2013;75:685-705. doi:10.1146/annurev-physiol-030212-183653.

264 Butz K, Geisen C, Ullmann A, Spitkovsky D, Hoppe-Seyler F. Cellular responses of HPV-positive cancer cells to genotoxic anti-cancer agents: Repression ofE6/E7-oncogene expression and induction of apoptosis. *Int. J. Cancer*. 1996;68(4):506-513. doi:10.1002/(SICI)1097-0215(19961115)68:4<506:AID-IJC17>3.0.CO;2-2.

265 van der Maaten L, Hinton G. Visualizing data using t-SNE. *Journal of machine learning research*. 2008;9(11).

266 Gilkes DM, Bajpai S, Wong CC, et al. Procollagen lysyl hydroxylase 2 is essential for hypoxia-induced breast cancer metastasis. *Mol Cancer Res*. 2013;11(5):456-466. doi:10.1158/1541-7786.MCR-12-0629.

267 Schietke R, Warnecke C, Wacker I, et al. The lysyl oxidases LOX and LOXL2 are necessary and sufficient to repress E-cadherin in hypoxia: insights into cellular transformation processes mediated by HIF-1. *J Biol Chem*. 2010;285(9):6658-6669. doi:10.1074/jbc.M109.042424.

268 Ebert BL, Firth JD, Ratcliffe PJ. Hypoxia and mitochondrial inhibitors regulate expression of glucose transporter-1 via distinct Cis-acting sequences. *J Biol Chem*. 1995;270(49):29083-29089. doi:10.1074/jbc.270.49.29083.

269 Azimi I, Petersen RM, Thompson EW, Roberts-Thomson SJ, Monteith GR. Hypoxia-induced reactive oxygen species mediate N-cadherin and SERPINE1 expression, EGFR signalling and motility in MDA-MB-468 breast cancer cells. *Sci Rep*. 2017;7(1):15140. doi:10.1038/s41598-017-15474-7.

270 García-Martínez JM, Alessi DR. mTOR complex 2 (mTORC2) controls hydrophobic motif phosphorylation and activation of serum- and glucocorticoid-induced protein kinase 1 (SGK1). *Biochem J*. 2008;416(3):375-385. doi:10.1042/BJ20081668.

271 Matsumoto K, Mizoue K, Kitamura K, Tse W-C, Huber CP, Ishida T. Structural basis of inhibition of cysteine proteases by E-64 and its derivatives. *Biopolymers*. 1999;51(1):99-107. doi:10.1002/(SICI)1097-0282(1999)51:1<99:AID-BIP11>3.0.CO;2-R.

272 Montaser M, Lalmanach G, Mach L. CA-074, but not its methyl ester CA-074Me, is a selective inhibitor of cathepsin B within living cells. *Biol Chem*. 2002;383(7-8):1305-1308. doi:10.1515/BC.2002.147.

273 Mauvezin C, Neufeld TP. Bafilomycin A1 disrupts autophagic flux by inhibiting both V-ATPase-dependent acidification and Ca-P60A/SERCA-dependent autophagosome-lysosome fusion. *Autophagy*. 2015;11(8):1437-1438. doi:10.1080/15548627.2015.1066957.

274 Sharifi MN, Mowers EE, Drake LE, Macleod KF. Measuring autophagy in stressed cells. *Methods Mol Biol*. 2015;1292:129-150. doi:10.1007/978-1-4939-2522-3_10.

275 Mauthe M, Orhon I, Rocchi C, et al. Chloroquine inhibits autophagic flux by decreasing autophagosome-lysosome fusion. *Autophagy*. 2018;14(8):1435-1455. doi:10.1080/15548627.2018.1474314.

276 Klionsky DJ, Abdel-Aziz AK, Abdelfatah S, et al. Guidelines for the use and interpretation of assays for monitoring autophagy (4th edition)1. *Autophagy*. 2021;17(1):1-382. doi:10.1080/15548627.2020.1797280.

277 Pierzyńska-Mach A, Janowski PA, Dobrucki JW. Evaluation of acridine orange, LysoTracker Red, and quinacrine as fluorescent probes for long-term tracking of acidic vesicles. *Cytometry A*. 2014;85(8):729-737. doi:10.1002/cyto.a.22495.

278 Eskelinen E-L. Maturation of autophagic vacuoles in Mammalian cells. *Autophagy*. 2005;1(1):1-10. doi:10.4161/auto.1.1.1270.

279 Hu Y-B, Dammer EB, Ren R-J, Wang G. The endosomal-lysosomal system: from acidification and cargo sorting to neurodegeneration. *Translational Neurodegeneration*. 2015;4(1):18. doi:10.1186/s40035-015-0041-1.

280 Ye X, Zhou X-J, Zhang H. Exploring the Role of Autophagy-Related Gene 5 (ATG5) Yields Important Insights Into Autophagy in Autoimmune/Autoinflammatory Diseases. *Front Immunol*. 2018;9:2334. doi:10.3389/fimmu.2018.02334.

281 Singh D, Vignat J, Lorenzoni V, et al. Global estimates of incidence and mortality of cervical cancer in 2020: a baseline analysis of the WHO Global Cervical Cancer Elimination Initiative. *Lancet Glob Health*. 2023;11(2):e197-e206. doi:10.1016/S2214-109X(22)00501-0.

282 Hockel M, Schlenger K, Aral B, Mitze M, Schaffer U, Vaupel P. Association between tumor hypoxia and malignant progression in advanced cancer of the uterine cervix. *Cancer Res*. 1996;56(19):4509-4515.

283 Höckel M, Schlenger K, Höckel S, Vaupel P. Hypoxic cervical cancers with low apoptotic index are highly aggressive. *Cancer Res*. 1999;59(18):4525-4528.

284 Muz B, La Puente P de, Azab F, Azab AK. The role of hypoxia in cancer progression, angiogenesis, metastasis, and resistance to therapy. *Hypoxia (Auckl)*. 2015;3:83-92. doi:10.2147/HP.S93413.

285 Butturini E, Carcereri de Prati A, Boriero D, Mariotto S. Tumor Dormancy and Interplay with Hypoxic Tumor Microenvironment. *Int J Mol Sci*. 2019;20(17). doi:10.3390/ijms20174305.

286 Vaupel P, Kallinowski F, Okunieff P. Blood flow, oxygen and nutrient supply, and metabolic microenvironment of human tumors: a review. *Cancer Res*. 1989;49(23):6449-6465.

287 Jiang BH, Semenza GL, Bauer C, Marti HH. Hypoxia-inducible factor 1 levels vary exponentially over a physiologically relevant range of O2 tension. *Am J Physiol*. 1996;271(4 Pt 1):C1172-80. doi:10.1152/ajpcell.1996.271.4.C1172.

288 Keith B, Johnson RS, Simon MC. HIF1α and HIF2α: sibling rivalry in hypoxic tumour growth and progression. *Nat Rev Cancer*. 2011;12(1):9-22. doi:10.1038/nrc3183.

289 Walton ZE, Patel CH, Brooks RC, et al. Acid Suspends the Circadian Clock in Hypoxia through Inhibition of mTOR. *Cell*. 2018;174(1):72-87.e32. doi:10.1016/j.cell.2018.05.009.

290 Hong J, Wuest TR, Min Y, Lin PC. Oxygen Tension Regulates Lysosomal Activation and Receptor Tyrosine Kinase Degradation. *Cancers (Basel)*. 2019;11(11). doi:10.3390/cancers11111653.

291 Glunde K, Guggino SE, Solaiyappan M, Pathak AP, Ichikawa Y, Bhujwalla ZM. Extracellular acidification alters lysosomal trafficking in human breast cancer cells. *Neoplasia*. 2003;5(6):533-545. doi:10.1016/s1476-5586(03)80037-4.

292 Achour O, Ashraf Y, Bridiau N, et al. Alteration of cathepsin D trafficking induced by hypoxia and extracellular acidification in MCF-7 breast cancer cells. *Biochimie*. 2016;121:123-130. doi:10.1016/j.biochi.2015.11.007.

293 Tournu C, Obled A, Roux MP, Deval C, Ferrara M, Béchet DM. Glucose controls cathepsin expression in Ras-transformed fibroblasts. *Arch Biochem Biophys*. 1998;360(1):15-24. doi:10.1006/abbi.1998.0916.

294 Bellot G, Garcia-Medina R, Gounon P, et al. Hypoxia-induced autophagy is mediated through hypoxia-inducible factor induction of BNIP3 and BNIP3L via their BH3 domains. *Mol Cell Biol*. 2009;29(10):2570-2581. doi:10.1128/MCB.00166-09.

295 Mazure NM, Pouysségur J. Hypoxia-induced autophagy: cell death or cell survival? *Curr Opin Cell Biol*. 2010;22(2):177-180. doi:10.1016/j.ceb.2009.11.015.

296 Plomp PJ, Gordon PB, Meijer AJ, Høyvik H, Seglen PO. Energy dependence of different steps in the autophagic-lysosomal pathway. *J Biol Chem*. 1989;264(12):6699-6704.

297 Park J-M, Lee D-H, Kim D-H. Redefining the role of AMPK in autophagy and the energy stress response. *Nat Commun*. 2023;14(1):2994. doi:10.1038/s41467-023-38401-z.

298 Brown JM. Tumor hypoxia in cancer therapy. *Methods Enzymol*. 2007;435:297-321. doi:10.1016/S0076-6879(07)35015-5.

299 Gray LH, Conger AD, EBERT M, HORNSEY S, SCOTT OC. The concentration of oxygen dissolved in tissues at the time of irradiation as a factor in radiotherapy. *Br J Radiol*. 1953;26(312):638-648. doi:10.1259/0007-1285-26-312-638.

300 Coppé J-P, Desprez P-Y, Krtolica A, Campisi J. The senescence-associated secretory phenotype: the dark side of tumor suppression. *Annu Rev Pathol*. 2010;5:99-118. doi:10.1146/annurev-pathol-121808-102144.

301 van Maanen JM, Retèl J, Vries J de, Pinedo HM. Mechanism of action of antitumor drug etoposide: a review. *J Natl Cancer Inst*. 1988;80(19):1526-1533. doi:10.1093/jnci/80.19.1526.

302 Montecucco A, Zanetta F, Biamonti G. Molecular mechanisms of etoposide. *EXCLI J*. 2015;14:95-108. doi:10.17179/excli2015-561.

303 Tan CY, Hagen T. Post-translational regulation of mTOR complex 1 in hypoxia and reoxygenation. *Cell Signal*. 2013;25(5):1235-1244. doi:10.1016/j.cellsig.2013.02.012.

304 Butz K, Geisen C, Ullmann A, Zentgraf H, Hoppe-Seyler F. Uncoupling of p21WAF1/CIP1/SDI1 mRNA and protein expression upon genotoxic stress. *Oncogene*. 1998;17(6):781-787. doi:10.1038/sj.onc.1201995.

305 Circu M, Cardelli J, Barr MP, O'Byrne K, Mills G, El-Osta H. Modulating lysosomal function through lysosome membrane permeabilization or autophagy suppression restores sensitivity to cisplatin in

refractory non-small-cell lung cancer cells. *PLoS One*. 2017;12(9):e0184922. doi:10.1371/journal.pone.0184922.

306 Wang S, Luke CJ, Pak SC, et al. SERPINB3 (SCCA1) inhibits cathepsin L and lysoptosis, protecting cervical cancer cells from chemoradiation. *Commun Biol*. 2022;5(1):46. doi:10.1038/s42003-021-02893-6.

307 Lin J-F, Lin Y-C, Tsai T-F, Chen H-E, Chou K-Y, Hwang TI-S. Cisplatin induces protective autophagy through activation of BECN1 in human bladder cancer cells. *Drug Des Devel Ther*. 2017;11:1517-1533. doi:10.2147/DDDT.S126464.

308 Sui X, Chen R, Wang Z, et al. Autophagy and chemotherapy resistance: a promising therapeutic target for cancer treatment. *Cell Death Dis*. 2013;4(10):e838. doi:10.1038/cddis.2013.350.

309 Lim SM, Mohamad Hanif EA, Chin S-F. Is targeting autophagy mechanism in cancer a good approach? The possible double-edge sword effect. *Cell Biosci*. 2021;11(1):56. doi:10.1186/s13578-021-00570-z.

310 Xu Y, Yu H, Qin H, et al. Inhibition of autophagy enhances cisplatin cytotoxicity through endoplasmic reticulum stress in human cervical cancer cells. *Cancer Lett*. 2012;314(2):232-243. doi:10.1016/j.canlet.2011.09.034.

311 Korsmeyer SJ, Wei MC, Saito M, Weiler S, Oh KJ, Schlesinger PH. Pro-apoptotic cascade activates BID, which oligomerizes BAK or BAX into pores that result in the release of cytochrome c. *Cell Death Differ*. 2000;7(12):1166-1173. doi:10.1038/sj.cdd.4400783.

312 Shelton SN, Shawgo ME, Robertson JD. Cleavage of Bid by executioner caspases mediates feed forward amplification of mitochondrial outer membrane permeabilization during genotoxic stress-induced apoptosis in Jurkat cells. *J Biol Chem*. 2009;284(17):11247-11255. doi:10.1074/jbc.M809392200.

313 Ferreira KS, Kreutz C, Macnelly S, et al. Caspase-3 feeds back on caspase-8, Bid and XIAP in type I Fas signaling in primary mouse hepatocytes. *Apoptosis*. 2012;17(5):503-515. doi:10.1007/s10495-011-0691-0.

314 Drobny A, Prieto Huarcaya S, Dobert J, et al. The role of lysosomal cathepsins in neurodegeneration: Mechanistic insights, diagnostic potential and therapeutic approaches. *Biochim Biophys Acta Mol Cell Res*. 2022;1869(7):119243. doi:10.1016/j.bbamcr.2022.119243.

315 Reiser J, Adair B, Reinheckel T. Specialized roles for cysteine cathepsins in health and disease. *J Clin Invest*. 2010;120(10):3421-3431. doi:10.1172/JCI42918.

316 Dai Y, Zhao X-J, Li F, et al. Truncated Bid Regulates Cisplatin Response via Activation of Mitochondrial Apoptosis Pathway in Ovarian Cancer. *Hum Gene Ther*. 2020;31(5-6):325-338. doi:10.1089/hum.2019.206.

317 Gavrieli Y, Sherman Y, Ben-Sasson SA. Identification of programmed cell death in situ via specific labeling of nuclear DNA fragmentation. *J Cell Biol*. 1992;119(3):493-501. doi:10.1083/jcb.119.3.493.

318 Schindelin J, Arganda-Carreras I, Frise E, et al. Fiji: an open-source platform for biological-image analysis. *Nat Methods*. 2012;9(7):676-682. doi:10.1038/nmeth.2019.

319 Dimri GP, Lee X, Basile G, et al. A biomarker that identifies senescent human cells in culture and in aging skin in vivo. *Proc Natl Acad Sci U S A*. 1995;92(20):9363-9367. doi:10.1073/pnas.92.20.9363.

320 Franken NAP, Rodermond HM, Stap J, Haveman J, van Bree C. Clonogenic assay of cells in vitro. *Nat Protoc*. 2006;1(5):2315-2319. doi:10.1038/nprot.2006.339.

321 Kuhn BJ. The LATS1 and LATS2 tumor suppressor kinases: a comprehensive multilayered MS-based analysis of their functional roles in breast cancer. *Heidelberg University Library*; 2022.

322 Ritchie ME, Phipson B, Di Wu, et al. limma powers differential expression analyses for RNA-sequencing and microarray studies. *Nucleic Acids Res*. 2015;43(7):e47. doi:10.1093/nar/gkv007.

323 Deutsch EW, Bandeira N, Perez-Riverol Y, et al. The ProteomeXchange consortium at 10 years: 2023 update. *Nucleic Acids Res*. 2023;51(D1):D1539-D1548. doi:10.1093/nar/gkac1040.

324 Perez-Riverol Y, Bai J, Bandla C, et al. The PRIDE database resources in 2022: a hub for mass spectrometry-based proteomics evidences. *Nucleic Acids Res*. 2022;50(D1):D543-D552. doi:10.1093/nar/gkab1038.

325 Subramanian A, Tamayo P, Mootha VK, et al. Gene set enrichment analysis: a knowledge-based approach for interpreting genome-wide expression profiles. *Proc Natl Acad Sci U S A*. 2005;102(43):15545-15550. doi:10.1073/pnas.0506580102.

326 Livak KJ, Schmittgen TD. Analysis of relative gene expression data using real-time quantitative PCR and the 2(-Delta Delta C(T)) Method. *Methods*. 2001;25(4):402-408. doi:10.1006/meth.2001.1262.

327 Fjeldbo CS, Aarnes E-K, Malinen E, Kristensen GB, Lyng H. Identification and Validation of Reference Genes for RT-qPCR Studies of Hypoxia in Squamous Cervical Cancer Patients. *PLoS One*. 2016;11(5):e0156259. doi:10.1371/journal.pone.0156259.